Chem Soc Rev

# Noncovalently bound and mechanically interlocked systems using pillar[*n*]arenes



| | |
|---|---|
| Journal: | *Chemical Society Reviews* |
| Manuscript ID | CS-REV-02-2022-000169.R1 |
| Article Type: | Review Article |
| Date Submitted by the Author: | 05-Apr-2022 |
| Complete List of Authors: | Kato, Kenichi; Kyoto University, Department of Synthetic Chemistry and Biological Chemistry, Graduate School of Engineering<br>Fa, Shixin; Kyoto University, Department of Synthetic Chemistry and Biological Chemistry, Graduate School of Engineering<br>Ohtani, Shunsuke; Kyoto University, Department of Synthetic Chemistry and Biological Chemistry, Graduate School of Engineering<br>Shi, Tan-hao; Kyoto University - Yoshida Campus<br>Brouwer, Albert; Van 't Hoff Institute for Molecular Sciences, ; Advanced Research Center for Nanolithography,<br>Ogoshi, Tomoki; Kyoto University, ; |
| | |

ARTICLE

# Noncovalently bound and mechanically interlocked systems using pillar[*n*]arenes

fReceived 00th January 20xx,
Accepted 00th January 20xx

DOI: 10.1039/x0xx00000x

Kenichi Kato,[†a] Shixin Fa,[†a] Shunsuke Ohtani,[a] Tan-hao Shi,[a] Albert M. Brouwer*[c] and Tomoki Ogoshi*[a,b]

Pillar[*n*]arenes are pillar-shaped macrocyclic compounds owing to the methylene bridges linking the para-positions of the units. Owing to their unique pillar-shaped structures, these compounds exhibit various excellent properties compared with other cyclic host molecules, such as, versatile functionality using various organic synthesis techniques, substituent-dependent solubility, cavity-size-dependent host–guest properties in organic media, and unit rotation along with planar chiral inversion. These advantages have enabled the high-yield synthesis and rational design of pillar[*n*]arene-based mechanically interlocked molecules (MIMs). In particular, new types of pillar[*n*]arene-based MIMs that can dynamically convert between interlocked and unlocked states through unit rotation, have been produced. The highly symmetrical pillar-shaped structures of pillar[*n*]arenes result in simple NMR spectra, which are useful for studying the motion of pillar[*n*]arene wheels in MIMs and creating sophisticated MIMs with higher-order structures. The creation and application of polymeric MIMs based on pillar[*n*]arenes is also discussed.

## Introduction

Mechanically interlocked molecules (MIMs), such as catenanes, rotaxanes, and polyrotaxanes, are composed of axles and rings.[1–10] As the ring molecules in MIMs are mechanically interlocked, they can rotate and move, despite these motions being restricted compared with ring molecules without mechanical interlocking. In some cases, this ring motion can be used to change the bulk macroscopic properties of MIMs. For example, topological gels, which were first reported by Ito and coworkers, are unique third-generation gel materials compared with typical gels produced by covalent and noncovalent intermolecular crosslinking between polymeric chains.[11–13] Based on their ring motion, topological gels show high swelling rates, elongation, stress-elongation, and self-healing properties similar to biological tissues. Furthermore, MIMs do not dissociate, even under highly dilute and concentrated conditions, while host–guest complexes rely on concentration-dependent noncovalent bonds.

Cyclodextrins,[14–16] cucurbit[*n*]urils,[17,18] crown ethers,[19] calix[*n*]arenes,[20–22] and blue boxes[23–25] are useful ring components for preparing MIMs. Based on their inherent properties, such as solubility, host–guest interactions, and functionality, various MIMs have been reported. These macrocyclic hosts have advantages and disadvantages for producing MIMs. In 2008, we first reported a new class of macrocyclic hosts, pillar[*n*]arenes (Fig. 1a).[26] Considerable research efforts have elucidated their fundamental properties, such as synthesis, structure, functionality, conformation, and host–guest properties.[27–31] In 2010, we reported the first pillar[5]arene-based MIM, a polyrotaxane constructed from pillar[5]arene wheels.[32,33] In 2011, a pillar[5]arene-based [2]rotaxane was first prepared by Stoddart and coworkers.[34] Subsequently, various types of pillar[*n*]arene-based MIMs have been synthesized and their unique properties, resulting from using pillar[*n*]arene wheels, evaluated.[35,36] Compared with other well-known macrocyclic hosts, pillar[*n*]arenes as wheels have the following advantages:

(i) Highly symmetrical pillar-shaped structure: Pillar[*n*]arenes show highly symmetrical pillar-shaped structures (Figs. 1a and b) in solid state, which is one of the stable structures. In solution, in many cases, the rotation of the aromatic units is fast on the NMR timescale at 25 °C, thus averaged proton signals are observed in $^1$H NMR. Higher analogues, such as pillar[*n*]arenes (n ≧ 7), possess high conformational freedom, thus the unit rotation is fast on the NMR timescale, resulting in simple $^1$H NMR spectra. Therefore, pillar[*n*]arene-based MIMs are relatively easy to analyse owing to the simple and symmetric structure of pillar[*n*]arene wheels.

(ii) Solubility: The solubility of pillar[*n*]arenes mainly depends on the substituents on the rims (R groups in Fig. 1a). Simple pillar[*n*]arenes, namely, peralkoxy-substituted pillar[*n*]arenes, are highly soluble in typical halogenated solvents including

[a] Department of Synthetic Chemistry and Biological Chemistry, Graduate School of Engineering, Kyoto University, Nishikyo-ku, Kyoto, 615-8510, Japan. E-mail: ogoshi@sbchem.kyoto-u.ac.jp
[b] WPI Nano Life Science Institute, Kanazawa University, Kakuma-machi, Kanazawa, 920-1192, Japan.
[c] Van't Hoff Institute for Molecular Sciences, University of Amsterdam P.O. Box 94157, 1090 GD Amsterdam, The Netherlands. E-mail: A.M.Brouwer@uva.nl
† These authors contributed equally.

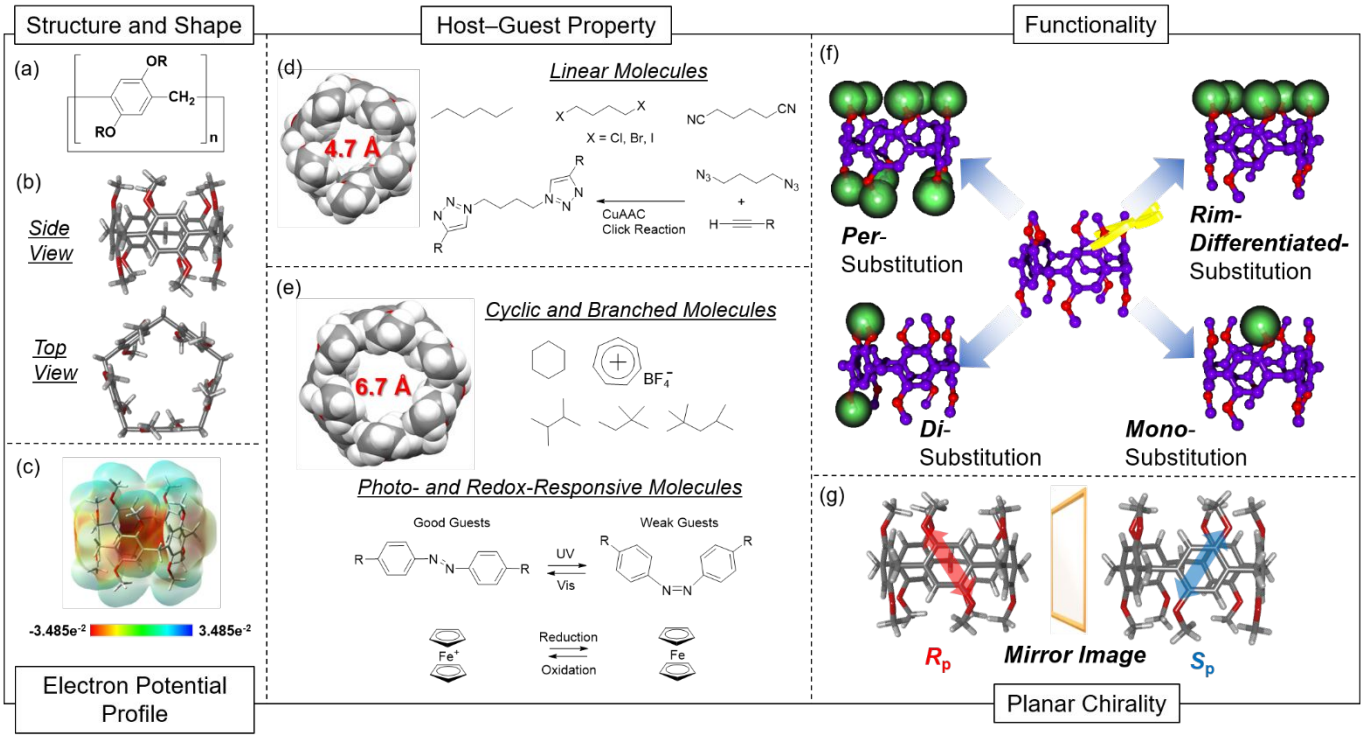


**Fig. 1** (a) Chemical structure of pillar[*n*]arenes. (b) Single-crystal structure of pillar[5]arene from side and top views. (c) Calculated electron potential profile (DFT calculation, B3LYP/6-31G(d,p)) of permethoxy-substituted pillar[5]arene. Cavity sizes and guests of (d) pillar[5]arenes and (e) pillar[6]arenes. (f) Mono-, di-, rim-differentiated, and per-functionalized pillar[*n*]arenes. (g) Planar chirality of pillar[*n*]arenes.

chloroform and dichloromethane, and aromatic solvents including toluene and benzene. Perhydroxy-substituted pillar[*n*]arenes, which can be produced by deprotection of the alkoxy groups, are soluble in polar organic solvents, including methanol, acetonitrile, DMF, and DMSO. Introducing ionic and nonionic hydrophilic groups on the rims results in water-soluble pillar[*n*]arenes.

(iii) Host–guest complexation in organic solvents: The formation of host–guest inclusion complexes is required to prepare MIMs. The pillar[*n*]arene cavity is electron-rich owing to the pillar[*n*]arene panels being electron-donating dialkoxybenzene units (Fig. 1c). Therefore, pillar[*n*]arenes can capture cationic guest molecules in their electron rich cavity. Furthermore, multiple C–H/$\pi$ interactions can form between the benzene rings of the panels and C–H groups of the guest molecules.[37–39] As almost all organic compounds have C–H groups, pillar[*n*]arenes are ideal host molecules for various organic compounds. Furthermore, O atoms of ether groups are arranged on both rims. Therefore, multiple C–H/O, O–H/O, and N–H/O interactions can form between the O atoms of pillar[*n*]arenes and C–H, O–H, and N–H groups of guest molecules. Each interaction is relatively weak (less than 10 kcal mol$^{-1}$), but multiple interactions between pillar[*n*]arenes and guests stabilize the host–guest complexes. Host–guest complexes can even be formed in good organic solvents for the pillar[*n*]arenes and guests. Therefore, various reactions that operate in organic solvents can be used to prepare MIMs. Various MIMs synthesis trials have shown that Huisgen-type copper(I)-catalysed azide–alkyne cycloaddition (CuAAC) "click" reactions are useful for preparing MIMs.[40] Furthermore, the triazoles produced by CuAAC reactions (Fig. 1d) are electron-withdrawing groups, which enhances the acidity of neighbouring C–H groups.[41] The acidic C–H groups promote C–H/$\pi$ hydrogen bond formation with the hydrogen-bond acceptors in pillar[*n*]arenes.

(iv) Cavity-size-dependent host–guest complexation: The cavity size of the cyclic pentamers, pillar[5]arenes, is approx. 4.7 Å (Fig. 1d). This size is suitable for linear-shaped molecules such as *n*-alkanes. Simple aromatic compounds are also good guest molecules for pillar[5]arenes.[42] The inclusion of linear-shaped molecules is among the advantages of preparing MIMs because such molecules are good linkers to connect guest stations for wheels. Fundamental molecular motion can be investigated by changing the linker length.[43] Furthermore, the cavity size of the cyclic hexamers, pillar[6]arenes, is 6.7 Å (Fig. 1e), which is suitable size for photoresponsive guests, such as azobenzenes,[44] and redox-responsive guests, such as ferrocenium cations.[45] The inclusion of these stimuli-responsive guests can be used to control the shuttling of pillar[6]arene wheels in MIMs.

(v) Versatile functionality: Simple alkoxy-substituted pillar[*n*]arenes can be converted to phenolic derivatives by

deprotection. As phenolic groups have high reactivity, hydroxy-substituted pillar[*n*]arenes are useful key compounds for producing various functional pillar[*n*]arenes. Mono-,[46,47] di-,[48,49] per-[50,51] and rim differentiated pillar[5.6]arenes[52–55] have been successfully synthesized by various organic reactions (Fig. 1f). Introducing triflate groups enables the use of cross-coupling reactions, such as Suzuki and Sonogashira couplings, to directly introduce aryl and alkynyl groups, respectively.[56–59] Based on this versatile functionality, stimuli-responsive and tag groups can be installed to control the motion and report the location of wheels in MIMs.

(vi) Planar chirality: The specific substitution pattern of the alkoxy substituents at 1,4-positions of the benzene units makes pillar[*n*]arenes chiral, namely, planar chiral $S_p$ and $R_p$ forms.[60] When the unit undergoes oxygen-through-the-annulus rotation, exchange between $S_p$ and $R_p$ forms (racemization) occurs. In contrast, the exchange does not occur when the unit rotation is inhibited. The formation of MIMs enables separation of the enantiomers by chiral chromatography because an axle or ring in the pillar[*n*]arene cavity inhibits unit rotation.[61]

This review first discusses the motion of pillar[*n*]arene wheels in pseudorotaxanes. The preparation of MIMs based on pillar[*n*]arenes will then be discussed. Generally, the use of strong host-guest interactions to form the stations results in the successful synthesis of MIMs. Solvent-free and ball-mill syntheses of MIMs are useful methods for improving the yields of MIMs, even when a weak host–guest complex combination is used for the station. The shuttling dynamics of pillar[*n*]arene wheels in MIMs are also described, followed by single-component mechanically self-locked molecules and MIM-based supramolecular polymers. Finally, polymeric MIMs, such as rotaxane dendrimers and polyrotaxanes, are discussed.

## MIMs and related molecules: Synthesis, dynamics, and functions

### Pillar[*n*]arene-based pseudorotaxanes

In the broadest possible sense, any complex between a pillar[*n*]arene and guest molecule without capping is called a pseudorotaxane, because the complex is an “interlaced compound”, which is generally more stable than the free components (the filamentous axle and cyclic wheel). However, this section focus only on structures that gain high stability through interactions in addition to the multiple C–H/π interactions within the pillar[*n*]arene cavities. These structures are usually stable enough for monitoring, capturing, and regulation.

Hou and coworkers reported a series of pseudo[2]rotaxanes constructed from linear diacids **A1**-*n* (*n*: carbon numbers, *n* = 3–10,12,15,18,20) and decaaminopillar[5]arene **P1** (Fig. 2).[62] The ionic interaction between the protonated amino groups on the rims of **P1** and the deprotonated acid groups at both ends of the linear diacids was the major driving force of complexation between **P1** and **A1**-*n*. Among all diacids, **A1**–8 with eight carbon atoms was the best fit for the cavity of **P1**, because the two acids at the ends of **A1**–8 were located close to the amines of **P1** for complexation. For shorter and longer diacids, **P1** might shuttle along their linear chains. The pseudo[2]rotaxanes constructed from **P1** and **A1**-*n* (*n* ≥ 15) can be further stabilized by capping with triethylamine (TEA). Adding 2 equiv. of TEA to the solution of **P1** and **A1**-*n* (*n* ≥ 15) resulted in the formation of new ion pairs between diacids and TEA, and capped the pseudo[2]rotaxanes, because TEA has substantially stronger basicity compared with primary amines. The formed ion pair-stopped [2]rotaxanes were detected using mass spectrometry and did not decompose, even at 70 °C.

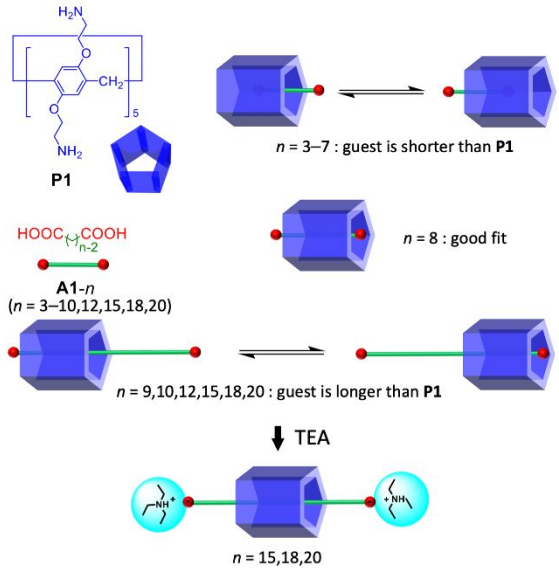


**Fig. 2** Wheel shuttling of pseudo[2]rotaxanes formed by **P1** and diacids, and formation of ion pair-stopped [2]rotaxanes. TEA = triethylamine.

The regulation of pseudorotaxanes is important for utilization of the interlaced structure features. Axle modification is one method for controlling the behaviour of pseudorotaxanes. Wei and coworkers designed tadpole-like axles **A2a** and **A2b** bearing imidazole derivatives and alkyl chains (Fig. 3a).[63] These axles formed pseudo[2]rotaxanes with perethylated pillar[5]arene **P2**. Owing to the unique shape of **A2a** and **A2b**, **P2** was found to move on the axles. Increasing the concentration of **P2** caused the pillar[5]arene wheel to gradually move from the imidazole part to the alkyl chains of the axles. Therefore, a unidirectional threading process seemed to occur within these pseudo[2]rotaxanes with an increasing concentration of **P2**. Our group carefully investigated the threading/dethreading exchange dynamics of three pseudo[2]rotaxanes, which were controlled by the ends of the axles.[64] Viologen axles with alkyl ends (**A3a**), carboxylic acid ends (**A3b**), and carbonylethyl ends (**A3c**) were synthesized and formed pseudo[2]rotaxanes with pillar[5]arene **P3** owing to interactions between the electron-rich cavity of **P3** and cationic viologen salts (Fig. 3b). The introduction of carbonyl groups significantly decreased the threading/dethreading exchange rates on the NMR timescale

by comparing the variable-temperature $^1$H NMR and two-dimensional exchange spectroscopy (2D EXSY) of the three pseudo[2]rotaxanes. This was because electronic repulsion between the electron-rich carbonyl groups and the electron-rich pillar[5]arene cavity led to an electric trap and decreased the exchange rate. The exchange rate constants of **P3** along **A3b** and **A3c** were about 2000 and 360 times smaller than that along **A3a**, respectively.

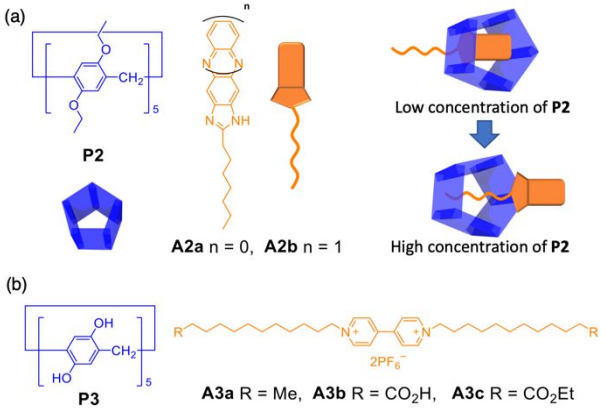


**Fig. 3** (a) Two inclusion-type pseudo[2]rotaxanes formed by **P2** and **A2**. (b) Chemical structures of **P3** and **A3a–c**.

External stimuli can change the properties of the axle or wheel in pseudorotaxanes, and further induce threading/dethreading processes. Li and coworkers reported a pH-responsive pseudo[2]rotaxane constructed from pillar[5]arene **P3** and 1,4-bisimidazolium butane **A4** (Fig. 4a).[65] **P3** formed a complex with protonated **A4** owing to cation/π interaction between the two imidazolium cations of **A4** and the pillar[5]arene backbone. In contrast, neutral **A4** hardly associated with **P3** owing to the lack of cation/π interaction. Therefore, the threading/dethreading process can be reversibly controlled through alternating addition of TEA and trifluoroacetic acid (TFA) to the pseudo[2]rotaxane solution. The same group also constructed a pH-responsive pseudo[2]rotaxane based on perethylated pillar[6]arene and bis(1,2,3-triazolium)butane dication using a similar concept.[66] Yao and coworkers controlled the threading/dethreading of a pseudo[2]rotaxane based on imidazolium cations and pillar[5]arene though alternating addition of silver(I) and TFA.[67] Adding silver oxide caused dissociation of the pseudorotaxane, owing to silver(I) coordinating with imidazolium cations. Adding TFA, which binds silver(I) more strongly, caused reconstruction of the pseudorotaxane. Arunachalam and coworkers reported an anion-responsive pseudo[3]rotaxane from difunctionalized pillar[4]arene[1]quinone **P4** and axle **A5** with two imidazolium ends (Fig. 4b).[68] The two wheels were separated by the aromatic spacer and located close to the imidazolium ends through hydrogen-bonding interactions. Upon neutralization by adding tetrabutylammonium chloride (TBACl), the pseudo[3]rotaxane was disassembled and guest **A5** was precipitated owing to formation of a stronger complex with chloride.

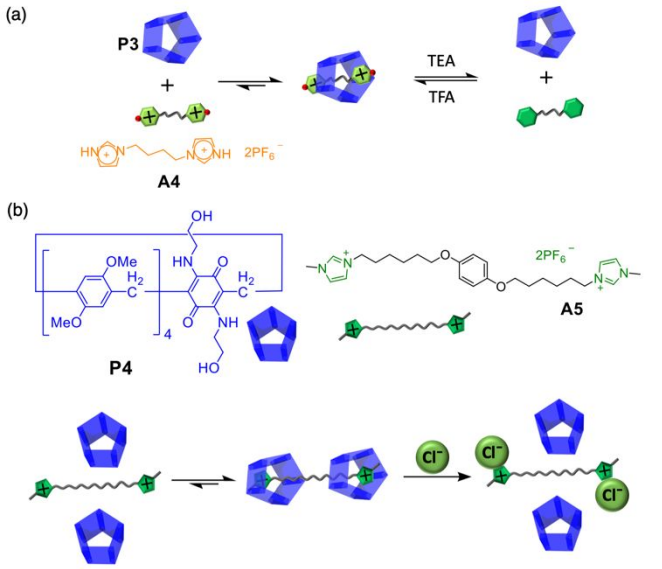


**Fig. 4** (a) pH-Responsive pseudo[2]rotaxane based on **P3** and **A4**. (b) Anion-responsive pseudo[3]rotaxane based on **P4** and **A5**. TFA = trifluoroacetic acid.

We developed a redox-responsive pseudo[2]rotaxane based on redox interconversion of pillar[4]arene[1]hydroquinone **P5**-red. The hydroquinone unit of **P5**-red can be oxidized to a benzoquinone unit, producing **P5**-ox (Fig. 5a).[69] **P5**-red binded filamentous axle **A6**, bearing an *n*-butylene bridged bis-triazole moiety, through hydrogen-bonding interactions, and generated the pseudo[2]rotaxane. In contrast, **P5**-ox did not form a stable complex with **A6** owing to the decreased electron density of the pillar[5]arene cavity after oxidization, resulting in decomposition of the pseudo[2]rotaxane. Upon addition of a reductant, the benzoquinone unit was converted to hydroquinone, leading to the rethreading of **P5**-red onto **A6**.

We subtly controlled the threading/dethreading speed of photoresponsive pseudo[2]rotaxane **A7@P3** between timescales of seconds and hours (Fig. 5b).[70] Filamentous axle **A7** was designed as the axle in this system. The central viologen group guaranteed complexation between **A7** and pillar[5]arene **P3**, while the bulky adamantyl stopper at one end of **A7** allowed the threading/dethreading process to only occur from the other end, to which a photoresponsive azobenzene group was connected. The wheel of **P3** shuttled through the *trans*-azobenzene smoothly, and the half-life of equilibration was only 3.33 s, as determined using $^1$H NMR and 2D EXSY. Under UV irradiation, the half-life of equilibration increased to 9.13 h, because azobenzene isomerization from the *trans*- to *cis*-form increased the free energy of activation of the wheel slipping over the end.

Lin and coworkers reported a novel photoresponsive [2]rotaxane constructed from photoresponsive carbamate derivative **A8** and **P2**.[71] The association constant between **A8** and **P2** was determined to be 856 ± 5 $M^{-1}$ owing to the multiple C–H/π interactions in the pillar[5]arene cavity and interactions between the carbamate groups and **P2**. Under UV irradiation, **A8** was cleaved (Fig. 5c). The product, *N*-carbobenzoxy-1,4-diaminobutane, was precipitated from the solvent, releasing **P2**.

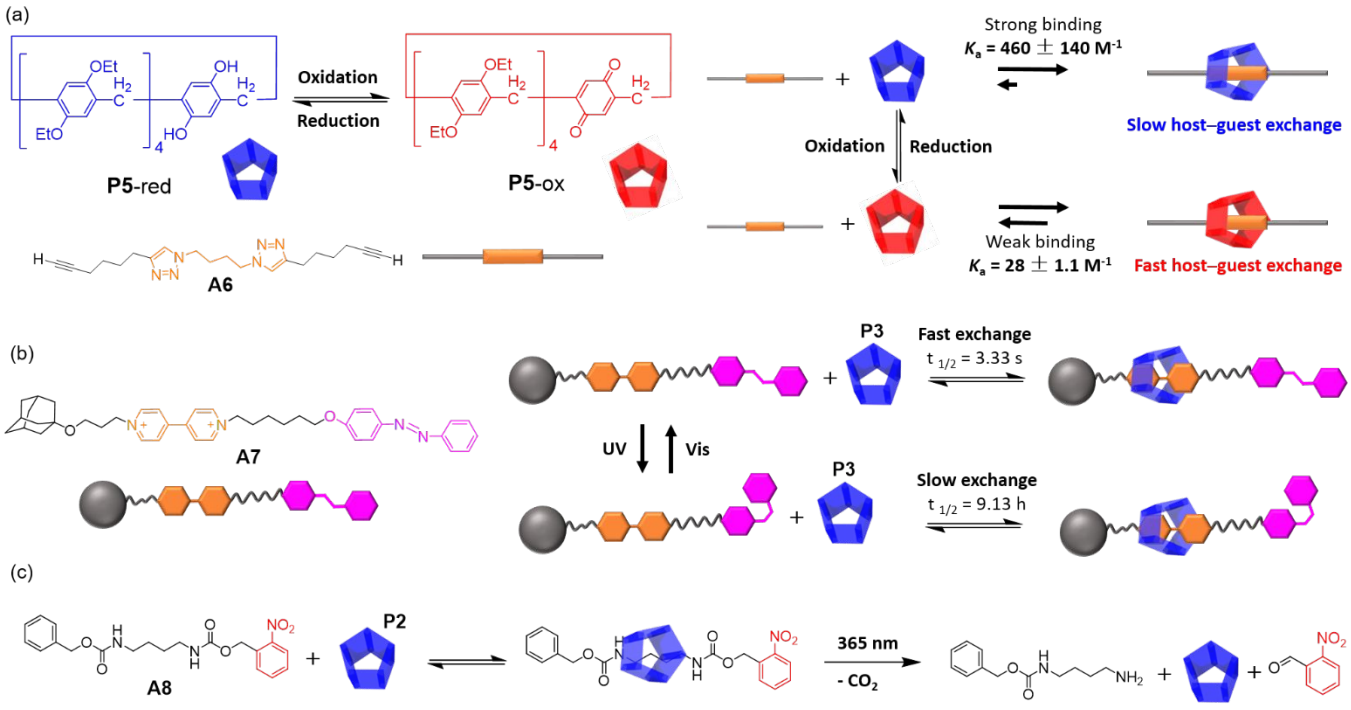


**Fig. 5** (a) Redox-responsive pseudo[2]rotaxane based on **P5** and **A6**. Photoresponsive pseudo[2]rotaxanes based on (b) **P3** and **A7**, and (c) **P2** and **A8**.

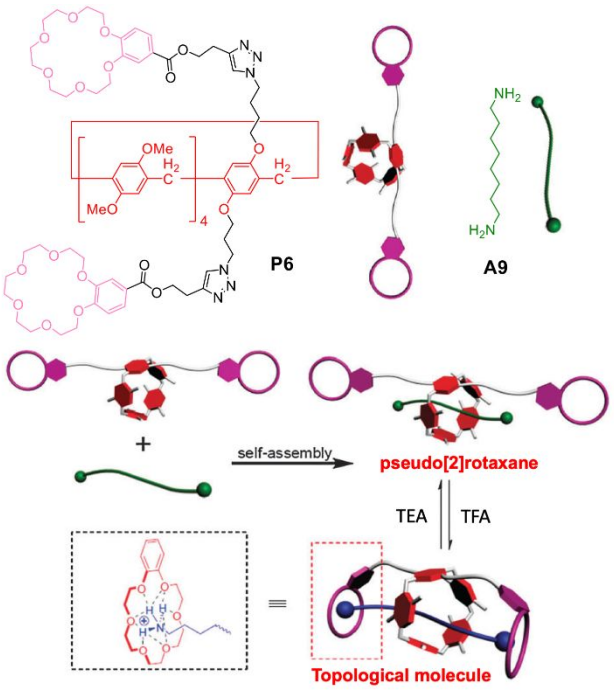


**Fig. 6** Dynamic pH-responsive [1]catenane based on **P6** and **A9**. Reproduced with permission from ref. 72. Copyright 2013 Royal Society of Chemistry.

Starting from pillar[*n*]arene-based pseudo[2]rotaxanes, more complex topological structures have been constructed through rational molecular design. In 2013, Huang and coworkers reported a pH-responsive topological molecule, which was described as a dynamic [1]catenane in the original paper, formed using the threading-followed-by-complexation strategy from the A1,A2-difunctionalized pillar[5]arene with two crown ether units **P6** and 1,8-diaminooctane **A9** (Fig. 6).[72] A pseudo[2]rotaxane was first formed by complexation between **P6** and **A9** through multiple C–H/π interactions in the pillar[5]arene cavity. Subsequent addition of TFA led to protonation of the amine groups, which further caused association between the two crown ether moieties and ammonium salts. Therefore, the topological molecule was constructed from the pseudo[2]rotaxane. The topological molecule and pseudo[2]rotaxane could be interconverted by alternating treatment with TEA and TFA.

**Synthesis of MIMs based on pillar[*n*]arenes**

Benefiting from the ability of pillar[*n*]arenes to recognize various guest molecules, especially linear alkyl moieties and their derivatives, interlocked structures including rotaxanes and catenanes can be conveniently obtained by simple capping.

**[2]Rotaxanes.** Rotaxanes based on pillar[*n*]arenes were initially synthesized using simple linear alkyl moieties as the station. In 2011, Stoddart and coworkers reported the first pillar[*n*]arene-based rotaxane. Permethylated pillar[5]arene **P7** was mixed with **A9** and formed a pseudo[2]rotaxane, which was capped with 3,5-di-*tert*-butylbenzaldehyde **1** through imine bond formation with the primary amino groups on the guest molecule (Scheme 1a).[34] Subsequent reduction of the imine bonds with

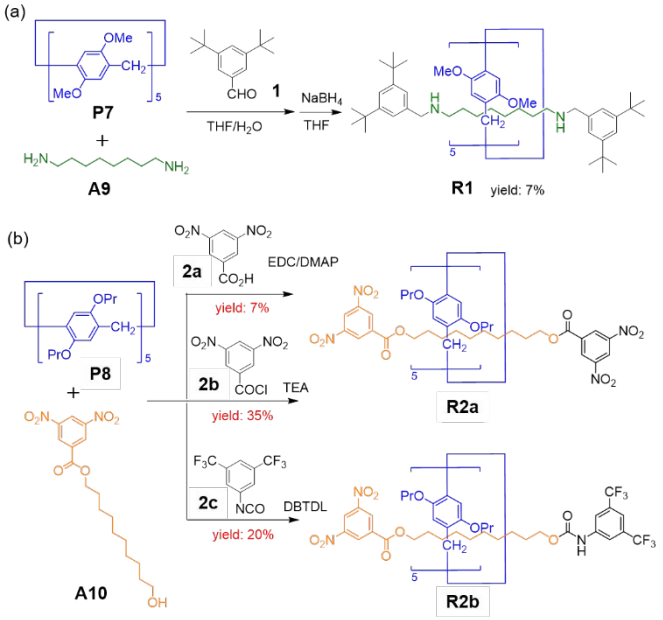


**Scheme 1** [2]Rotaxanes constructed by (a) **P7** and **A9**, and (b) **P8** and **A10**. EDC = 1-Ethyl-3-(3-dimethylaminopropyl)carbodiimide, DMAP = 4-Dimethylaminopyridine, DBTDL = Dibutyltin dilaurate.

sodium borohydride gave [2]rotaxane **R1** in 7% yield. The low yield was due to the weak host–guest interaction in the pseudo[2]rotaxane ($K_a$ = 70 ± 10 $M^{-1}$). Similarly, Huang and coworkers synthesized [2]rotaxanes based on the interaction between 1,10-decanediol and *n*-perpropylated pillar[5]arene **P8** (Scheme 1b).[73] 1,10-Decanediol was initially capped at one end by 3,5-dinitrobenzoic acid to form axle **A10**, and then formed an interlaced structure with **P8**. The complex was capped by stoppers **2a–c** through ester and uretane formation of the remaining OH group. The yields of rotaxanes **R2a**,**b** were higher than that of **R1**. The longer aliphatic station probably increased the stability of the host–guest complex during rotaxane synthesis.

Nierengarten and coworkers used dodecanedioyl chloride **A11** as the axle and obtained pillar[5]arene-based [2]rotaxanes in high yield.[74] When perethylated pillar[5]arene **P2** was used as the wheel and 3,5-bis(trifluoromethyl)aniline **3** as stopper, the yield of rotaxane **R3** in chloroform was up to 63% (Scheme 2a). The electron-withdrawing properties of acyl chloride increased the interactions between the electron-rich pillar[5]arene cavity and alkyl chains, making the host–guest complex more stable and increasing the yield of rotaxane formation. Furthermore, the end-capping reaction of acyl chloride with amines to form amides was highly efficient, which helped to increase the yield. The authors found that decreasing the axle length and increasing the length of rim substituents in the pillar[5]arene also influenced the efficiency of rotaxane formation, because amide formation was inhibited in these cases by steric hindrance between the acyl chlorides and amines. Furthermore, electron-rich aromatic stoppers did not work as well as their electron-deficient counterparts, owing to negative interactions with the electron-rich cavity of the pillar[5]arene receptors.

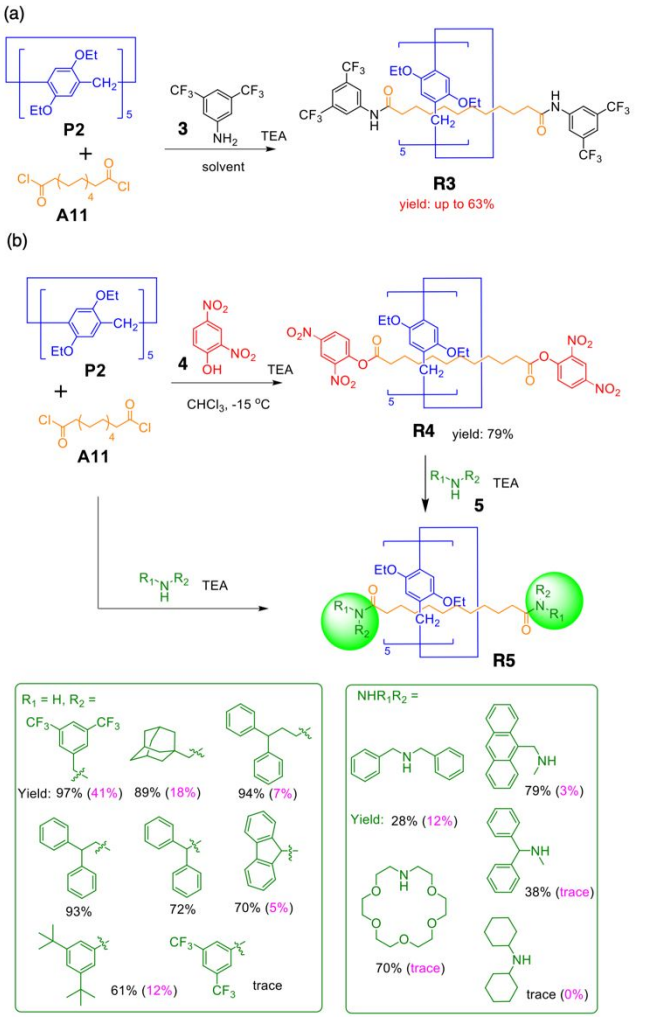


**Scheme 2** (a) Preparation of [2]rotaxane **R3** from acyl chloride **A11**. (b) Preparation of [2]rotaxanes using a stopper exchange strategy. The yields in parentheses were obtained by direct introduction of the two amide stoppers in a single synthetic step.

To solve this problem, the same group used a stopper exchange strategy to prepare [2]rotaxanes that were difficult or impossible to obtain by direct introduction of the two amide stoppers in a single synthetic step.[75] Rotaxane **R4** was first synthesized by capping the host–guest complex of dodecanedioyl and **P2** with 2,4-dinitrophenol **4** in 79% yield (Scheme 2b). The subsequent replacement of **4** with various commercially available secondary amines **5** through an addition–elimination mechanism prevented decomposition of the [2]rotaxane structure, generating a series of diamide [2]rotaxanes **R5** in good yields. This two-step synthesis improved the yield of some [2]rotaxanes that were difficult or impossible to prepare by direct capping of two ends with bulky amines. Interestingly, these diamide [2]rotaxanes were also synthesized under mechanochemical solvent-free conditions.[76] In this strategy, the complex between **P2** and **A11** was first formed in chloroform at −15 °C. The solvent was then evaporated, and the resulting solid was mixed with specific

amines using ball-milling methods, providing the corresponding diamide [2]rotaxanes in excellent yields (up to 87%). The solvent-free conditions might prevent dissociation of the uncapped complex during stoppering reactions. Therefore, rotaxane formation was highly efficient.

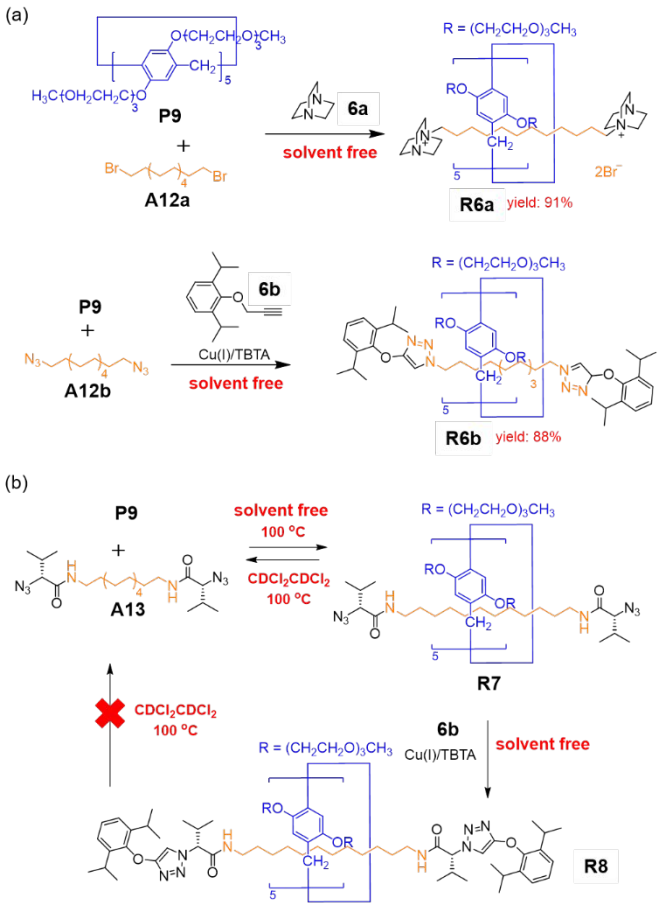


**Scheme 3** (a) Preparation of [2]rotaxanes based on liquid pillar[5]arene **P9**. (b) Preparation of pseudo[2]rotaxane **R7** using the slippage approach, and the capping reaction for synthesis of [2]rotaxane **R8**. TBTA = Tris[(1-benzyl-1H-1,2,3-triazol-4-yl)methyl]amine.

We developed another solvent-free strategy for rotaxane synthesis using liquid pillar[5]arene **P9** as the wheel.[77] **P9** with tri(ethylene oxide) chains on both rims existed in the liquid state even at −50 °C, and did not decompose at up to 250 °C. By dissolving axles **A12a**,**b** and stoppers **6a**,**b** in **P9**, [2]rotaxanes **R6a** and **R6b** were obtained in high yields by cationization and CuAAC reactions, respectively, between the axles and stoppers (Scheme 3a). Surprisingly, the association constants between **P9** and **A12a**,**b** were determined to be 10–15 $M^{-1}$ in chloroform. Complexation was clearly extremely efficient in liquid pillar[5]arene **P9** compared with that in solution. This solvent-free strategy provided an approach for the synthesis of rotaxanes, even with unfavourable statistical combinations for host–guest complexation.

We also demonstrated the slippage behaviour of **P9** on axle **A13**, which possessed bulky ends (Scheme 3b).[78] Pseudo[2]rotaxane **R7** was formed by heating a mixture of **P9** and **A13** at 100 °C, with **P9** slipping across the bulky ends of **A13**. The pillar[5]arene wheel of rotaxane **R7** was released by heating in tetrachloroethane or trapped on the axle by capping the ends of **A13** with stopper **6b** via CuAAC reaction to form [2]rotaxane **R8**.

In addition to solvent-free synthesis, another common strategy for improving the yield of rotaxane synthesis involves introducing a station on the axle in advance to increase complex stability between the axle and wheel. We synthesized a cationic axle **A14** bearing a central pyridinium moiety that helped to increase the stability of the host–guest complex between **A14** and **P2** (Scheme 4a).[61] The association constant was determined to be (7.6 ± 1.1) × $10^4$ $M^{-1}$. The pseudo[2]rotaxane was capped with an azide-terminated stopper **7** via the CuAAC reaction to produce [2]rotaxane **R9** in 75% yield. The two stable isomers of **R9** with planar chirality were isolated in a 1:1 ratio by chiral HPLC. This was the first example of chiral rotaxanes based on pillar[*n*]arenes

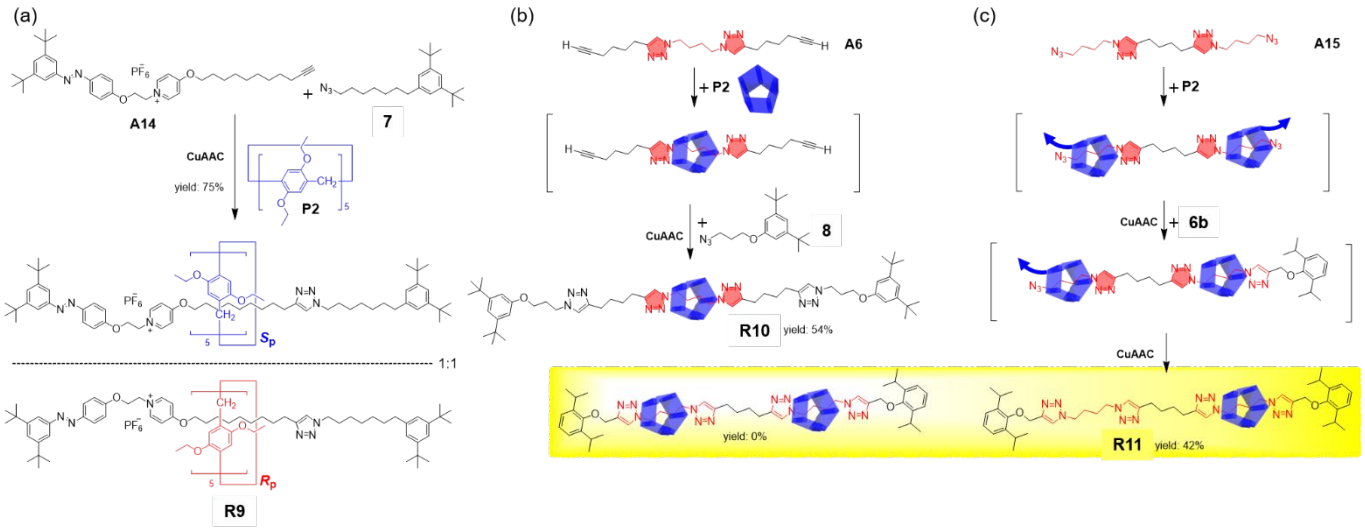


**Scheme 4** Preparation of [2]rotaxanes (a) **R9**, (b) **R10**, and (c) **R11** using station-containing axles.

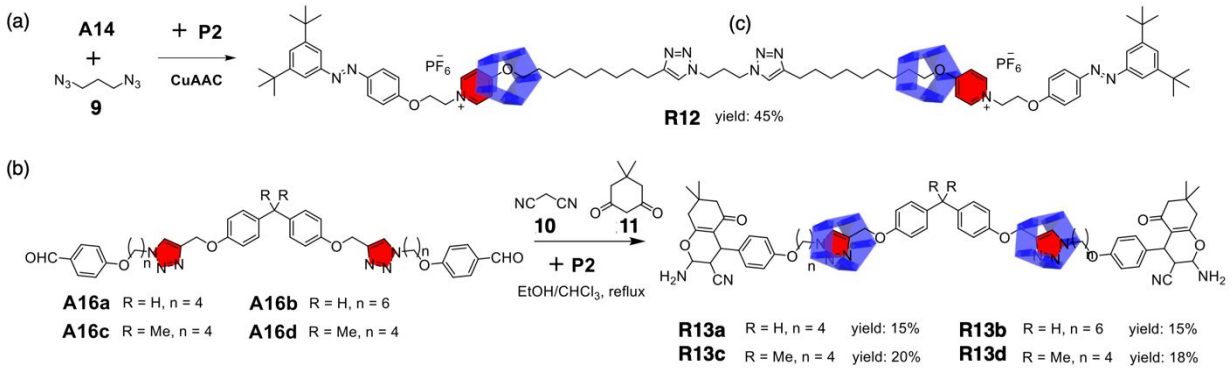


**Scheme 5** Preparation of [3]rotaxanes (a) **R12** and (b) **R13** using axles containing multiple stations.

1,2,3-Triazole is another group that helps to increase complex stability between pillar[5]arenes and linear guests, especially when two triazoles are linked with an *n*-butylene group. We synthesized [2]rotaxane **R10** in 54% yield via the one-pot CuAAC reaction of **P2**, axle **A6**, and stopper **8** (Scheme 4b).[79] Interestingly, axle **A15**, which formed a 1:2 complex with **P2**, also provided the corresponding [2]rotaxane in 42% yield, instead of the [3]rotaxane, by capping with stopper **6b** via the one-pot CuAAC reaction (Scheme 4c). **A15** had weak binding sites for **P2**. When **A15** was reacted with **6b**, an axle with a good station formed in situ and complexed with **P2**. Capping the second end of the axle provided [2]rotaxane **R11**. From the synthesis of [2]rotaxanes **R10** and **R11**, the *N*-terminated butylene linker was clearly a better station for pillar[5]arenes than the *C*-terminated butylene linker. Huang and coworkers also used a bis-triazole derivative bearing an *n*-pentylene linker as the axle to synthesize [2]rotaxanes in yields of 16–27%.[80]

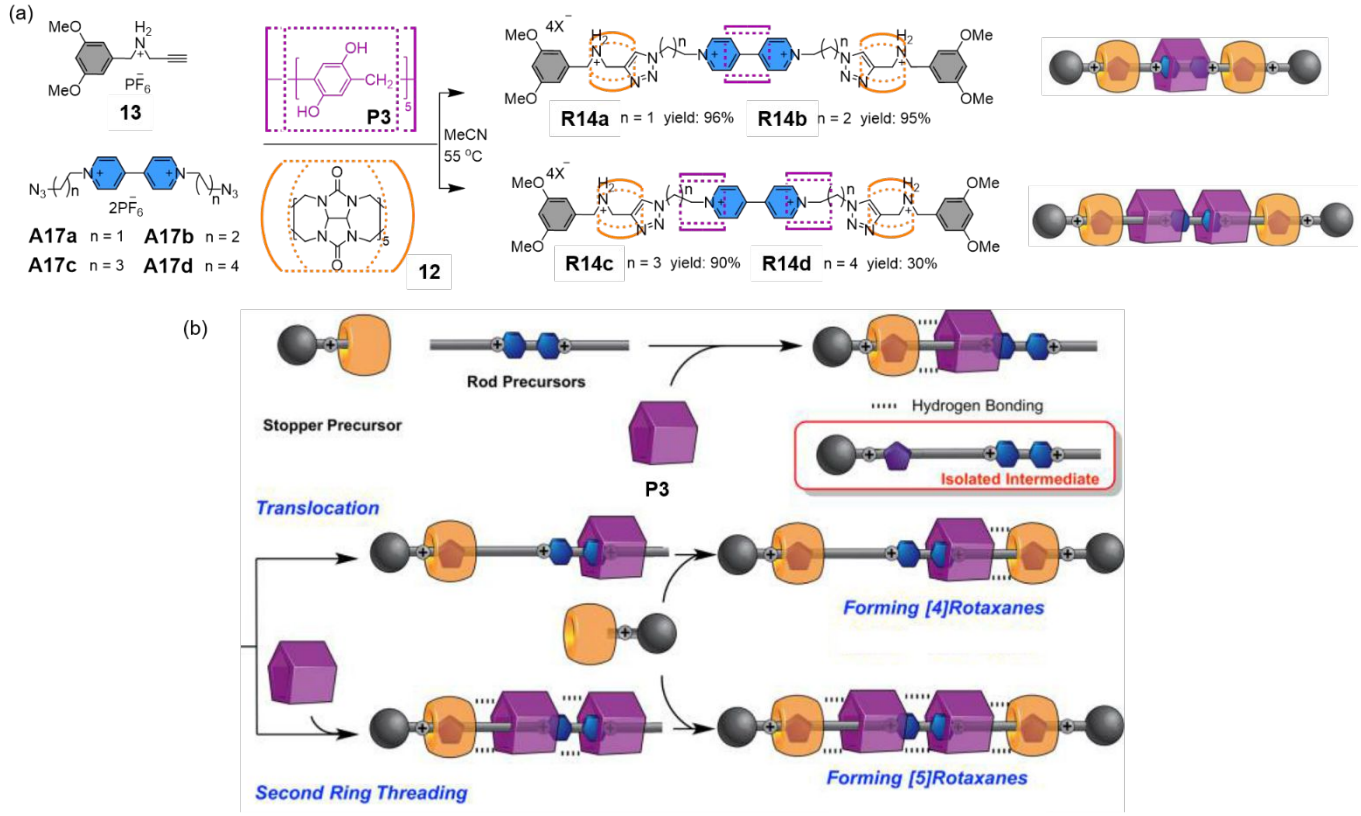


**Scheme 6** (a) Preparation and (b) mechanism of hetero[4]rotaxanes and hetero[5]rotaxanes **R14**. Reproduced with permission from ref. 82. Copyright 2013 American Chemical Society.

**[3]Rotaxanes and hetero[*n*]rotaxanes.** The synthesis of [*n*]rotaxanes of higher order than [2]rotaxane is important in the field of MIMs, but is difficult owing to cross-action between the various components. To obtain [*n*]rotaxanes, multiple stations on the axle provide a useful approach. We used pyridinium-containing axle **A14**, **P2**, and diazidopropane **9** to synthesize [3]rotaxane **R12** in one-pot via CuAAC reaction (Scheme 5a).[61] Two pseudo[2]rotaxanes formed by complexation of **A14** and **P2** were connected by linker **9** to provide **R12** in 45% yield. Yao and coworkers synthesized [3]rotaxanes using axles containing two separated triazole stations and two multicomponent stoppers (Scheme 5b).[81] By mixing axles **A16a–d**, **P2**, malononitrile **10**, and dimedone **11** in one pot, two wheels could be initially threaded by the axles through interactions between **P2** and the triazole stations, providing pseudo[3]rotaxanes. The subsequent base-catalysed three-component reaction of **10**, **11**, and the benzaldehyde units on **A16a–d** capped the pseudo[3]rotaxanes in situ to generate [3]rotaxanes **R13a–d** in 15–20% yields.

Stoddart and coworkers reported the synthesis of hetero[4,5]rotaxanes based on cucurbit[6]uril (**12**) and perhydroxy-substituted pillar[5]arene **P3** (Scheme 6a).[82] Axles **A17a–d**, bearing a positively charged bipyridinium moiety, and stopper **13**, containing a secondary amine, were rationally designed and synthesized. **A17a–d** bound **P3** strongly through cation/π interactions between bipyridinium and the electron-rich pillar[5]arene cavity, and **13** had high affinity for **12** after protonation due to the charge–dipole and hydrogen-bonding interactions between the ammonium ions and carbonyl groups around the rims of **12**. Therefore, pseudorotaxanes of **P3** onto the axles and **12** onto **13** were formed in advance in the system (Scheme 6b) before 1,3-dipolar cycloadditions occurred between the azides at the axle ends and alkynes on the stopper. The capping reaction of the preorganized pseudorotaxanes provided hetero[4,5]rotaxanes **R14a–d** depending on the spacer length of the axles. Longer axles provided more space for wheels and resulted in the formation of high-order rotaxanes. During the reaction, hydrogen-bonding interactions between the wheels (**12** and **P3**) not only stabilized the intermediates, but also accelerated the 1,3-dipolar cycloaddition reactions owing to complexation between the produced triazole groups and the cavity of **12** (Scheme 6b). Therefore, heterorotaxane formation was highly efficient, even at room temperature without a copper catalyst. Furthermore, the authors found that **P3** in the rotaxanes adopted various conformations that were frozen on the axles, suggesting strong interactions between **P3** and **12** during the reaction. Owing to its larger cavity compared with **P3**, perhydroxy-substituted pillar[6]arene nestled between two **12** rings in hetero[4]rotaxanes was conformationally mobile in solution.[83] A hetero[4]rotaxane consisting of one crown ether and two pillar[5]arene macrocycles, and perylenediimide diimidazolium axle was recently reported by Champness and coworkers.[84] The hetero[4]rotaxane showed photoinduced charge separation between crown ether macrocycle and the perylenediimide, which are different from a homo[3]rotaxane consisting of the same axle and two pillar[5]arene macrocycles (without the crown ether macrocycle).

Champness and coworkers reported handcuff rotaxanes based on host–guest complexation between pillar[5]arenes and imidazoles, and π–π stacking between rylene diimides.[85] Bis-pillar[5]arene-functionalized species **P10**, in which the two pillar[5]arene moieties were separated by the perylene diimide (PDI) aromatic core, and bisimidazole species **A18**–*n*, in which the two arms were separated by PDI or naphthalene diimide (NDI) aromatic cores, were mixed with bulky aryl iodide **14** to give handcuff rotaxanes **R15**–*n* in high yields (Scheme 7). Rotaxane formation probably involved the initial pseudorotaxane, in which each imidazole group on **A18**–*n* sat within a pillar[5]arene host. These handcuff-shaped rotaxanes produced dimers of rylene diimide, such that the two components freely stacked compared with covalently bound systems. Therefore, **R15**–*n* exhibited unusual behaviour, such as H-aggregate formation.

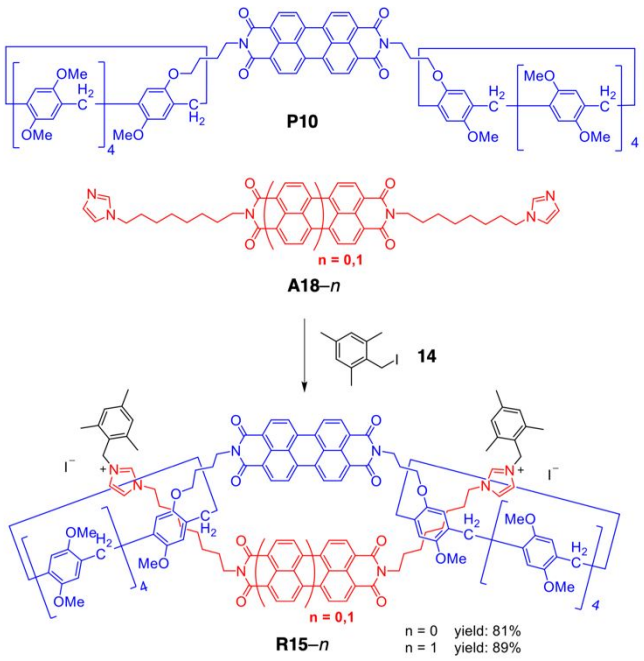


**Scheme 7** Synthesis of handcuff [2]rotaxanes **R15**–*n*.

**Catenanes.** The synthesis of pillar[*n*]arene-based catenanes follows a similar strategy to that of [*n*]rotaxanes, namely, introducing a station on the axle in advance to increase the stability of the complex between the axle and macrocycle. We reported the synthesis of the first pillar[*n*]arene-based catenane using **P2** and 4-alkoxy-substituted pyridine derivative **A19** with vinyl groups at opposite ends (Scheme 8a).[86] Owing to the strong interaction between the pyridinium moiety and the cavity of **P2**, the central part of **A19** was included in **P2** to form a pseudo[2]rotaxane. A subsequent ring-closing reaction via intramolecular olefin metathesis produced the target [2]catenane **C1** in 24% yield.

Based on the aforementioned synthetic strategy for pillar[*n*]arene-based rotaxanes and catenanes, topologically complicated structures could be obtained. Wen and coworkers reported a [2]rota[2]catenane, obtained by fusing a pillar[5]arene-based [2]rotaxane and a crown ether-tetracationic cyclophane [CBPQT]$^{4+}$-based [2]catenane (Scheme 8b).[87] The synthesis started from bicyclic host **P11**, which consisted of a pillar[5]arene and naphthalene-containing crown ether. Two axles, **A20** and **A21**, complexed with the pillar[5]arene cavities and crown ether through cation/π interactions, respectively. The ends of **A20** were capped by stopper **15**, and the ends of **A21** were connected by spacer **16**, forming [2]rota[2]catenane **RC1**. Interestingly, the order of the capping reaction to form the rotaxane subunit and ring-closing reaction to form the catenane subunit was important for efficient target molecule formation, with construction of the rotaxane subunit prior to the catenane subunit being optimal.

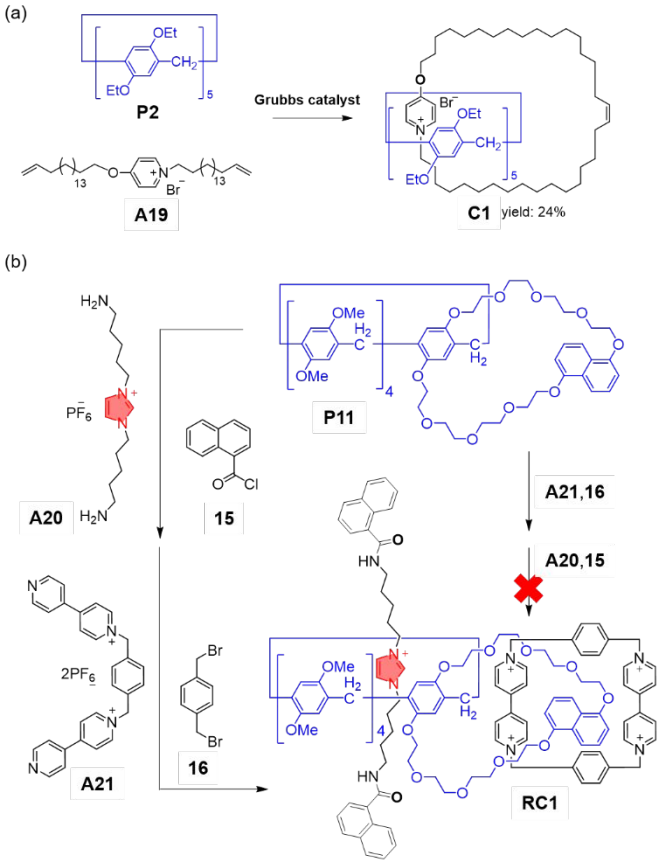


**Scheme 8** (a) Synthesis of (a) [2]catenane **C1** and (b) [2]rota[2]catenane **RC1**.

### Shuttling dynamics of pillar[*n*]arene rings in rotaxanes

The movement of components in MIMs is typically a thermally activated process that occurs spontaneously under experimental conditions, with the rate determined by the activation energies of barrier crossings. Degenerate molecular shuttles are suitable for kinetic studies using dynamic NMR spectroscopy. In such systems, two chemically equivalent binding sites exist on the axle, and the wheel moves back and forth between them. When the exchange frequency is low, compared to the differences in resonance frequencies, the NMR spectrum shows separate signals resulting from the part of the axle bound to the wheel and the part not bound. At the fast exchange limit, a single set of signals is found, and intermediate regime line shape analysis allows for accurate determination of the exchange rates. Furthermore, owing to the potentially wide range of temperatures that can be used, accurate activation parameters $\Delta G^{\ddagger}$, $\Delta H^{\ddagger}$, and $\Delta S^{\ddagger}$ can be determined.

Using this methodology, our groups showed that the observed rates of shuttling in a series of pillar[5]arene rotaxanes (**R16$^4$–*n*** (*n* = 4,8,12,16) in Fig. 7a) were independent of the distance between the binding stations.[43] This could be explained by considering the energy landscape, namely, for the wheel to move from one station to the other, it must unbind from the initial station (local minima $M_1$ and $M_{1'}$ in Fig. 7b), which requires a certain activation energy, and then finds itself weakly bound to the axle. Simulations indicate that shallow local minima ($M_2$, $M_{2'}$) exist for the wheel on the centre axle. To reach the other stable station, a barrier crossing is required ($TS_{12}$ or $TS_{1'2'}$). This barrier is much higher than the barriers for movement of the wheel along the centre of the axle ($TS_{22'}$). As a result, the wheel can move back and forth along the central connector several times, caught between two barriers, before finally reaching one of the stable sites again. In this situation, the movement along the middle thread is not rate-limiting for the overall process, and the distance between the stations does not affect the rate. At the same time, the fraction of the molecules in which the wheel resides on the axle between the stations is small enough to escape detection, such that shuttling looks like a one-step process.

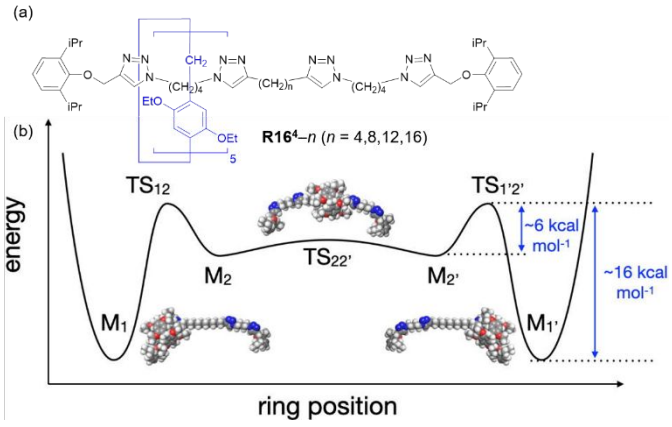


**Fig. 7** (a) Structure of rotaxanes **R16$^4$–*n*** (*n* = 4, 8, 12, 16). (b) Energy profile for shuttling; $M_1$ and $M_{1'}$ are the stable structures, $M_2$ and $M_{2'}$ are local minima in which the wheel is on the axle. Reproduced with permission from ref. 43. Copyright 2018 Wiley-VCH Verlag GmbH & Co. KGaA.

The dynamics of rotaxane molecular shuttles can be changed under the influence of external stimuli. We can distinguish

between changing the preferred structure or changing the rate at which the wheel shuttles along the axle. In the former case,

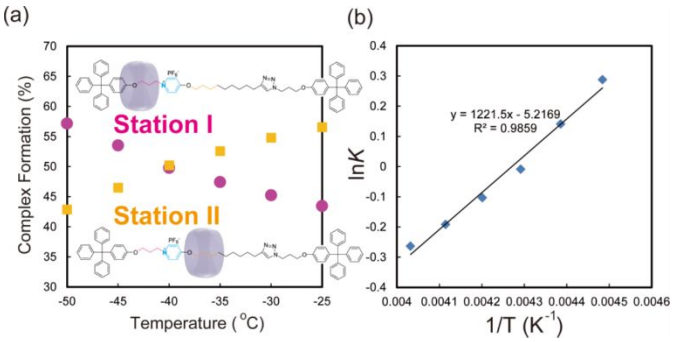


**Fig. 8** (a) Temperature-dependent binding of perethoxy-substituted pillar[6]arene wheel to the two different stations in rotaxane **R17**, and (b) van't Hoff plot for binding to station I, giving thermodynamic parameters $\Delta H$ = –10.2 ± 0.6 kJ mol$^{-1}$ and $\Delta S$ = –43.4 ± 0.3 J mol$^{-1}$ K$^{-1}$. Reproduced with permission from ref. 88. Copyright 2012 Royal Society of Chemistry.

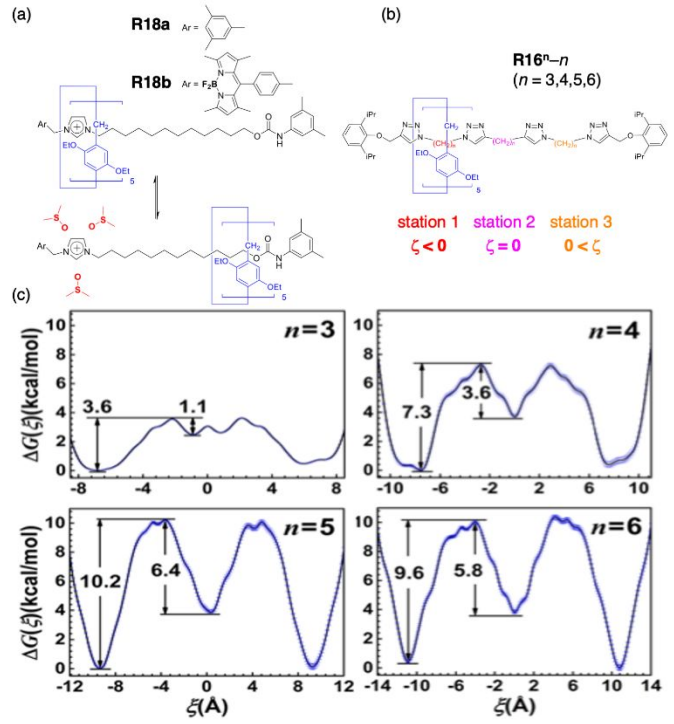


**Fig. 9** (a) Working principle of solvent-controlled pillar[5]arene molecular shuttles. Strongly coordinating DMSO displaces wheel from imidazolium station. (b) Chemical structures of four-triazole pillar[5]arene rotaxanes **R16$^{n}$**–*n* and (c) their energy profiles simulated by Wang et al. Reproduced with permission from ref. 94. Copyright 2017 American Chemical Society.

chemical modification of a binding station, such as protonation/deprotonation, reduction/oxidation, or photoisomerization, can be conducted. While such methods have been abundantly applied to other types of rotaxanes,[2] no such applications to pillar[*n*]arenes were found in the literature. Changes in the external conditions (solvent, temperature) can also influence the equilibrium between different conformational states. Our groups showed that temperature changes alone can change the preferred structure of a pillar[6]arene rotaxane **R17** owing to differences in the entropy of conformations (Fig. 8).[88] At low temperature, "tight" binding site I is preferred (–50 °C, $\Delta G$ = –0.48 kJ mol$^{-1}$), while at high temperatures, more flexible site II is favoured (60 °C, $\Delta G$ = 0.60 kJ mol$^{-1}$).

Similar temperature effects were later reported for pillar[5]arene rotaxanes (**R18** in Fig. 9a).[89,90] In the latter cases, a change of solvent was also shown to change the preferred conformation. This solvent switch is based on competition between the interactions of the imidazolium unit in the axle with the pillar[5]arene wheel and with the polar solvent DMSO. In $CDCl_3$, the wheel is located near the cationic unit, but when DMSO is added, the wheel is displaced because the solvent interacts more strongly with the charged group. The same effect, with a urea unit instead of an imidazolium unit, had already been used in 2012 to compress and elongate a "molecular spring".[91]

Similarly, Li et al. used acetate ions as competitive binders to break the bonds between thiourea units and pillar[5]arene wheels, which moved the wheels closer to fluorescent units (see below, Fig. 14).[92]

The solvent effect was studied by Liu et al. using free energy calculations.[93] They concluded that hydrogen-bond-accepting solvents interacted strongly with the imidazolium unit and displaced the wheel towards the carbamate stopper, while non-basic solvents chloroform, dichloromethane, and benzene interacted more strongly with the hydrocarbon part of the axle, and did not compete with the hydrogen-bond-accepting wheel to bind imidazolium.

The same group also modelled pillar[5]arene rotaxanes with four neutral triazole linkers (**R16$^{n}$**–*n* (*n* = 3,4,5,6) in Fig. 9b).[94] At each energy minimum, the wheel interacted with two triazoles. At axle centre, the C-termini of the two triazoles were linked by an oligo-methylene chain. This formed a less stable binding arrangement than the other two sites, where the N-termini of two triazoles were closer to the wheel. The activation energies were predicted to increase in the order (*n* = 3) < (*n* = 4) < (*n* = 5) ≈ (*n* = 6). This result was in marked contrast to that obtained with the four-triazole rotaxanes studied by our groups, where a spacer-length-independent rate was found (Fig. 7).[43] As an

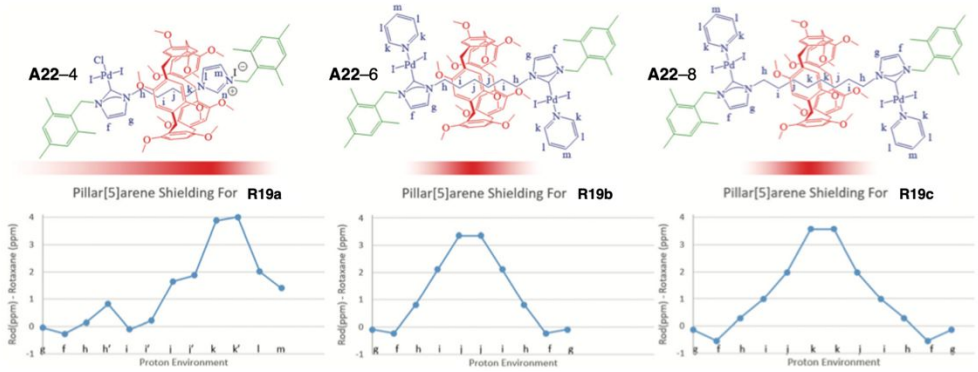


**Fig. 10** Control of the wheel position on the axle by complexation of *N*-heterocyclic carbenes in the axle. Top: Structures of rotaxanes **R19**; bottom: Calculated magnetic shielding of $^1$H. Reproduced with permission from ref. 95. Copyright 2019 Royal Society of Chemistry.

important difference between the two systems, in the computational study, the structures of all stations changed with n, while the stable station in our rotaxanes always had four $CH_2$ groups, with only the central linker varying.

A different method for modifying the wheel position through complexation was explored by Champness and coworkers. The authors used the complexation of bulky ions to imidazole-derived *N*-heterocyclic carbenes in the axle to restrict the space available for the wheel to certain parts of the axle (**A22**–*n* (*n* = 4,6,8) in Fig. 10). The location of the pillar[5]arene ring was derived from shielding of the axle protons in $^1$H NMR.[95]

In addition to controlling the preferred position of the axle on the wheel in pillar[*n*]arene rotaxanes, another goal is controlling the movement of the wheel along the axle, preferably in a reversible manner. This has been achieved using photoisomerization reactions. As discussed above, we determined the rate of threading/dethreading for axles capped with *E*- and *Z*- azobenzene groups (Fig. 5b).[70] Slipping the macrocycle over the *E*-isomer proceeded four orders of magnitude faster than slipping over the *Z*-isomer. Yu et al. showed that the binding mode of azobenzene in a pillar[6]arene pseudorotaxane **A23@P12** was different for the *E*- and *Z*-isomers, as the *E*-isomer fits inside the cavity, while the *Z*-isomer does not (Fig. 11).[44] This difference was expressed by the physical properties of the isomeric complexes, which had quite different aggregation behaviour.

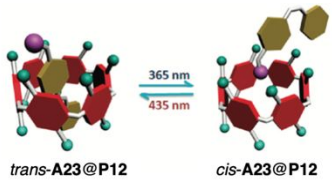


**Fig. 11** Different binding modes of *E*- and *Z*-azobenzene in the pillar[6]arene cavity. Purple sphere represents an $NMe_3^+$ group; green balls represent *n*-propyl groups. Reproduced with permission from ref. 44. Copyright 2012 American Chemical Society.

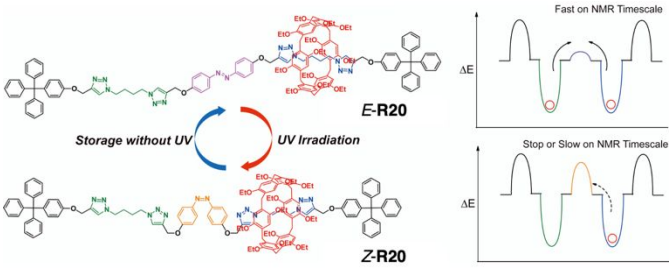


**Fig. 12** Photoregulated molecular shuttle. Reproduced with permission from ref. 96. Copyright 2020 Royal Society of Chemistry.

As *E*-azobenzene fits in the cavity of pillar[6]arene, but *Z*-azobenzene does not, our group designed photoregulated molecular shuttle **R20**, as shown in Fig. 12.[44,96] In this system, the azobenzene unit links two equivalent binding stations, consisting of two imidazoles linked by a C4 chain. In the *E*-configuration, the wheel can pass and the $^1$H NMR spectrum shows fast exchange at room temperature. However, when the azobenzene is switched to the *Z*-form, shuttling is inhibited. The same binding motif of two triazoles linked by a C4 chain at their nitrogen atoms was used as in the shuttles with different central axle parts **R16$^n$** described above, but binding of the pillar[5]arene to this station in **R16$^n$** was considerably stronger than that of the pillar[6]arene used in **R20**. As a result, the rate of degenerate shuttling at room temperature was ~400 times faster in **R20** than in **R16$^n$**.

**MIM-based functional systems**

Rotaxane architectures allow functional units to be brought together in a flexible manner, with control over the distance between them. Interactions between functional units and with external agents can often be probed using fluorescence spectroscopy. Förster resonance energy transfer (FRET) was studied in a pillar[5]rotaxane with pyrenes attached to the wheel and perylene as a stopper.[97] Later, FRET was used to read out the state of a photoswitching unit in a pillar[5]arene pseudo[3]rotaxane.[98] Pillar[5]arenes were synthesized with a

fullerene attached to the wheel and porphyrin[99] or BODIPY[100] chromophores, and FRET was deemed responsible for fluorescence quenching of the chromophore in both cases.

Compared with simpler axle-only molecules, pillar[*n*]arene rotaxanes can have different self-assembly properties. Unexpected supramolecular gel formation was observed by Dong et al. for rotaxane **R18a**, as shown in Fig. 9a. The self-assembly behaviour of this system was attributed to its amphiphilic character, with the charged imidazolium ion and hydrophobic alkyl chain. It was also shown to be dependent on the bromide counterion, with the gel collapsing upon bromide removal by capture with $CF_3CO_2Ag$, but being restored by subsequent bromide addition. Structurally similar compound **R18b**, containing a BODIPY fluorophore (Fig. 9a), showed similar self-assembly behavior.[101] Sun et al. showed that this behaviour was also temperature sensitive, with a transition from gel to solution in DMSO at 338 K, and that the BODIPY fluorescence was modulated by acid and base.

The Nierengarten group reported several examples of functional pillar[*n*]arene rotaxanes organized into higher-level structures, such as Langmuir–Blodgett films, in which self-assembly was subtly dependent on the molecular structure,[102] and electroactive monolayers on gold.[103] In another study, the same group explored the possibility of multivalent interactions in biological target recognition, provided by the two ends of the axle and the ten substituents on the wheel of a pillar[5]arene.[104]

Utilizing the self-assembly tendency of pillar[*n*]arene rotaxanes, Yu et al. designed organic nanoparticles for theranostic applications, consisting of multifunctional pillar[5]arene rotaxanes **R21** (Fig. 13).[105] The axle stoppers were a triphenylphosphonium ion for mitochondria recognition, and tetraphenylethylene (TPE) as a fluorescent label that only operates in the aggregated state (aggregation-induced emission, AIE), while the pillar[5]arene macrocycle contained two doxorubicin (DOX) units. The luminescence of the nanoparticles was quenched by FRET from TPE to DOX, while DOX did not fluoresce due to being nonfluorescent when aggregated (aggregation-caused quenching, ACQ). When the rotaxane interacted with mitochondria, and the DOX units were released after hydrolysis, TPE emission was turned on, but DOX also became fluorescent due to no longer being aggregated. This work constitutes a proof-of-principle, because this combination of target selectivity, imaging, and drug delivery can be extended to other drugs.

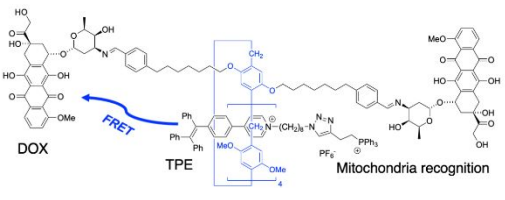


**Fig. 13** Multifunctional theranostic rotaxane **R21**.

By combining AIE with the planar chirality of the pillar[5]arene wheel, Li et al. demonstrated circular polarized luminescence in the aggregated state of rotaxane **R22** (Fig. 14).[106,107] The degree of polarization could be switched between a lower level, when the wheel was relatively far from the AIE chromophore, and a higher level, when it was brought closer to the chromophore. This switching was induced by competitive binding of acetate ions to the thiourea units of axle **A24**.

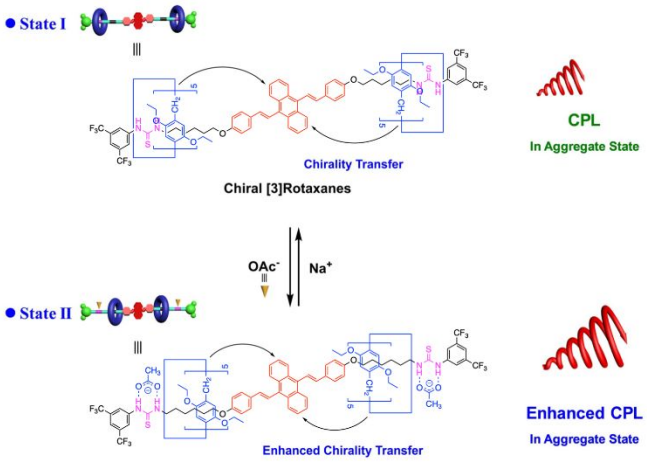


**Fig. 14** Enhancement of circular polarized luminescence in [3]rotaxane **R22** in aggregated state when the pillar[5]arene wheels are brought closer to the chromophore after displacement from the preferred thiourea binding sites of **A24**. Reproduced with permission from ref. 107. Copyright 2021 Wiley-VCH Verlag GmbH & Co. KGaA.

Pillar[5]arene rotaxanes have also been used as fluorescent sensors. Li et al. demonstrated the detection of fluoride ions through cleavage and dissociation of rotaxane **R23**, in which a fluorophore, forming part of the wheel, was released from the quenching group in the axle, which turned on fluorescence (Fig. 15).[108]

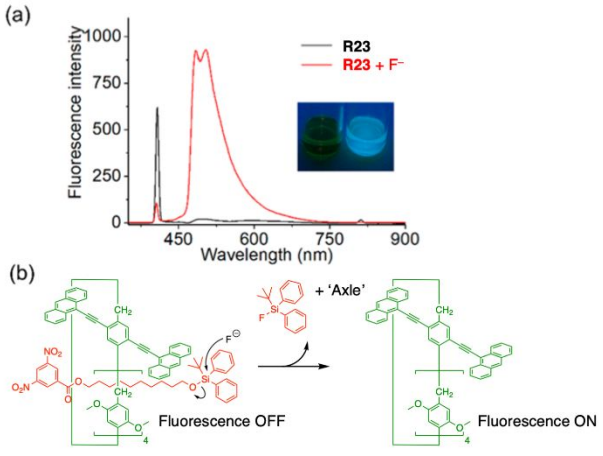


**Fig. 15** Fluoride detection through disassembly of rotaxane **R23**, allowing fluorescence turn-on by disrupting the fluorescence quenching pathway. Reproduced with permission from ref. 108. Copyright 2020 American Chemical Society.

Chong et al. showed that nitrobenzene explosives can be detected using a pillar[5]arene-based supramolecular

assembly.[109] The authors constructed a poly(pseudorotaxane) organo-gel through complexation of $Zn^{2+}$ with terpyridine attached to pillar[5]arene **P13** and axle **A25** containing triazole groups. The fluorescence of the organo-gel was quenched when picric acid (**17**) was added. Although the two fluorescent sensor applications described here elegantly explore the supramolecular properties of pillar[5]arene pseudorotaxanes, their practical application remains to be reported. Other examples of fluorescent pillar[*n*]arene rotaxanes are discussed below, in the context of polyrotaxanes.

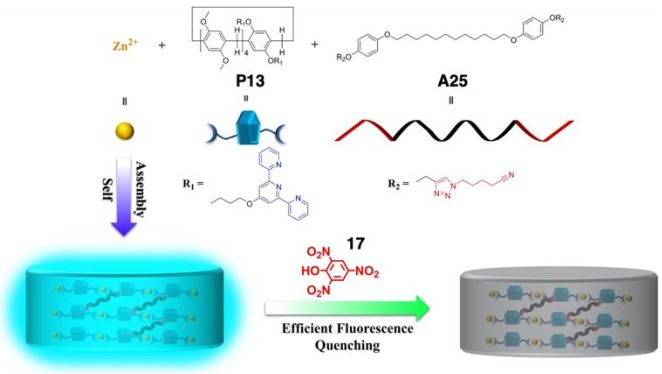


**Fig. 16** Schematic illustration of supramolecular organo-gel for picric acid sensing. Reproduced with permission from ref. 109. Copyright 2021 Wiley-VCH Verlag GmbH & Co. KGaA.

## Single-component mechanically self-complexed molecules and related compounds

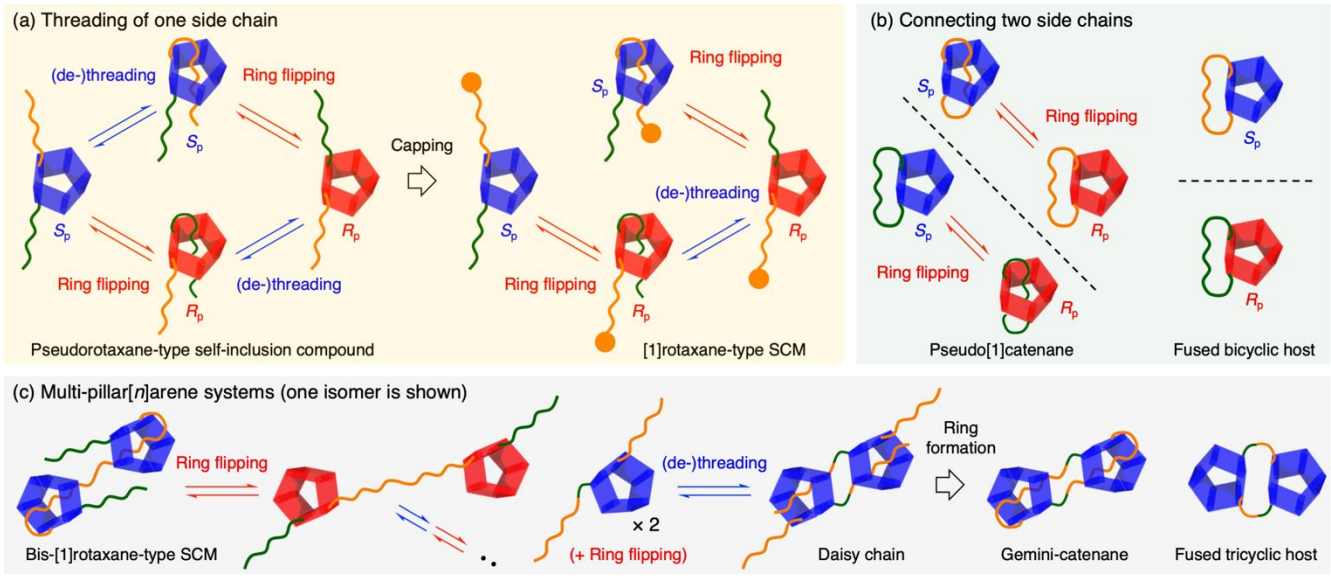


**Fig. 17** Structures of single-component self-complexed molecules and related compounds. Compounds with (a) one threaded side chain, (b) connected two side chains at the same unit, and (c) two pillar[*n*]arene cores. Molecular conformations and their interconversion are restricted by the topology and bulkiness.

Pillar[*n*]arenes are readily functionalized at the rims by both mixed condensation of different panel units and late-stage modification, including partial deprotection of alkyl groups, etherification of phenolic OHs, coupling reactions with triflate, and other reactions on the side chains.[31] As-incorporated functionalized side chains can thread into the cavities of pillar[*n*]arenes, providing self-inclusion compounds. Such species can also be produced by connecting side chains of pillar[*n*]arene hosts and threading guest molecules with covalent bonds.

Fig. 17 shows single-component self-complexed molecules (SCMs) and related compounds. When one of the pillar[*n*]arene side chains is simply threaded, a pseudorotaxane-type self-inclusion compound is obtained (Fig. 17a). A bulky stopper can be attached to the side chain, giving a [1]rotaxane-type SCM. Before capping, the side chain is in a threading/de-threading equilibrium between complexed and free states. On the other hand, the free state was only accessible through a flip motion of the pillar[*n*]arene ring after capping. This flip motion makes the discrimination of [1]rotaxane/catenane and pseudo[1]rotaxane/catenane inappropriate for most pillar[5]arene-based systems because they might dethread regardless of bulky stoppers. For several systems, such behaviour has not been surveyed or described in detail. Therefore, most compounds in this chapter are designated as "rotaxane/catenane-type" SCMs, except for a few molecules that match the conventional designation well. When two side chains at the same unit of a pillar[*n*]arene are linked to each

other, a [1]catenane-type SCM is obtained (Fig. 17b). The pseudo[1]catenane inverts its chirality between self-included and expelled states via flip motion. Some pillar[*n*]arenes form linkages outside the macrocycles and do not take up self-inclusion states. In such cases, the products behave as fused bicyclic hosts with the chirality fixed as synthesized. Single-component mechanically self-locked molecules and related compounds have also been constructed from two or more pillar[*n*]arene components, yielding bis-[1]rotaxane-type SCMs, daisy chains, gemini-catenanes, and fused tricyclic hosts, among other compounds.

**Rotaxane and related compound based on a functionalized pillar[*n*]arene**

**Rotaxane and related compounds: Self-inclusion and capping.** The functionalized side chain of a pillar[*n*]arene sometimes threads into its own cavity to provide a single-component pseudorotaxane. Such a self-inclusion compound was first reported by our group in 2011 (**P14** in Fig. 18a),[46] although molecules in equilibrium with a supramolecular assembly were identified by Huang and coworkers earlier (vide infra).[38] We prepared a monohydroxy pillar[5]arene by partial demethylation and attached an ammonium cation with a C8 alkyl linker ($K_a$ = 8×10$^2$ M$^{-1}$ in $CDCl_3$ for a model system). The functional side chain was included in the cavity in $CDCl_3$, but expelled from it in acetone-$d_6$, as shown by NMR studies. The spectral changes were concentration-independent, clearly indicating single-molecule behaviour, not an intermolecular process. Similar self-inclusion molecules were synthesized by Cao, Meier, and coworkers using 6-bromohexoxy[110] and ester-containing side chains **P15–17**.[111] Although acetate-type compound **P16** showed self-inclusion characteristics, butylate-type counterpart **P17** did not. The single-crystal structure of **P16a** showed a flat and nonflexible ester unit exhibiting C–H/O interactions with methoxy groups, indicating the importance of the ester group location. The side chain competed against external guests. 1,4-Dihydroxybutane (**18**) did not form a complex with **P16b** owing to the self-complexed state being more stable, while 1,4-diiodobutane (**19**) afforded a host–guest complex with the side chain expelled (Fig. 18b). These results demonstrated that self-inclusion molecules were useful for guest molecule discrimination. This selectivity was tuned by changing the competing side chain[111] or the eight substituents on the rims of pillar[5]arenes (**P18**).[112]

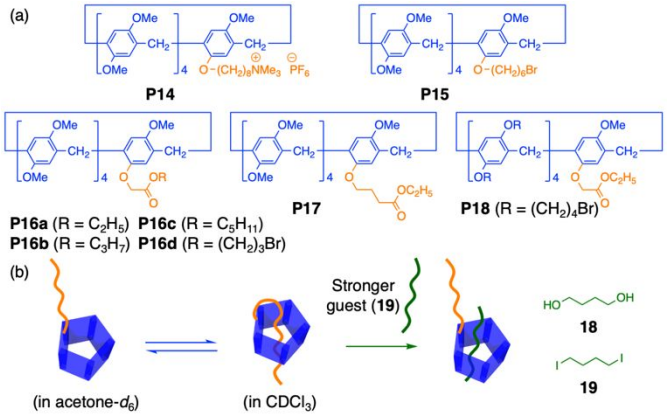


**Fig. 18** (a) Chemical structures of self-inclusion compounds with alkyl and ester side chains and (b) their solvent- and guest-dependent conformations.

The appended ester groups can be transformed into amides, enabling functionalization of the threading side chains. In 2014, Xue and coworkers condensed monocarboxylic acid-appended pillar[5]arene **P19a** and alkylamine **20** bearing a stopper to yield the first [1]rotaxane-type SCM based on pillar[5]arene (**P20** in Scheme 9).[113] Owing to the ionic interaction between ammonium and carboxylate ions ($K_a$ = 1.5×10$^4$ M$^{-1}$ in $CDCl_3$ for a model system), the preformed pseudo[2]rotaxane was well organized and led to the product in high yield. In addition to the precapping strategy, sequential formation of [1]rotaxane-type SCMs has been widely employed using alkylene diamines as threading linker units. Terminal amines were capped through condensation with aryl aldehydes (**P22–23**)[114,115] and carboxylic acids (**P24–25**),[116,117] $S_N2$ reaction with an alkyl bromide (**P26**),[118] reacting with isothiocyanates (**P27**),[119] and their combination (**P28**).[120] When the linker units in condensation-based capping schemes were shorter than propylene diamine,[114–116] the side chains did not complex with pillar[5]arene cores, but existed in free states. When the threading units had sufficient length, many types of [1]rotaxane-type SCM were obtained, as confirmed by NMR spectroscopy and X-ray crystallography. Most of these [1]rotaxane-type SCMs were highly stable, not only in $CDCl_3$, but also in polar DMSO-$d_6$, indicating that the amide-containing loop segments were relatively rigid owing to multiple noncovalent interactions and prevented ring flipping.

In 2015, a photo-induced thiol–ene reaction was also used in the capping step to prepare [1]rotaxane-type SCM **P30** with an imidazolium-containing side chain ($K_a$ = 1.0×10$^4$ M$^{-1}$ in $CDCl_3$ for a model system).[121]

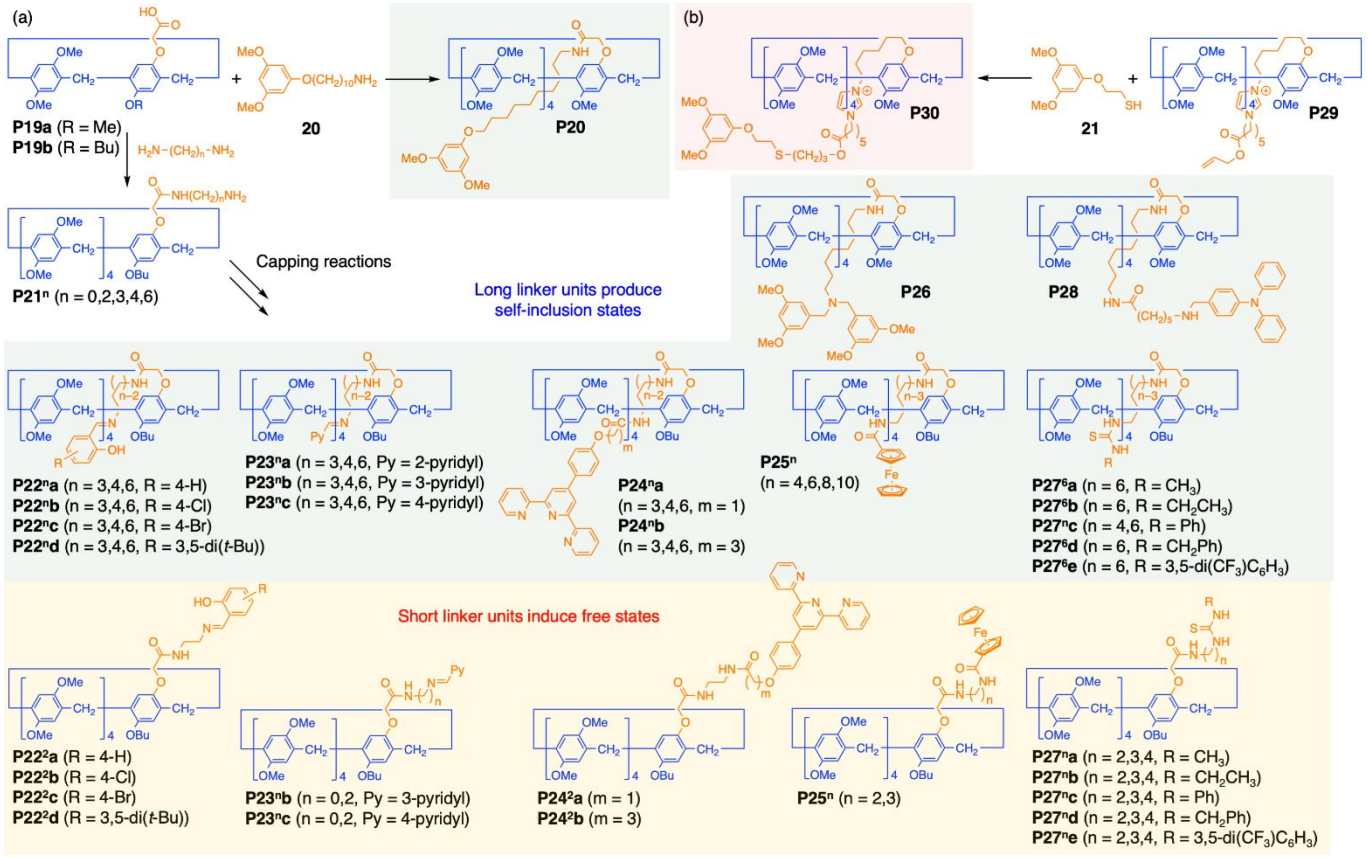


**Scheme 9** Chemical structures of self-inclusion and related compounds with (a) amide- and (b) imidazolium-containing side chains.

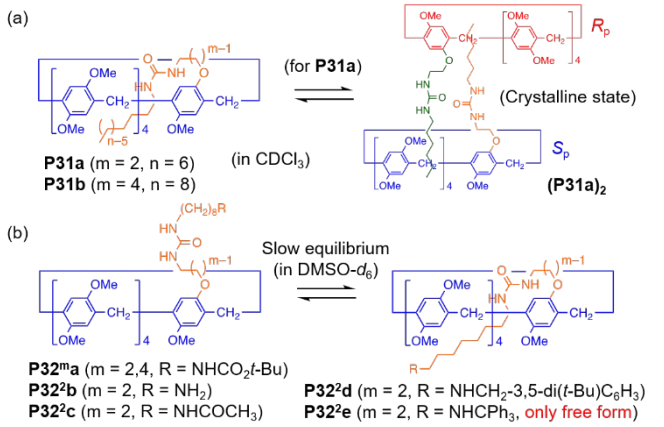


**Scheme 10** Chemical structures of urea-functionalized self-inclusion compounds and their interconversion (a) with a [*c*2]daisy chain and (b) with free side-chain states.

**Rotaxane and related compounds: Dynamic structure and functionalization.** The side chains of self-inclusion pillar[5]arenes have been endowed with various functions other than guest characteristics. In 2014, Hu and coworkers reported a series of urea-functionalized pillar[5]arenes **P31**,**32** (Scheme 10).[122,123] The ureido groups did not show a typical anion-binding nature nor form an α-tape motif. In 0.5–100 mM solutions in $CDCl_3$, **P31** was monomeric and included the side chains in its own cavities, while **P31a** gave a dimeric [*c*2]daisy chain with an $S_p$–$R_p$ configuration in the crystalline state. The self-inclusion state was quite stable and not even completely lost in a 1:1 mixture of $CDCl_3$ and DMSO-$d_6$. When the side-chain terminals were replaced with a medium-sized Boc-protected amine, a slow equilibrium between a free state, loosely included state, and deeply threaded state was realized in DMSO-$d_6$ (**P32**). The rate of self-inclusion dynamics was dependent on the size of the side-chain ends. The threaded form was destabilized by increasing the distance between the ring and urea units (**P32⁴a**). The authors also tested the synthesis of bulky $CPh_3$-terminated compound **P32²e** and obtained it in the free state. Therefore, in these molecules, the side-chain reaction is thought to be followed by threading, instead of a reverse-order process and the involvement of ring-flipping.

The CuAAC reaction is among the most versatile methods for introducing functional moieties into pillar[*n*]arene side chains. When biotin was attached to self-inclusion systems (**P34** in Fig. 19), the bioactivity could be switched on along with the de-threading process caused by the strongly polar environment and competitive guest.[124] Simple ethylene glycol chains also responded to the addition of $NaBF_4$ in DMSO-$d_6$ (**P35**).[125] $^1$H NMR peak shifts indicated tightly included structures, in which a sodium ion was thought to be located inside the loop moieties. A pyridine ring was attached to a self-inclusion system as the

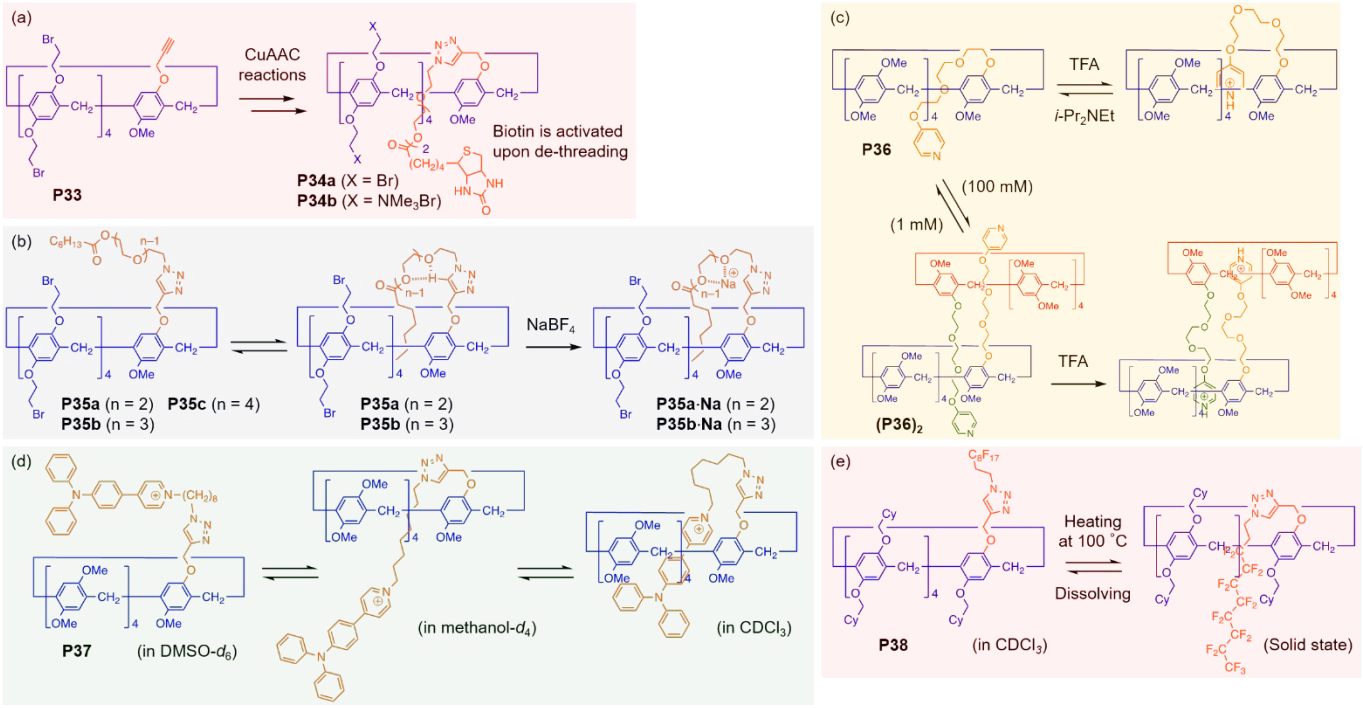


**Fig. 19** Chemical structures of stimuli-responsive self-inclusion compounds with (a) biotin, (b) cation-binding ethylene oxide, (c) pyridine, (d) pyridinium, and (e) fluoroalkyl segments.

ethylene glycol chain terminal using an $S_N2$ reaction on the rim (**P36**).[126] In $CDCl_3$, the ethylene glycol segment was located inside the cavity, while adding acid resulted in protonation of the pyridine unit and inclusion of the pyridinium terminal. Such shuttling was controlled by adding trifluoroacetic acid (TFA) and *N*,*N*-diisopropylethylamine. Click chemistry afforded a pyridinium-containing [1]rotaxane-type SCM **P37** with a side chain contained an alkyl linker and triphenylamine stopper.[127] As the affinity between the pyridinium ion and solvents increased, **P37** changed from a pyridinium-capturing state (in $CDCl_3$) to an alkyl-inclusion state (in methanol-$d_4$), and then a dethreaded free state (in DMSO-$d_6$). A fluoroalkyl chain was also incorporated into a pillar[5]arene with bulky cyclohexylmethoxy substituents via CuAAC reaction (**P38**).[128] In the presence of small solvent molecules, such as $CDCl_3$, the dethreaded form was solely observed. Heating at 100 °C for approx. 20 h in the solid state converted 85% of molecules to a self-inclusion state. This was reversed in $CDCl_3$ at 25 °C with a half-life of 2.89 h.

**Light- and redox-responsive compounds.** [1]Rotaxane-type SCMs can be responsive to light irradiation and changes in redox potentials. When a rigid stilbene unit was incorporated into a side chain along with two alkyl domains and a bulky stopper (**P39** in Fig. 20),[129] the stilbene unit caused *E*/*Z*-photoisomerization upon irradiation with 360 and 387 nm light, providing *Z*-rich and *E*-rich states, respectively. The *Z*-isomer preferred self-inclusion in the alkyl region next to stilbene, while the *E*-isomer underwent self-complexation in the region next to stopper, which realized nanometre-scale translational motion. To our knowledge, this is the only photocontrolled molecular shuttle reported in the field of pillar[*n*]arene rotaxanes to date. Several systems have been described that contain photoswitchable azobenzenes, but photoswitching only controls the dynamics of these systems, not the supramolecular geometry. In another monofunctionalized system, redox-responsive disulfide bond was introduced into a linker segment with a long ethylene glycol tail (**P40**).[130] The alkylated pillar[5]arene core was hydrophobic, such that the molecule behaved as an amphiphilic compound to form spherical supramolecular vesicles in aqueous media. Upon exposure to a high concentration of glutathione (GSH), disulfide bonds were cleaved and exchanged, causing the vesicles to collapse. This behaviour was exploited for encapsulation and release of anticancer drug DOX as a GSH-responsive drug delivery system. In this system, a vulnerable disulfide bond was sterically protected inside the pillar[5]arene cavity to increase the vesicle stability.

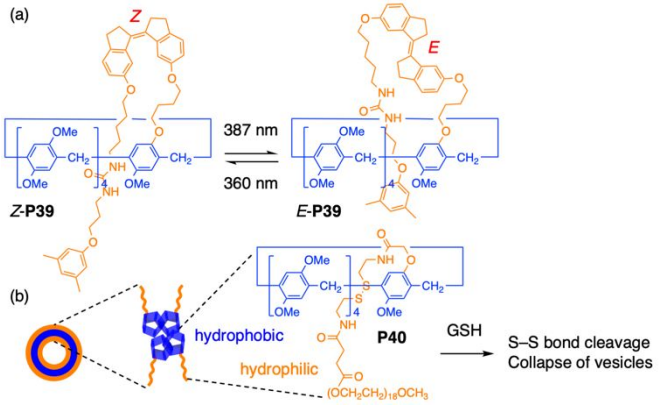

**Fig. 20** (a) Chemical structure of a photoswitching [1]rotaxane-type self-complexed molecule and (b) illustration of a supramolecular vesicle of a disulfide-containing self-inclusion compound. GSH = glutathione.

## Catenane and related compound based on functionalized pillar[*n*]arene

**Catenane-type molecules and their chirality switching.** Pillar[*n*]arenes with two functional groups at the same unit are readily accessible via condensation using two types of monomers[131] and the partial oxidation of peralkoxy-substituted pillar[*n*]arenes.[48,49] Two functionalized sites can be covalently connected with the linker segment included inside the pillar[*n*]arene cavity. The resulting pseudo[1]catenane exists as a pair of enantiomers, each of which undergoes chirality inversion through ring flipping (Fig. 17). Therefore, pseudo[1]catenanes are an ideal platform for chirality switching and have attracted intensive research. This advantage was first exploited by our group in 2013 (Fig. 21)[132] by applying CuAAC reactions to a dipropargyloxy-substituted pillar[5]arene and 1,12-diazidododecane, which afforded pseudo[1]catenane **P41a** in 17% yield. In noncomplexing $CDCl_3$, pseudo[1]catenane **P41a** existed mainly in a self-inclusion state, but changed into an expelled state upon adding 1,4-dicyanobutane **22** or alkylammonium ion **23**, as stronger guests for the pillar[5]arene cavity. In the case of optically resolved fractions, the conformational change was observed through the inversion of circular dichroism (CD) signals. The reversed signals were recovered by adding 24-crown-8, which extracted **23** from the complex with the pillar[5]arene unit. Pseudo[1]catenanes **P42**–**44** were also prepared via amide formation from acid and amine units,[133] adding isocyanate to the amine ends,[134] and the $S_NAr$ reaction of chloropyrazine moieties with phenolic OHs.[135] The conformation of **P42$^8$** was very stable, while those of **P43**,**44** were dynamic. Pseudo[1]catenanes **P44** were in a self-inclusion state in bulky solvent $CDCl_3$, but in equilibrium with an expelled state in guest solvent $CD_2Cl_2$. Furthermore, the self-inclusion conformer was not fully inverted into an expelled state when the alkyl linker was shortest (**P44$^4$**), underlining the importance of linker structures. Water-soluble pseudo[1]catenane **P41b** was also produced by attaching tri(ethylene oxide) chains to remaining sites on the pillar[5]arene rims.[136] Chirality inversion that was responsive to metal ions was achieved using a thia-crown-type linker, which provided soft metal-binding sites.[137] Pseudo[1]catenane **P45** favoured a self-inclusion state in $CDCl_3$, but its CD signal was reversed upon adding $Hg(ClO_4)_2$. The signal was reversed again by subsequent addition of tetrabutylammonium iodide. These responses were explained by *endo*-coordination of a $Hg^{2+}$ ion in an expelled state and *exo*-coordination of a $HgI_2$ in a self-inclusion state, respectively, as demonstrated by single-crystal X-ray analysis. The latter state was also accessible from the initial state by direct addition of $HgI_2$, while the initial state could be recovered from the former state by removing $Hg^{II}$ species via $Na_2S$-induced precipitation of HgS. When aza-crown-type linkers were introduced into pseudo[1]catenanes, acid/base-responsive systems **P46** were produced.[138] Pseudo[1]catenanes **P46** showed self-inclusion states in THF-$d_8$ and $CHCl_3$/EtOH (1:1). The conformation and accompanying CD signal of **P46b** could be switched repeatedly by sequential addition of HCl (aq) and NaOH (aq).

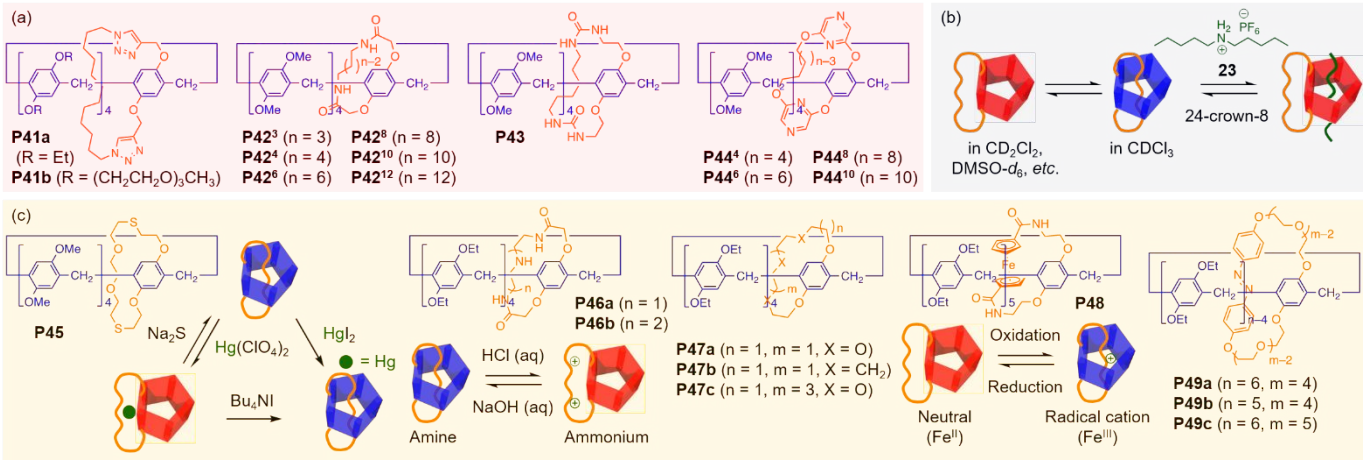


**Fig. 21** (a) Chemical structures of pseudo[1]catenanes and (b) their typical ring flipping behaviour. (c) Chemical structures of pseudo[1]catenanes with switching moieties.

Stimuli other than chemicals have also been examined for pseudo[1]catenane-based chirality switching by Yang and coworkers since 2017. The authors prepared alkyl chain- and ethylene glycol-linked molecules **P47**.[139] Owing to the delicate balance between two conformations, the equilibria were not only dependent on solvents, as observed for other molecules, but also highly dependent on temperature. For example, the CD signal of **P47a** was drastically inverted in nonpolar methylcyclohexane, from –0.012 at >10 °C to +0.019 at –90 °C on the dissymmetry factor (*g*) scale. This behaviour was quite different among various solvents and linker segments with different characters. For example, the longer ethylene glycol chain in **P47c** induced relatively large spectral changes in $CH_2Cl_2$ and MeCN, while the alkyl chain in **P47b** led to CD signal

inversion only in polar MeCN, in addition to the opposite temperature-dependent CD sign change. The authors also tested mixing two organic solvents to manipulate the inversion temperature.[140] Ring flipping was also evaluated in terms of enthalpic and entropic factors from the desolvation and self-inclusion processes versus exclusion and solvation processes of the linked side chains. Furthermore, the self-inclusion/exclusion equilibria were highly susceptible to hydrostatic pressure.[141] In polar MeCN, the CD signal of **P47b** changed from $g = -0.0016$ at 0.1 MPa to +0.0034 at 320 MPa. Redox-responsive system **P48** was developed by combining a ferrocene-containing linker and pillar[6]arene scaffold.[142] Similarly to pillar[5]arene pseudo[1]catenanes, **P48** exhibited a solvent- and temperature-dependent self-inclusion/exclusion equilibrium. Furthermore, **P48** exhibited a CD sign inversion through chemical oxidation with $Fe(ClO_4)_3$ and reduction with sodium ascorbate, and under applied potentials between +0.5 V and −0.5 V in MeCN. The incorporation of an azobenzene into the linker component was accomplished to produce photoswitchable chiroptical molecules **P49**.[143] *E*/*Z*-Photoisomerization of the azobenzene units was achieved by photoirradiation with 365 and 510 nm light, giving *cis*- and *trans*-enriched photostationary states (PSS), respectively. In contrast, thermal equilibrium in the dark yielded the stable *trans*-isomer exclusively. In addition to the responses to solvents and competitive guests, the conformations and CD signals of **P49** were repeatedly switched by photoirradiation. In *n*-hexane at 20 °C, *trans*-**P49a** favoured a self-inclusion form, which was converted into an expelled state by 365 nm light and recovered by 510 nm light because the bulky *cis*-azobenzene segment was a poor guest for the pillar[6]arene cavity. In contrast, pillar[5]arene **P49b** preferred an expelled state in the dark state and a PSS under 510 nm light, while the inverse CD signal was observed in a PSS under 365 nm light. The difference was probably due to the stretched *trans*-linker not being suitable for self-inclusion conformation and the flexible *cis*-linker allowing partial inclusion of the ethylene glycol segment. The long and flexible ethylene glycol chain afforded the same CD peak sign for all states of pillar[6]arene **P49c**, with only partial exclusion of the side chain in the *cis*-isomer. These results again exemplified the importance of molecular design. As increase of the temperature accelerated the thermal equilibrium favouring *trans*-isomers, heating led to a decrease in photoswitching efficiency to give the same sign of CD signal for the two PSSs above a critical temperature, which can be regarded as an over-temperature protection function.

**Nonthreaded fused bicyclic host.** Some linkages do not enter the pillar[*n*]arene cavities, but exist solely outside the macrocycles to give conformationally stable fused bicyclic hosts. Such a molecule was first reported by Ma, Li, Jiang, Wen, and coworkers in 2014. The authors used the $S_N2$ reaction of an A1,A2-dihydroxy pillar[5]arene and a ditosylate containing a bulky naphthalene segment to construct another macrocycle (Fig. 22).[144] The resulting bicyclic host, **P11**, showed independent guest binding, reflecting the characters of pillar[5]arene- and crown ether-like cavities. Linear-shaped neutral guest **22** was captured inside the pillar[5]arene subunit, while viologen **24**, a cationic aromatic-based guest, formed a complex with the crown ether moiety through a π-stacking-induced charge transfer (CT) interaction. When the guest for the

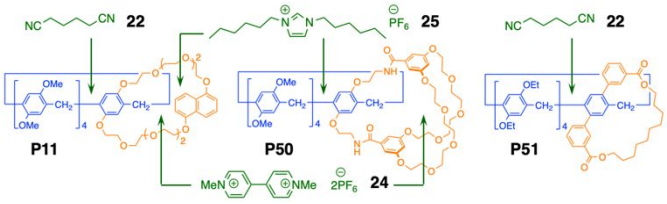


**Fig. 22** Chemical structures of fused bicyclic compounds and their site-selective guest binding.

pillar[5]arene subunit was replaced with cationic imidazolium ion **25**, the association constants for the second step forming the 1:1:1 complex clearly decreased (from 51 to 7.0 $M^{-1}$ for **25** and $7.7\times10^2$ to $1.1\times10^2$ $M^{-1}$ for **24** in acetone-$d_6$).[145] The negative cooperativity was rationalized by repulsive Coulombic interactions between positively charged guests. Bis-(*m*-phenylene)-32-crown-10 (BMP32C10) cryptand was also combined with pillar[5]arene unit (**P50**).[146] Selective and orthogonal guest binding was used in formation of the supramolecular polymer by complexing with ditopic guests. As another example, A1,A2-bis-(*m*-benzoic acid)-appended pillar[5]arene formed a bicyclic structure by linking its side chains with 1,10-decanediol (**P51**).[147] The alkyl chain was located outside the pillar[5]arene ring, probably owing to the rigid *m*-benzoate segment, allowing host–guest chemistry with **22** in the pillar[5]arene cavity.

### Multi-pillar[*n*]arene-based self-complexed molecules

**Multi-[1]rotaxane-type compounds.** When two pseudorotaxane-type self-inclusion compounds are connected at the ends of threading side chains, bis-[1]rotaxane-type SCMs are obtained, in which each pillar[*n*]arene acts as the stopper for the other. Bis-[1]rotaxane-type SCMs are also produced via double-threaded pseudo[3]rotaxanes by connecting a ditopic guest and two monofunctionalized pillar[*n*]arenes. Similar to the synthesis of [1]rotaxane-type SCMs, amide formation was used as a versatile and reliable method. In 2016, Yang, Jiang, and coworkers combined a long-chain diamine and two carboxylic acid-appended pillar[*n*]arenes in 23% yield (**P52**, Scheme 11).[134] The obtained structure was confirmed to be a bis-[1]rotaxane-type SCM by the large upfield shifts of alkyl chain signals in the $^1H$ NMR spectrum. Self-inclusion was disrupted by adding strong guest **22**. On the basis of similar methods, several [1]rotaxane-type SCMs were produced (**P54–60**,**P62**).[148–154] The alkyl chain length was again of great importance for the threaded structures. When the alkyl segments did not possess sufficient length (**P54**), only one of the two pillar[5]arenes adopted the self-inclusion form. One of

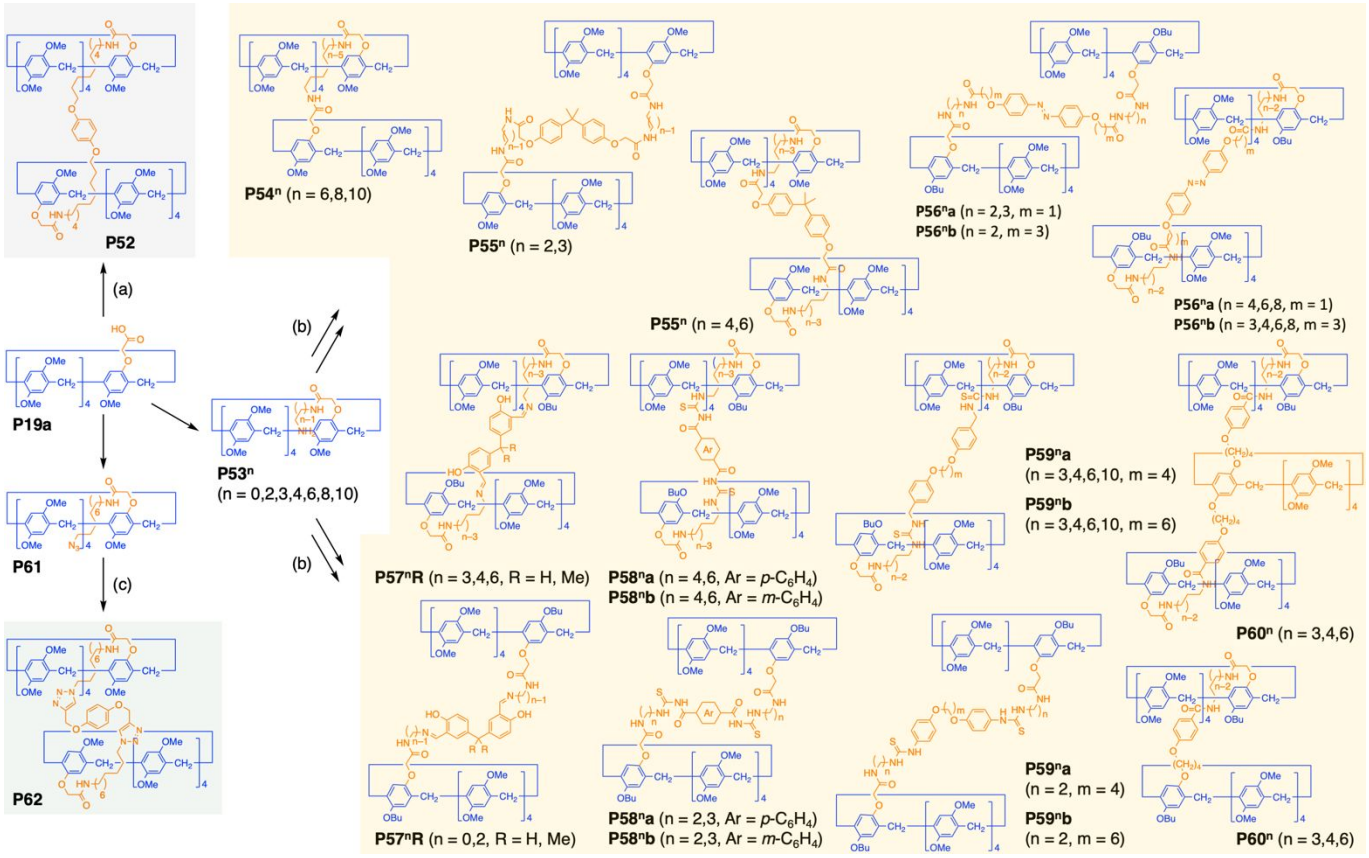


**Scheme 11** Chemical structures of bis-[1]rotaxane-type SCMs and related compounds prepared (a) directly from carboxylic acid, (b) via diamine-appended self-inclusion compounds, and (c) via an azido-appended self-inclusion compound.

these compounds was confirmed by single-crystal X-ray analysis (**P54**$^{6}$).[148] Various units have been introduced at the centre of the linker units to date, including azobenzene (**P56**),[149] the imine of salicylaldehyde (**P57**),[150] thiourea (**P58**,**59**),[151,152] imidazole (**P62**),[153] and another pillar[5]arene segment (**P60**).[154] Pillar[*n*]arene-based [1]rotaxane-type SCMs usually exist as a pair of enantiomers that interconvert via free states if they are accessible through dethreading or ring flipping. The racemization kinetics and other chiral aspects of [1]rotaxane-type SCMs have received little study, perhaps owing to the fast racemization. Bis-[1]rotaxane-type SCMs have diastereomers in addition to enantiomers but such stereochemistry has yet to be surveyed, probably because tuning the flexibility of loop segments and coupling two pillar[*n*]arene moieties with non-weak interactions remains difficult. We hope that such challenges will be overcome for the development of stimuli-responsive systems like pseudo[1]catenanes.

**Daisy chains and gemini-catenanes.** Pseudorotaxane-type self-inclusion occurs not only within intramolecular systems, but also intermolecularly to form dimeric and polymeric species, typically under concentrated conditions. In some cases, dimeric species are obtained with moderate or high selectivity. In 2011, Huang and coworkers reported ($S_p$,$R_p$)-dimeric assembly **(P63a)$_2$** and its crystal structure (Scheme 12).[155] In $CDCl_3$, the $^1$H NMR peaks corresponding to the four-methylene segment adjacent to the bromo end were in fast exchange on the NMR timescale, and showed marked shifts in the dilute concentration range of 0.25–8 mM. At higher concentrations (8–48 mM), the peak shifts were not large and diffusion coefficients based on DOSY measurement did not change much. These results were in sharp contrast with a nonbrominated compound that exhibited continuous signal changes owing to linear-type aggregation (vide infra).[38] The crystal structure of **(P63a)$_2$** contained van der Waals interactions between noncomplexing five-methylene segments, as well as multiple C–H/π and C–H/O interactions. The former was realized by complexation at the terminal part with an electron-withdrawing bromo group and was not observed in linear aggregates. A 6-hydroxyhexoxy side chain also enabled selective dimerization in solution and crystalline states (**P63b**),[156] while the bromo-counterpart formed a self-complexed species (**P15** in Fig. 18).[110] In **P63b**, dimer formation was supported by a very low specific viscosity and its linear correlation with concentration. Similar dimeric assemblies were observed for an benzyl-substituted molecule (**P63c**),[157] and some self-inclusion molecules described above in the crystalline state (**P31a** in Scheme 10)[122] and under concentrated conditions (**P36** in Fig. 19).[126]

In solution, the equilibrium favouring dimeric species could be modified by changing the solvent and temperature, and by adding competitive guests and hydrogen-bonding molecules.[155,156] The assembly/disassembly behaviour was coupled with fluorescence response using a pillar[5]arene bearing A1-anthracene- and A2-ammonium-terminated side

chains (**P64**).[158] In the dimeric state, restricted anthracene motion led to a highly emissive nature, which was greatly influenced by solvent, temperature, competitive guests, pH, and counter anions, providing an on–off switching system. Huang and coworkers replaced the bromo group of **P63a** with an amino group and capped the molecule with an isocyanate in 30% yield.[159] In interlocked dimer **P65**, the pillar[5]arene units were located close to the stopper in $CDCl_3$, but around the middle of the methylene segment in DMSO-$d_6$. The shuttling motion resulted in the stretching of **P65**, with its length changing from 31 to 37 Å. Without capping, similar shuttling-induced molecular extension was realized with **(P36)$_2$** by protonation of the pyridine ends in response to TFA.[126]

The dimeric assemblies introduced above are sometimes known as [*c*2]daisy chains. Two threading side chains in a [*c*2]daisy chain can be connected to form another macrocycle. The resulting self-locked molecule is denoted as a gemini-catenane, and was synthesized by Liu and coworkers in 2015.[133] The authors attempted the condensation of A1,A2-dicarboxylic acid-appended pillar[5]arene **P66** and 1,8-octanediamine, obtaining gemini-catenanes **P67** in addition to pseudo[1]catenane **P42** in Fig. 21a. Owing to their dimeric structure, the gemini-catenanes existed as two diastereomers with $S_2$- and $C_2$-symmetry. The former was achiral owing to ($S_p$,$R_p$)-pillar[5]arenes, while the latter was a pair of enantiomers with ($S_p$,$S_p$)- and ($R_p$,$R_p$)-configurations. The planar chirality in **P42** and **P67** was highly robust, even upon addition of 10 equiv. of **22** and heating in DMSO-$d_6$, in sharp contrast to that in normal pseudo[1]catenanes. Gemini-catenanes were also obtained with longer diamines ($n$ = 10,12) along with a decreased preference for $C_2$-isomers, while only pseudo[1]catenanes formed with shorter diamines ($n$ = 3,4,6).

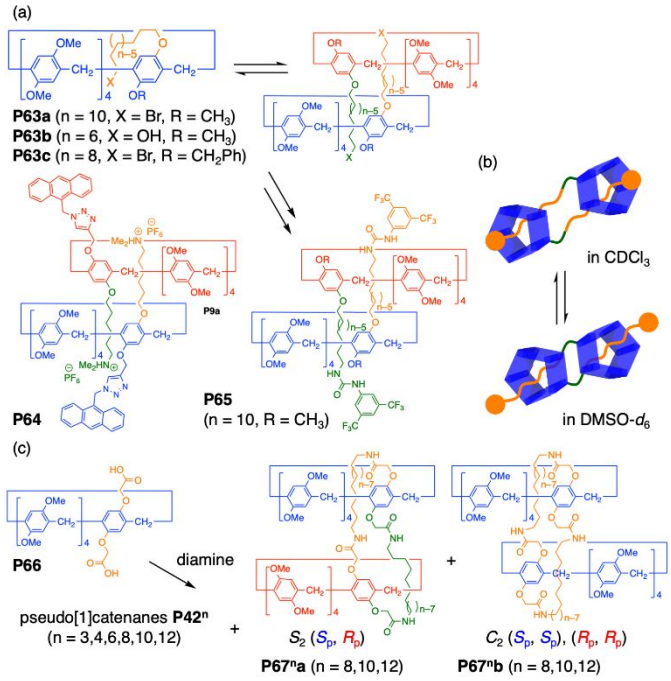


**Scheme 12** (a) Chemical structures of [*c*2]daisy chains and (b) shuttling motion of **P65**. (c) Synthesis of gemini-catenanes.

**Nonthreaded fused tricyclic host.** Similar to fused bicyclic hosts, tricyclic hosts can be constructed from two pillar[5]arene units and nonthreading linkers. In 2015, two A1,A2-dihydroxypillar[5]arenes and tetra(ethylene glycol)s were combined via sequential tosylation and $S_N2$ reactions (**P68** in Fig. 23).[160] Although the authors did not mention the stereochemistry, all crystal structures contained solely heterochiral ($S_p$,$R_p$)-diastereomers. The cavities of the pillar[5]arenes and crown ether hosted linear-shaped neutral guest **22** and aromatic dication **24** with 1:2 and 1:1 stoichiometry, respectively. For the binding of **24**, negative cooperativity was clearly observed between **P68** and (**22**)$_2$@**P68** ($9.1\times10^2$ and $2.3\times10^2$ $M^{-1}$, respectively) in $CDCl_3$/DMSO-$d_6$ (3/1). In 2020, a series of doubly *m*-phenylene-bridged pillar[5]arene dimers was prepared via $S_NAr$ reactions (**P69**).[161] The tricyclic products were separated by chromatography on silica gel and chiral column to give an achiral ($S_p$,$R_p$)-isomer (**P69a**) and an enantiomeric pair of ($S_p$,$S_p$)- and ($R_p$,$R_p$)-isomers (**P69b**). The two pillar[5]arene cavities were used to bind two axle molecules and produce many kinds of chiral supramolecular systems with one and two rotaxane structures after capping.

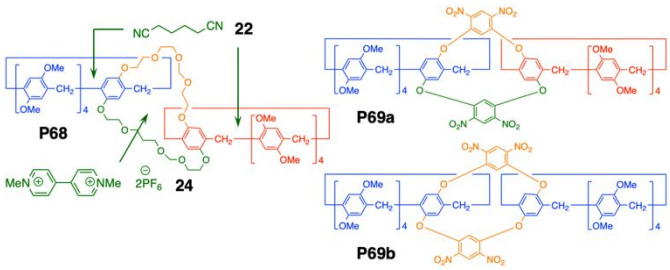


**Fig. 23** Chemical structures of fused tricyclic compounds and their site-selective guest binding.

## MIM-based supramolecular systems

### Interlocked supramolecular polymers based on pillar[*n*]arenes

The host–guest properties of pillar[*n*]arenes make them good candidates to "polymerize" through self-inclusion of heteroditopic pillar[*n*]arenes fusing a pillar[*n*]arene part and a guest part, and host–guest conjugation between pillar[*n*]arene hosts and guests with multiple sites of action.

In some cases, pillar[*n*]arenes with functionalized side chains that act as guests do not form single-component pseudorotaxanes, but cause supramolecular polymerization based on intermolecular complexation. In 2011, Huang and coworkers reported a supramolecular polymer from a simple pillar[5]arene bearing one *n*-octyl group, **P70a** (Fig. 24a).[38] At low concentration in $CDCl_3$ (1 mM), *n*-octyl groups rapidly exchanged between uncomplexed and intramolecular self-complexation states. In contrast, increasing the concentration resulted in sharp $^1H$ NMR peak shifts attributed to the formation

of linear supramolecular polymers. Viscosity measurements in $CHCl_3$ gave a critical polymerization concentration (CPC) of 275 mM. The resulting polymer was confirmed as a head-to-tail linear polymer with quadruple C–H/π interactions by single-crystal X-ray analysis. Stoddart and coworkers used a viologen unit as a stronger guest component ($K_a$ = 1.3×10$^5$ M$^{-1}$ in $CH_2Cl_2$/MeCN (24:1) for a model system), which was introduced to monofunctionalized pillar[5]arene **P70b** via CuAAC reaction.[162] Owing to stronger complexation of the pillar[5]arene cavity with the viologen units on the rim, supramolecular polymerization occurred at lower concentration (CPC, approx. 15 mM).

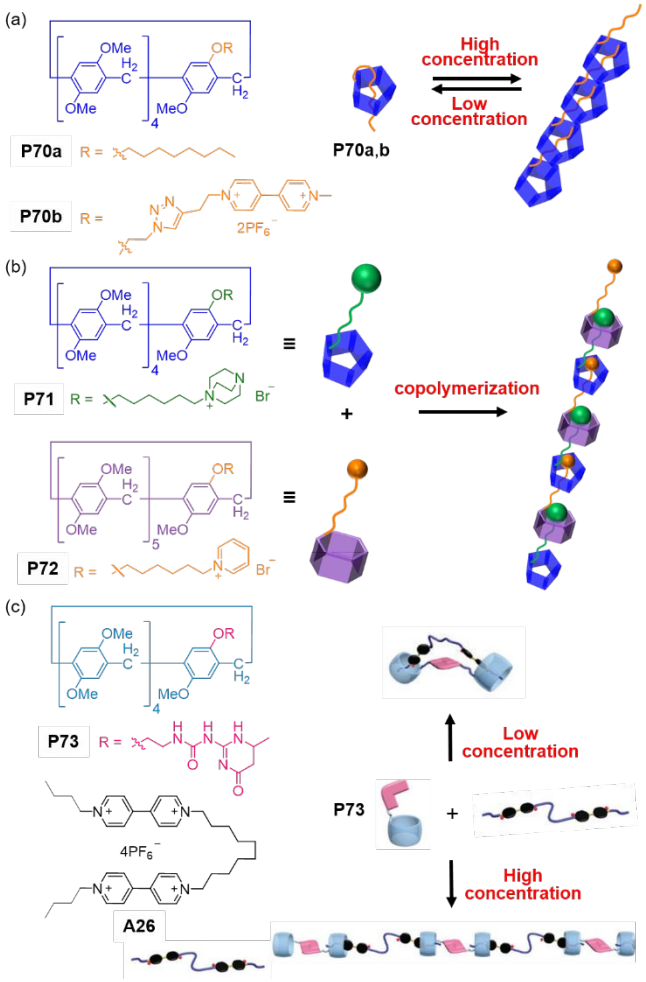


**Fig. 24** Concentration-dependent (a) supramolecular polymerization of **P70a** and **P70b**, and (b) co-polymerization of **P71** with **P72**.(c) Polymerization of **P73** with ditopic guest **A26** via the cross-action of host–guest interaction and hydrogen bonding between hosts. Reproduced with permission from ref. 164. Copyright 2012 Royal Society of Chemistry.

Supramolecular polymers of pillar[*n*]arenes can also be prepared based on various multicomponent systems. We reported a supramolecular polymer by mixing two heterotopic host–guest conjugates, a monofunctionalized pillar[5]arene bearing a DABCO cation at the terminal of the substituent (**P71**), and a monofunctionalized pillar[6]arene bearing a terminal pyridinium cation (**P72**).[163] As the cavities of pillar[5]arene and pillar[6]arene preferred to bind pyridinium and DABCO cations,

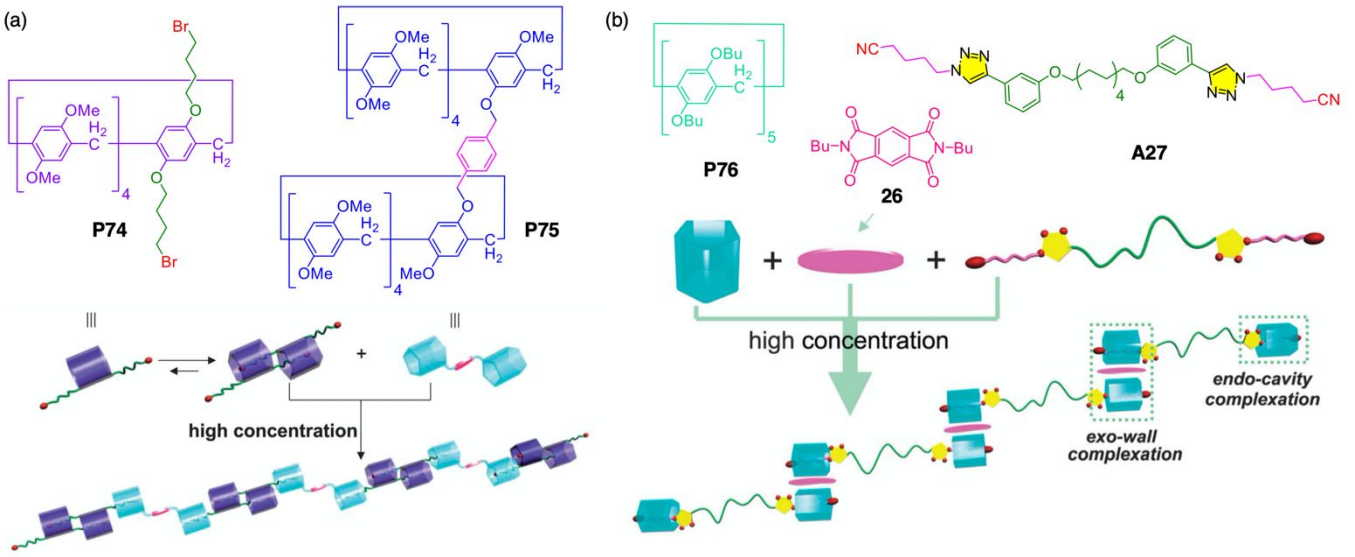


**Fig. 25** Supramolecular polymerization of pillar[5]arene dimers. (a) $A_2B$-type polymer of **P74** and **P75**. Reproduced with permission from ref. 166. Copyright 2013 Royal Society of Chemistry. (b) $A_2B$-type polymer of **P76** and **A27**. Reproduced with permission from ref. 167. Copyright 2015 Royal Society of Chemistry.

respectively, the constructed supramolecular polymer alternated between pillar[5]arene and pillar[6]arene units (Fig. 24b). Wang and coworkers prepared a pillar[5]arene with a ureidopyrimidinone segment, **P73**, which caused facile dimerization via self-complementary quadruple hydrogen bonds (Fig. 24c).[164] When excess **P73** was added to a 2.5 mM solution of ditopic guest **A26** ($K_a = 4.46\times10^3$ $M^{-1}$ in $CHCl_3$/MeCN (1:1) for a model system) in $CDCl_3/CD_3CN$ (1:1), host–guest complexation occurred at both outer alkylpyridinium segments. At higher concentration, a 2:1 mixture of **P73** and **A26** showed a clear decrease in diffusion coefficients and increase in viscosity with a CPC of 13.2 mM. These results demonstrated that a supramolecular polymer was successfully constructed based on an alternate two-component system with orthogonal noncovalent interactions.

Li, Jia, and coworkers realized neutral supramolecular polymers using linear alkyl chains with electron-withdrawing cyano and triazolyl moieties.[165] The authors used a combination of a pillar[5]arene dimer and guests with two and three binding sites under AA/BB- and $A_2/B_3$-type schemes. Linear and hyperbranched supramolecular polymers were produced with CPCs of 18 and 22 mM, respectively. The same group reported another heterotritopic $AB_2$-type system with two types of pillar[5]arene, **P74** and **P75** (Fig. 25a).[166] Owing to the presence of two bromobutoxy chains, **P74** self-assembled into a [*c*2]daisy-chain pseudorotaxane **$(P74)_2$** bearing additional unbound recognition sites at both ends. A linear supramolecular polymer was produced when pillar[5]arene dimer **P75** and supramolecular dimer **$(P74)_2$** were mixed in 1:1 molar ratio ([**P75**]/[**P74**] = 1:2), and the CPC was determined to be 95 mM for **P74**. The same group also polymerized guest **A27** with a supramolecular dimer of **P76**, which was dimerized by forming a 2:1 sandwich-type structure with electron-deficient planar

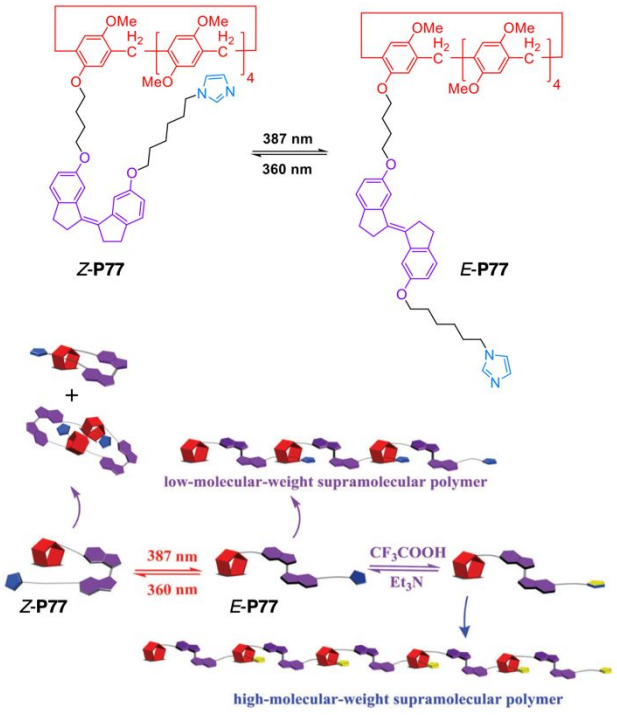


**Fig. 26** Photoresponsive supramolecular polymer of **P77**. Reproduced with permission from ref. 170. Copyright 2014 Royal Society of Chemistry.

molecule **26** via a π–π donor–acceptor interaction (Fig. 25b).[167] Similarly, Wang, Fan, and coworkers constructed a linear supramolecular polymer in an $A_2B_2$-type scheme from a supramolecular dimer of **P76** and a dimerized linear monomer.[168] Three types of noncovalent recognition motif

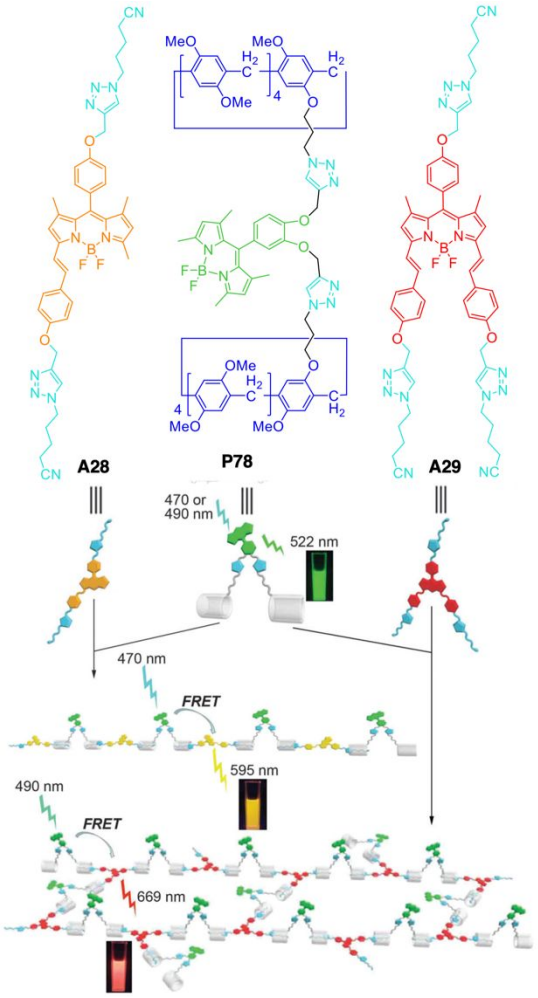


**Fig. 27** FRET-capable supramolecular polymers based on BODIPY-bridged molecules. Reproduced with permission from ref. 172. Copyright 2015 Royal Society of Chemistry.

were included in this system, namely, π–π donor–acceptor interactions, quadruple hydrogen-bonding interactions between two linear monomers, and host–guest interactions between the pillar[5]arene cavity and linear monomer.

Supramolecular polymers with stimuli-responsiveness were achieved when specific functional groups were introduced into the system. We prepared an azobenzene-bridged pillar[5]arene dimer, which formed a linear supramolecular polymer with a homoditopic linear guest bearing two pyridinium ends.[169] The supramolecular polymer photoreversibly switched between assembly and disassembly owing to the change in conformation of the azobenzene-bearing pillar[5]arene dimer. Yang and coworkers prepared monofunctionalized pillar[5]arene **P77**, which contained a photoresponsive rigid stilbene in the middle and an imidazole moiety at the end of the substituent (Fig. 26).[170] **P77** exhibited *E*/*Z*-isomerization under irradiation with different wavelengths of UV light. *Z*-**P77** tended to form a self-complexing pseudo[1]rotaxane and a double-threaded dimer. In contrast, *E*-**P77** formed a low-molecular-weight supramolecular polymer via host–guest interactions between imidazoles and pillar[5]arene cavities. Protonation of the imidazoles enhanced host–guest complexation, resulting in the formation of high-molecular-weight polymers.

The incorporation of fluorescent moieties allows the construction of fluorescent polymers. Yang and coworkers prepared a tetraphenylethene-bridged pillar[5]arene tetramer and a distyrylanthracene-bridged pillar[5]arene dimer, both of which copolymerized with a bistriazole guest linker to form supramolecular polymers.[106,171] Owing to the AIE of both tetraphenylethene and distyrylanthracene, the constructed supramolecular polymers showed remarkable fluorescence emission enhancement in solution and solid states. Wang and coworkers reported FRET-capable supramolecular polymers based on BODIPY-bridged pillar[5]arene dimer **P78** and two BODIPY-bearing guests, in which two (for **A28**) or three (for **A29**) "tails" with a triazole-cyano station at the end were linked by a BODIPY moiety (Fig. 27).[172] Strong host–guest complexation between the pillar[5]arene cavity and guest tails allowed the copolymerization of **P78** with **A28**/**A29**, which brought the BODIPY moieties on the pillar[5]arene dimer and guests close to each other. Consequently, both polymers exhibited efficient FRET effects, with transfer efficiencies of 51% and 63%, respectively. Stoddart and coworkers introduced a porphyrin unit and viologen cations onto a pillar[5]arene derivative to self-assemble into a linear supramolecular polymer, which showed the potential for photoinduced electron transfer processes between porphyrins and viologens.[173]

Recently, Lin and coworkers reported a multifunctional supramolecular polymer network based on pillar[5]arene trimer **P79** and triquaternary ammonium guest **A30** (Fig. 28).[174] Both the pillar[5]arenes in **P79** and terminal ammonium ions in **A30** were linked by a triacylhydrazone group, which provided an additional driving force for copolymerization through multiple hydrogen-bonding interactions. Therefore, the supramolecular network of the mixture of **P79** and **A30** stacked with each other formed a bundle and then gelated. The gel showed excellent conductivity ($\sigma$ = 22.7 mS $m^{-1}$) owing to the abundance of free counter-anions, and AIE behaviour owing to restriction of the intramolecular motion of the pillar[5]arene units. Owing to the coordination properties of the triacylhydrazone groups, the gel also bound various metal ions and showed regulated fluorescent properties. In particular, the colour of the $Co^{2+}$-coordinated polymer was extremely sensitive to temperature, changing from light yellow to dark green in DMSO/water solution when the temperature was increased from 75 to 80 °C. Furthermore, the $Fe^{3+}$-, $Hg^{2+}$-, and $Cu^{2+}$-coordinated polymers showed high selectivity and quick fluorescent responses for anions $H_2PO_4^-$, $I^-$, and $H_2PO_4^-$, respectively, among 11 common monovalent anions.

### Supramolecular polymers of pillar[*n*]arene-based MIMs

**Construction of supramolecular polymers containing MIMs based on noncovalent intermolecular interactions.** To date, mechanically interlocked architectures based on pillar[*n*]arenes have been successfully installed into polymer chains using

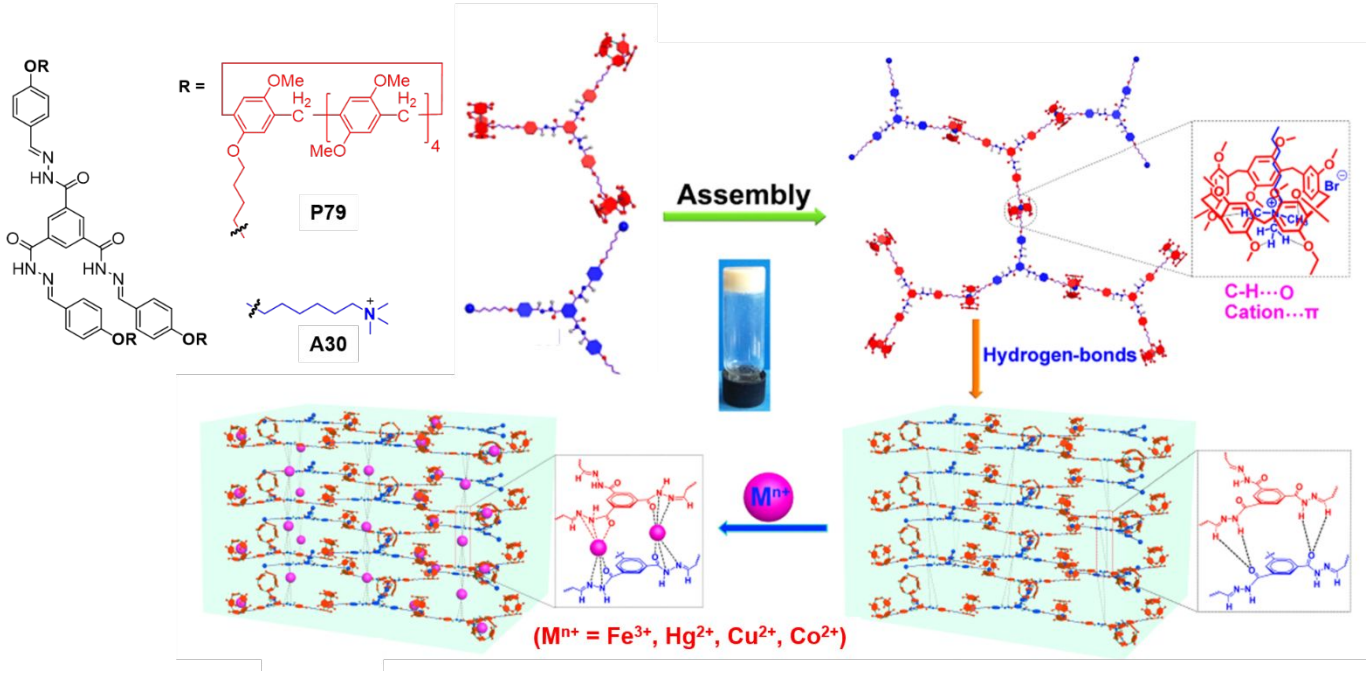


**Fig. 28** Multifunctional supramolecular polymer network based on **P79** and **A30**. Reproduced with permission from ref. 174. Copyright 2021 American Chemical Society.

various types of noncovalent intermolecular interaction. In 2012, Wang and coworkers successfully prepared the first noncovalently bonded dynamic polyrotaxanes constructed by the quadruple hydrogen bonding of ureidopyrimidinone motifs (**27**) on the end groups of threaded axles into pillar[5]arene cavities (Fig. 29a).[175] In this system, the quadruple hydrogen bonds of **27** played dual roles as the end-capping and interlocking units. The symmetric and unsymmetric [2]rotaxanes (**$27_2$·A31@P7** and **$27_2$·A9@P7**, respectively) based on permethylated pillar[5]arene (**P7**) wheels were obtained using 1,4-butanediamine (**A31**) and 1,8-octanediamine (**A9**) as axles, respectively. In concentration-dependency tests, the average measured diffusion constant of **$27_2$·A9@P7**, calculated from DOSY NMR measurements, sharply decreased from $3.49\times10^{-10}$ $m^2$ $s^{-1}$ at 5 mM to $1.38\times10^{-10}$ $m^2$ $s^{-1}$ at 150 mM, which indicated the formation of much larger polyrotaxane poly(**$27_2$·A9@P7**) at higher concentrations. Upon increasing the concentration of **$27_2$·A31@P7** from 5 to 300 mM, the average measured diffusion constant decreased from $5.28\times10^{-10}$ to $1.36\times10^{-10}$ $m^2$ $s^{-1}$. This also indicated the concentration dependence of the supramolecular polymerization of **$27_2$·A31@P7** to form polyrotaxane poly(**$27_2$·A31@P7**). These results clearly indicated that polyrotaxanes based on pillar[5]arenes were successfully obtained.

The same group also reported supramolecular poly(pseudorotaxane)s constructed from bifunctional pillar[5]arene **P80** as the wheel and **A31** as the axle (Fig. 29b).[176] Concentration-dependency tests of **P80** and **A31** at concentrations in the range of 1–200 mM using $^1$H NMR showed that the N–H signals of ureidopyrimidinone motif had large downfield shifts with lower intensity, indicating dimerization of the ureidopyrimidinone units. As the concentrations in the mixture of **P80** and **A31** increased, the signals of the diamine protons showed significant upfield shifts, suggesting host–guest interactions between the pillar[5]arene and diamine in solution. Furthermore, all proton signals became broad at high concentrations, strongly indicating the formation of linear supramolecular poly(pseudorotaxane) poly(**A31@P80**).

Halogen bonding shows potential as a design element in crystal engineering and molecular recognition. Połoński and coworkers reported the formation of crystalline poly(pseudorotaxane)s (Fig. 29c).[177] Pseudorotaxane **A32@P7** was constructed by combining **P7** as a macrocyclic wheel with 1,4-bis(1-imidazolyl)butane (**A32**). 1,4-Bis(iodoethynyl)benzene (**28**) or 1,4-diiodo-1,3-butadiyne (**29**) linkers formed halogen bonding with **A32@P7** and provided polyrotaxanes poly(**28·A32@P7**) and poly(**29·A32@P7**). The single-crystal structures of poly(**28·A32@P7**) and poly(**29·A32@P7**) showed that infinite chains of alternating **A32** and **28** or **A32** and **29** molecules were formed, which were connected by halogen bonds to form the poly(pseudorotaxane) axis with the threaded pillar[5]arene **P7** beads. The halogen bonds connecting **A32** with **28** or **A32** with **29** were nearly linear (C–I···N angles of 172°) and quite strong, as evidenced by the short I···N distances of 2.734–2.794 Å.

Huang and coworkers also accomplished synthesis of the side-chain poly(pseudorotaxane) with a supramolecular polymer backbone through halogen bonds and pillar[5]arene-based host–guest interactions both in solution and solid states (Fig. 29d).[178] The supramolecular poly(pseudorotaxane) poly(**30·A31@P81**) was prepared by adding *n*-hexane (**31**) to a

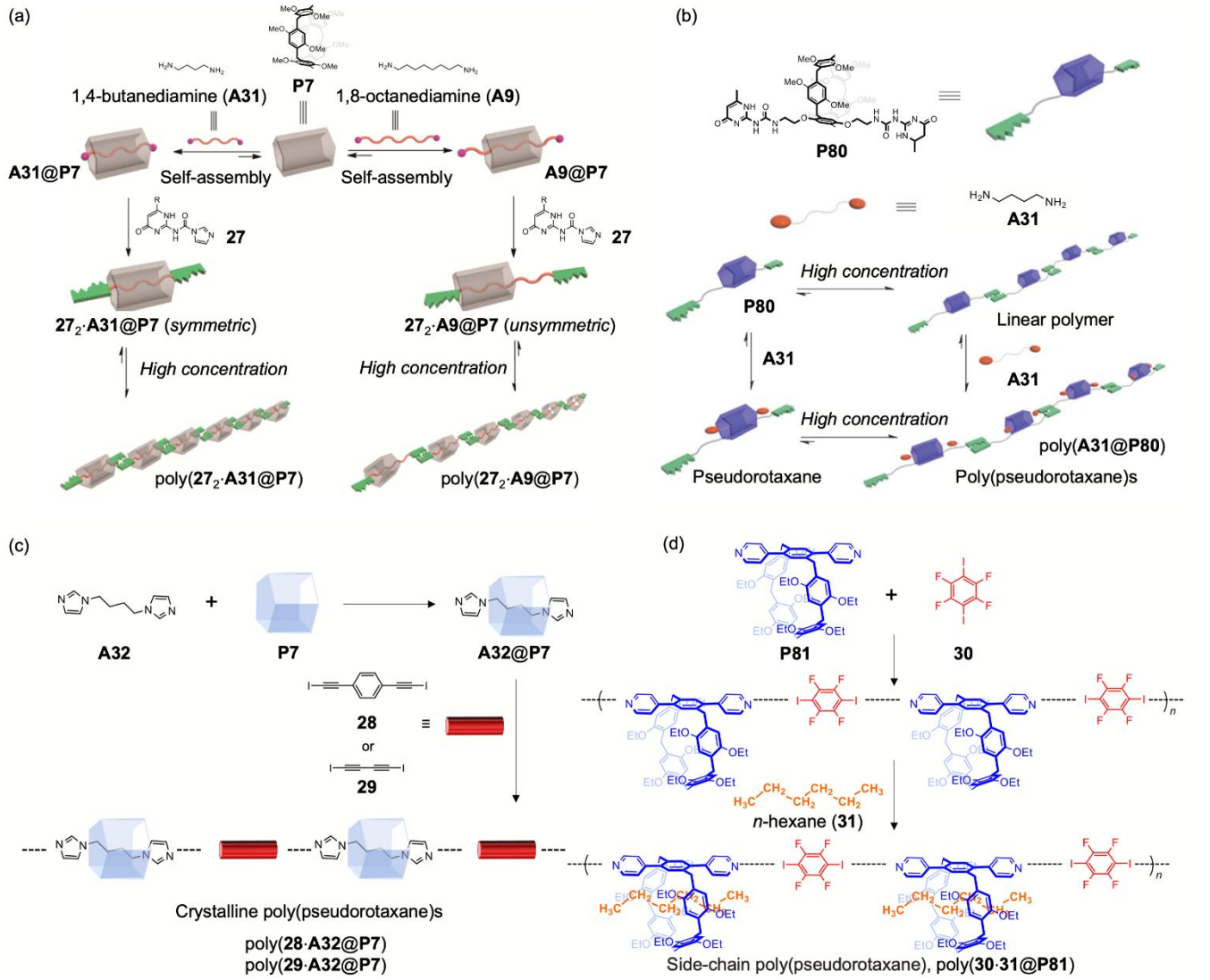


**Fig. 29** (a) Schematic representation of the construction of dynamic polyrotaxanes poly(**27**$_2$·**A31@P7**) and poly(**27**$_2$·**A9@P7**). Reproduced with permission from ref. 175. Copyright 2012, American Chemical Society. (b) Schematic representation of the construction of poly(pseudorotaxane) poly(**A31@P80**). Reproduced with permission from ref. 176. Copyright 2012 Royal Society of Chemistry. (c) Schematic representation of the approach to the formation of designed poly(pseudorotaxane)s poly(**28**·**A32@P7**) and poly(**29**·**A32@P7**). (d) Schematic representation of formation of the supramolecular polymer backbone and side-chain poly(pseudorotaxane) poly(**30**·**A31@P81**).

solution of equimolar pillar[5]arene derivative **P81** containing pyridyl groups as a halogen bond acceptor and 1,4-mixture confirmed the presence of halogen-bonding interactions owing to downfield and upfield shifts of the peaks related to protons in the pyridine groups and adjacent phenyl groups, respectively. These were due to the loss of electron density upon association of the pyridine N-atoms with the electron deficient I-atoms, indicating halogen-bonding interactions between **P81** and **30**. Furthermore, the diffusion coefficient calculated from the $^1$H DOSY measurements (298 K) for free **P81** (10.0 mM) was $1.21\times10^{-4}$ m$^2$ s$^{-1}$. In contrast, the diffusion coefficient was decreased to $1.44\times10^{-5}$ m$^2$ s$^{-1}$ by adding **30** to a solution of **P81** (10.0 mM), suggesting formation of the linear supramolecular polymer. The diffusion coefficient diiodotetrafluorobenzene (**30**) as the divalent halogen bond donor in $CDCl_3$. The $^1$H NMR study of equimolar **P81** and **30** further decreased to $4.13\times10^{-6}$ m$^2$ s$^{-1}$ after adding *n*-hexane to the solution of **P81** and **30**, indicating the formation of linear poly(pseudorotaxane) poly(**30**·**A31@P81**). Single-crystal X-ray analysis elucidated the structure of the supramolecular poly(pseudorotaxane), wherein the pseudorotaxane units are connected by halogen bonds to form a linear sidechain poly(pseudorotaxane) throughout the entire crystal. This was in agreement with the NMR experiments in solution and indicated that the supramolecular poly(pseudorotaxane) architecture existed not only in solution, but also in the solid state.

Metal coordination is beneficial for the construction of stable and complex poly(pseudorotaxane) structures through

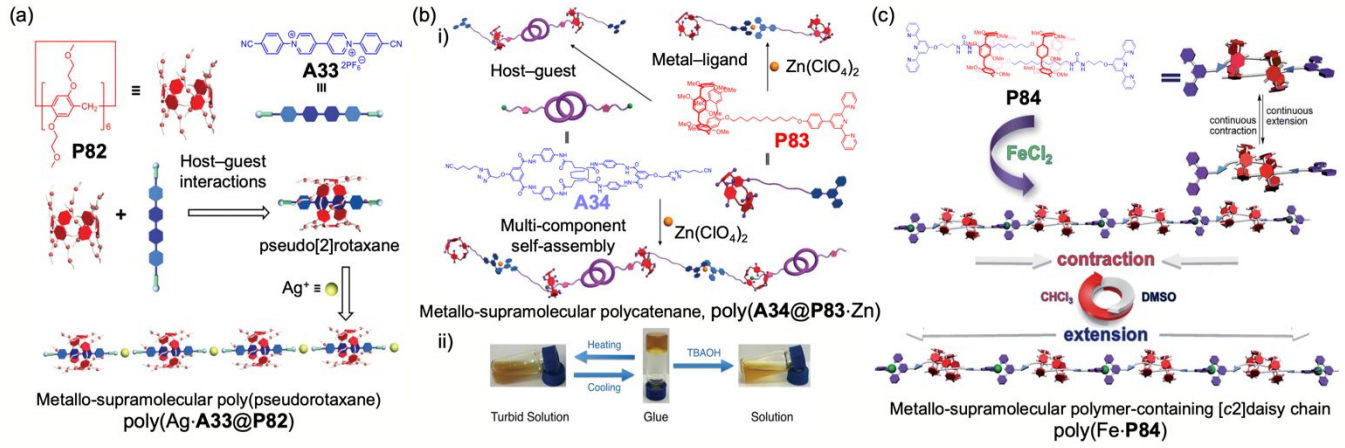


**Fig. 30** (a) Chemical structures of compounds **P82** and **A33** used in this study, and cartoon representation of the formation of metallo-supramolecular poly(pseudorotaxane) poly(Ag·**A33**@**P82**) driven by metal coordination. Reproduced with permission from ref. 179. Copyright 2019 Royal Society of Chemistry. (b) (i) Cartoon representation of the formation of supramolecular main-chain polycatenanes poly(**A34**@**P83**·Zn) based on orthogonal host–guest interaction and metal ion coordination; (ii) glue–sol transitions of the supramolecular polymers triggered by different stimuli. Reproduced with permission from ref. 180. Copyright 2016 Royal Society of Chemistry. (c) Cartoon representation of the formation of metallo-supramolecular polymer containing [*c*2]daisy chain, poly(Fe·**P84**), and the corresponding integrated translational motion based on individual contraction and extension of each daisy chain repeating unit. Reproduced with permission from ref. 181. Copyright 2014 Royal Society of Chemistry.

spontaneous formation of metal–ligand bonds. Xia, Chen, Wang, and coworkers synthesized a pseudo[2]rotaxane **A33**@**P82** based on a mono(ethylene oxide)-substituted pillar[6]arene **P82** and a paraquat derivative guest **A33** (Fig. 30a).[179] After adding $Ag^+$ to **A33**@**P82**, a coordination polymer backbone was constructed between metal cation $Ag^+$ and the cyano groups on **A33** moieties, and then metallo-supramolecular poly(pseudorotaxane) poly(Ag·**A33**@**P82**) was successfully formed, as confirmed by various techniques, including $^1$H NMR, 2D DOSY, dynamic light scattering (DLS), and scanning electron microscopy (SEM).

Xing and Shi constructed linear metallo-supramolecular polycatenane poly(**A34**@**P83**·Zn) using metal ion coordination and host–guest interactions between pillar[5]arene monomer **P83** and [2]catenane guest monomer **A34** bearing two cyano groups (Fig. 30b).[180] This supramolecular polycatenane exhibited dual-stimuli responsiveness to both temperature and $OH^-$ by taking advantage of the reversibility of host–guest and metal–ligand interactions. By adding **A34** (100 mM), **P83** (200 mM), and $Zn^{2+}$, a glue-like solution was formed, while the glue-like viscous liquid gradually changed to a turbid solution in response to increasing temperature. This dynamic behaviour was explained by the fact that heating could induce disassembly of the supramolecular polymer backbone. In contrast, the glue-like supramolecular polymer was disassembled by adding several drops of a $CH_3CN/CHCl_3$ (1:1, *v*/*v*) solution of tetrabutylammonium hydroxide (TBAOH) at 200 mM owing to the strong binding ability of $OH^-$ ions toward Zn ions. Correspondingly, the glue-like supramolecular polymers dissociated into a transparent solution within a short time of 1 min.

In 2014, Huang and coworkers reported metallo-supramolecular polymers from a pillar[5]arene-based [*c*2]daisy chain (Fig. 30c).[181] Daisy chains are a species of MIM that exhibit unique intramolecular motions, such as elongation and contraction, which can be controlled by external inputs. Upon adding $Fe^{2+}$ to [*c*2]daisy chain monomer **P84**, metal-coordination with the terpyridine ligand on both ends of the [*c*2]daisy chain initiated polymerization and metallo-supramolecular polymer poly(Fe·**P84**) was obtained. Importantly, when the solvent polarity was increased in DLS experiments of poly(Fe·**P84**), the hydrodynamic radius ($R_h$) of the aggregates increased correspondingly (from an average $R_h$ of 104 nm in $CHCl_3$ to an average $R_h$ of 254 nm in DMSO), meaning that the increase in solvent polarity caused movement of the pillar[5]arene cavities on **P84** and led to its extension. Therefore, the length of polymer poly(Fe·**P84**) changed continuously according to the solvent polarity based on individual contraction or extension of each daisy chain repeating unit.

**Crosslinking MIMs based on noncovalent intermolecular interactions.** Crosslinking via noncovalent intermolecular interactions provides network structures with further functionalities, such as gel forming abilities and stimuli-responsivity. In 2016, Hu, Wang and coworkers obtained supramolecular gel poly(Pd·**A35**@**P7**) (Fig. 31a).[182] First, a linear pillar[5]arene-based polyrotaxane was synthesized by adding $Pd(OAc)_2$ to pseudo[2]rotaxane **A35**@**P7**. Subsequently, the polyrotaxane was crosslinked via intermolecular hydrogen bonding interactions, affording poly(Pd·**A35**@**P7**). The $^1$H NMR spectra from a variable-concentration study showed that the chemical shift of the proton assigned to the amide group exhibited concentration-dependent properties. Therefore, the formation of a supramolecular gel might be caused by further self-assembly between amide groups on the polyrotaxane

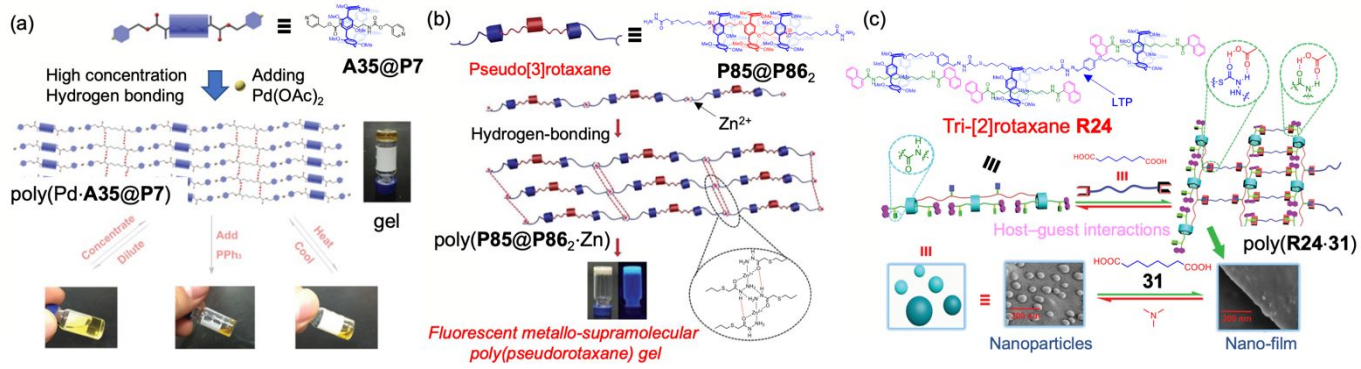


**Fig. 31** (a) Schematic of the formation of crosslinked polyrotaxane poly(Pd·**A35@P7**) and its thermo- and dilution-induced reversible sol–gel transformation. Reproduced with permission from ref. 182. Copyright 2016 Royal Society of Chemistry. (b) Cartoon representation of the formation of metallo-supramolecular poly(pseudorotaxane) gel poly(**P85@P86**$_2$·Zn). Reproduced with permission from ref. 183. Copyright 2018 Royal Society of Chemistry. (c) Diagram of nano-thin film construction by guest induction to regulate fluorescent nanoparticles formed from tri-[2]rotaxane **R24**. Reproduced with permission from ref. 184. Copyright 2021 Royal Society of Chemistry.

backbone through hydrogen-bonding interactions. Importantly, the obtained supramolecular polymeric network gel exhibited thermo- and dilution-induced reversible gel–sol transformation. The gel–sol transformation might be due to the weakened noncovalent hydrogen bonding resulting from diluting and heating. In contrast, adding a $PPh_3$ ligand resulted in irreversible transformation, because the competitive binding of $PPh_3$ with $Pd(OAc)_2$ destroyed the polyrotaxane structures.

Similarly, Lin, Wei, and coworkers prepared metallo-supramolecular poly(pseudorotaxane) gel poly(**P85@P86**$_2$·Zn) via pillar[5]arene-based pseudo[3]rotaxane **P85@P86**$_2$ and zinc ion coordination (Fig. 31b).[183] The 2D networks of poly(**P85@P86**$_2$·Zn) were organized through intermolecular hydrogen-bonding interactions among the hydrazide groups of thioacetylhydrazine in the pseudo[3]rotaxane structure. As an important feature, this supramolecular poly(pseudorotaxane) showed highly sensitive fluorescence recognition of metal ions. In fluorescence spectra, the emission band at 460–560 nm disappeared only when a water solution containing $Fe^{3+}$ and $Cu^{2+}$ was added to metallo-supramolecular poly(pseudorotaxane) gel poly(**P85@P86**$_2$·Zn). IR spectra suggested that the recognition mechanism of poly(**P85@P86**$_2$·Zn) for $Fe^{3+}$ and $Cu^{2+}$ was based on the coordination of $Fe^{3+}$ and $Cu^{2+}$ with –C=O and C–S–C moieties in poly(**P85@P86**$_2$·Zn).

More recently, Lin, Wei, and coworkers constructed stimuli-responsive fluorescent polymer poly(**R24**·**31**) from pillar[5]arene-based tri-[2]rotaxane **R24** consisting of linear tri-pillar[5]arene (LTP), a 1,10-diaminodecane thread guest, and a naphthyl stopper (Fig. 31c).[184] With formation of the tri-[2]rotaxane, the fluorescence intensity was enhanced compared with that of LTP and tri-pseudo[2]rotaxane systems, owing to the introduction of fluorescent naphthyl groups. Furthermore, with the addition of suberic acid (**31**), the fluorescence emission of the tri-[2]rotaxane exhibited distinct enhancement, but did not show similar response for other dicarboxylic acids. From the morphological study using SEM and transmission electron microscopy (TEM), adding **31** induced a transformation from spherical nanoparticles to nanofilms. $^1$H NMR titration experiments of **R24** and **31** showed that tri-[2]rotaxane **R24** with a nanoparticle structure was changed to a nanofilm by guest crosslinking with tri-[2]rotaxane through multiple intermolecular hydrogen bonds. Furthermore, alternating addition of **31** and trimethylamine to tri-[2]rotaxane systems based on competitive hydrogen bonds reversibly changed the tri-[2]rotaxane from nanoparticles to a nanofilm.

Jia, Li, Fang, and coworkers designed a [2]rotaxane consisting of a pillar[5]arene wheel, linear alkane chain axle, and pyromellitic diimide (PDI) stopper (Fig. 32a).[185] The [2]rotaxane **R25** formed supramolecular polymer poly(**R25**) through CT interactions between the π-electron rich pillar[5]arene wheel and electron-deficient PDI stopper. In variable-concentration $^1$H NMR experiments, when the concentration of **R25** increased, the signals derived from the PDI units and the aromatic protons of pillar[5]arenes were shifted upfield owing to the ring current effects of π–π stacking, suggesting wheel-stopper CT interactions. Furthermore, viscosity and DOSY measurements clearly demonstrated that the supramolecular polymerization proceeded with increased concentrations of monomer **R25**. Single-crystal X-ray diffraction measurements of **R25** revealed the assembly motifs of the supramolecular polymer, with both face-to-face and edge-to-face π–π stacking interactions between the exo walls of the pillar[5]arenes and PDI units being responsible for supramolecular polymerization.

Lee and coworkers also reported poly(pseudorotaxane) crystalline products based on the self-assembly of ditopic pillar[5]arene monomer **P87** and silver(I) trifluoroacetate in the presence of linear dinitrile guests (Fig. 32b).[186] Importantly, the poly(pseudorotaxane) structure could be controlled by adjusting the length of the dinitrile guest, with short dinitrile guest **32** affording one-dimensional (1D) poly(pseudorotaxane) poly(**32@P87**), while two-dimensional (2D) poly(pseudorotaxane) poly(**33@P87**) was formed by long dinitrile guest **33**, in which the same guest threaded into the

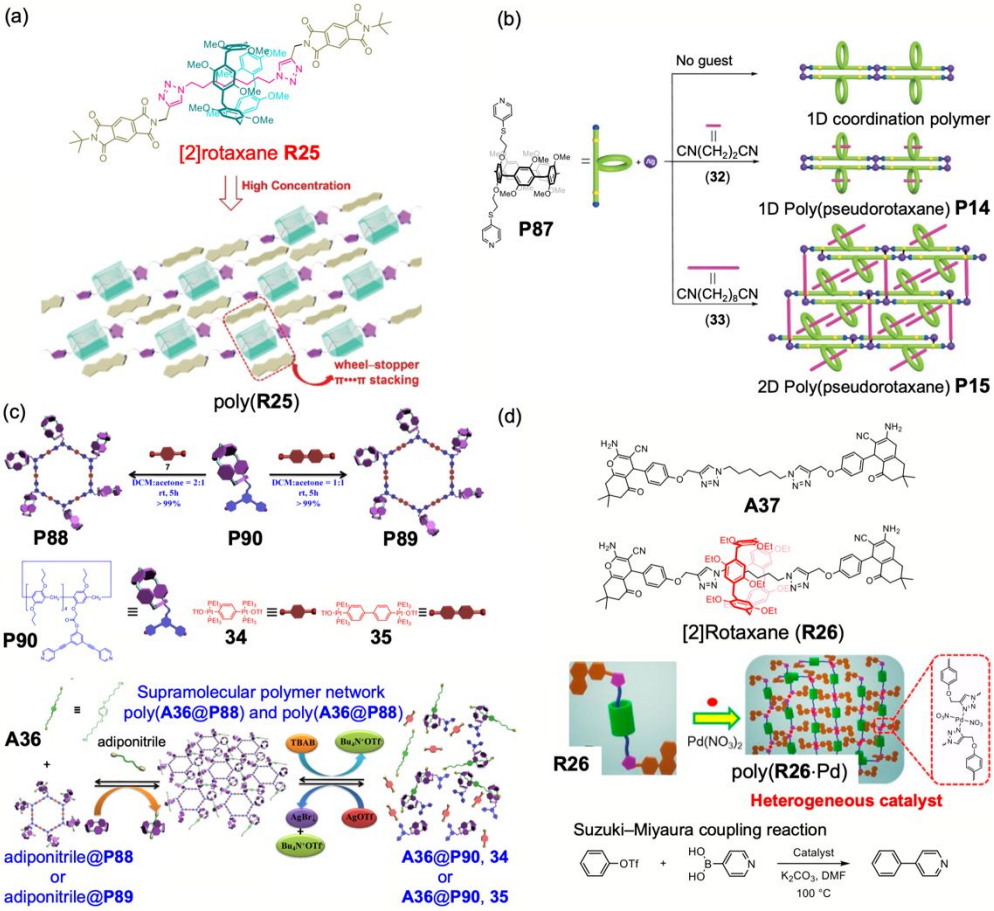


**Fig. 32** (a) Chemical structure of [2]rotaxane **R25** and cartoon representation of the formation of crosslinked supramolecular polymer poly(**R25**). Reproduced with permission from ref. 185. Copyright 2018 Royal Society of Chemistry. (b) Formation of infinite coordinative products, including 2D poly(pseudorotaxane) poly(**32**@**P87**), by threading and crosslinking of the same guest molecules (**33**). Reproduced with permission from ref. 186. Copyright 2019 Wiley-VCH Verlag GmbH & Co. KGaA. (c) Chemical structures of **P88**–**P90**, **34**, **35**, and **A36**, and a schematic representation of the disassembly and reassembly of supramolecular polymer gels induced by a competitive guest and bromide anions as stimuli. Reproduced with permission from ref. 187. Copyright 2014, American Chemical Society. (d) Chemical structures of **A37** and **R26**, and cartoon representation of the formation of poly(**R26**·Pd) and its application in the coupling reaction. Reproduced with permission from ref. 188. Copyright 2020, American Chemical Society.

pillar[5]arene cavity and crosslinked two parallel 1D poly(pseudorotaxane)s. The use of a long dinitrile guest allowed not only the formation of a 1D pseudorotaxane, but also crosslinking toward higher dimensionality by minimizing steric hindrance between short-range and long-range order.

Yang and coworkers synthesized two different-sized hexakis-pillar[5]arene metallacycles **P88** and **P89** via coordination-driven self-assembly between pillar[5]arene containing dipyridyl donors (**P90**) and linear di-Pt(II)acceptors **34** and **35**, respectively (Fig. 32c).[187] Subsequently, crosslinked supramolecular polymers poly(**A36**@**P88**) and poly(**A36**@**P89**) were successfully constructed at the same time as the pseudorotaxane structures from hexakis-pillar[5]arene metallacycles (**P88** or **P89**, respectively) and neutral ditopic guest **A36**. The crosslinked supramolecular polymers were destroyed by adding competitive guest adiponitrile owing to the stronger binding ability of pillar[5]arene with adiponitrile compared with ditopic guest **A36**. Furthermore, the crosslinked supramolecular polymers formed supramolecular gels at higher concentrations. Owing to the dynamic nature of hierarchical self-assembly, the reversible gel–sol transitions can be controlled through disassembly and reassembly by changing the temperature and adding or removing bromide anions.

Yan, Yao, and coworkers successfully obtained organometallic crosslinked pillar[5]arene-based [2]rotaxane poly(**R26**·Pd) via coordination, and demonstrated that it was a good catalyst for the Suzuki–Miyaura coupling reaction, with excellent stability and repeatability (Fig. 32d).[188] After pillar[5]arene-based [2]rotaxane **R26** was prepared from perethylated pillar[5]arene and aliphatic chain axle **A37** by the threading-stopper method, metal-coordination between triazole groups on the axle and $Pd(NO_3)_2$ afforded $Pd^{2+}$-loaded supramolecular polymer poly(**R26**·Pd). Compared with $Pd(NO_3)_2$ and non-pillar[5]arene-containing catalyst Pd·**A37**, which was synthesized by crosslinking linear axle **A37**, poly(**R26**·Pd) showed better catalytic activity in the Suzuki–Miyaura coupling reaction and could be reused in several cycles without any loss of conversion. Although polymeric poly(**R26**·Pd) was nonporous with a

Brunauer–Emmett–Teller surface area ($S_{BET}$) of 8.45 $m^2$ $g^{-1}$, it had a larger surface area than Pd·**A37**. This might be due to the large-sized pillar[5]arene framework inhibiting close stacking of the molecules.

**Supramolecular self-assembly of MIMs.** The formation of a pseudorotaxane structure can be useful for constructing dynamic and stimuli-responsive supramolecular polymer networks. In 2013, Zhao and coworkers reported switchable supramolecular polymer assemblies from host–guest complexation between star-shaped pillar[5]arene trimer **P91** and bis-viologen guest **A38** (Fig. 33a).[189] Morphological analysis using TEM and SEM showed that, although the complexation of permethoxy-substituted pillar[5]arene **P7** with **A38** afforded zero-dimensional (0D) lamellar vesicles owing to their amphiphilic nature, which did not change with increasing concentration, the initial 0D assembly of the inclusion complex between **P91** and **A38** transformed into 1D tubular objects, 2D layers, and three-dimensional (3D) stacked layers with increasing sample concentration. Owing to the star-shaped structure of **P91** with three recognition sites, linear fibres formed flat layers, which then stacked together regularly at high concentration.

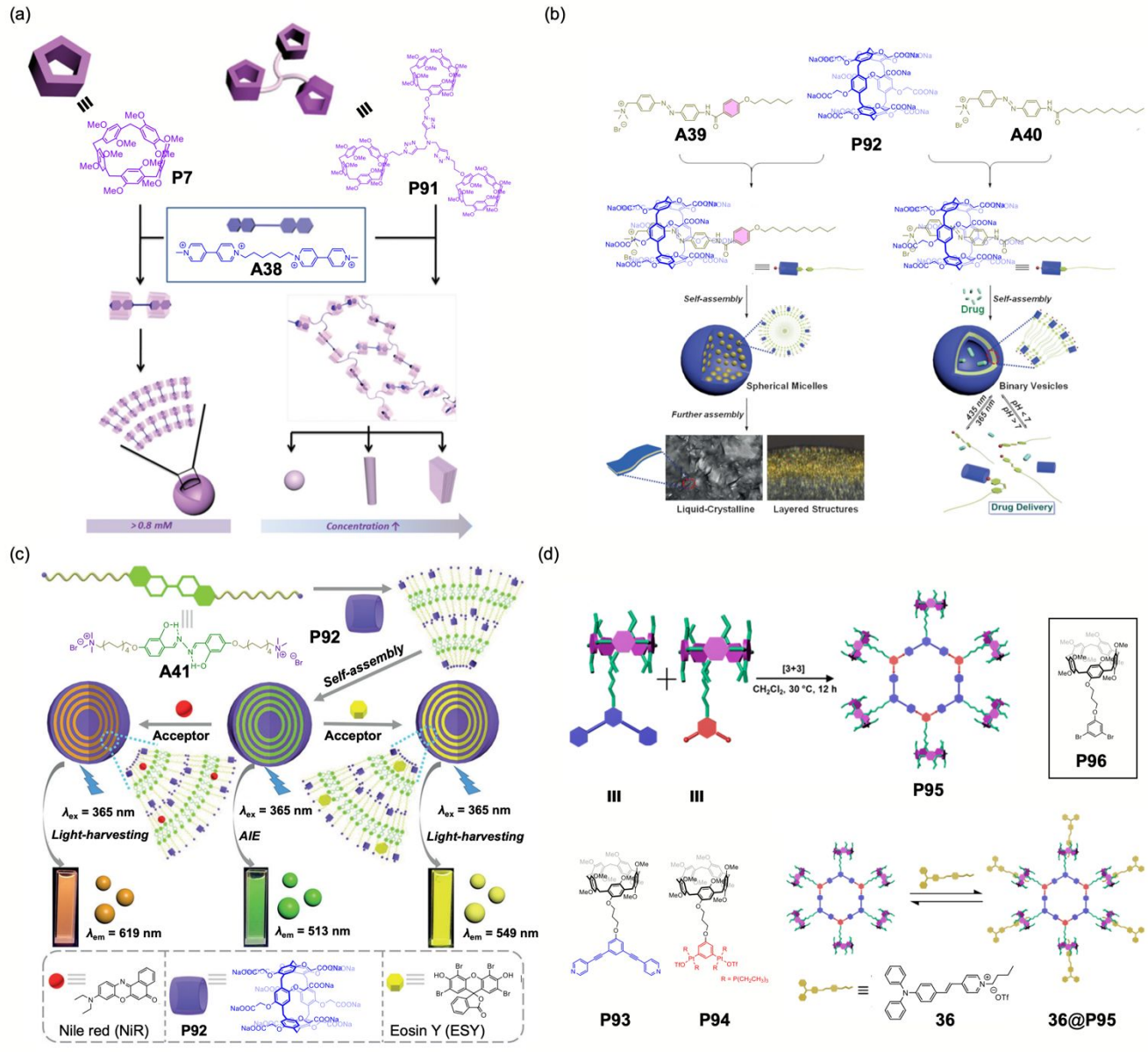


**Fig. 33** (a) Structural representations of **P7**, pillararene trimer **P91**, and bis-viologen **A38**, and the proposed mechanism for the formation of multidimensional assemblies at different concentrations. Reproduced with permission from ref. 189. Copyright 2013 Royal Society of Chemistry. (b) Schematic illustration of the construction of supramolecular micelles (**39**@**P92**) or vesicles (**40**@**P92**), and the application of supramolecular vesicles in drug delivery. Reproduced with permission from ref. 190. Copyright 2015 Wiley-VCH Verlag GmbH & Co. KGaA. (c) Representation of the self-assembly of pillar[6]arene-based aqueous light-harvesting systems. Reproduced with permission from ref. 191. Copyright 2018 Wiley-VCH Verlag GmbH & Co. KGaA. (d) Chemical structures of pillar[5]arene derivatives **P93**, **P94**, and **P96**, and guest molecule **36**, and a schematic illustration of the formation of pillar[5]arene-based hexagonal Pt(II) metallacycle **P95**. Reproduced with permission from ref. 192. Copyright 2020 American Chemical Society.

Wang and coworkers constructed duel photo- and pH-responsive supramolecular nanocarriers based on the pH responsive ability of water-soluble pillar[6]arene **P92** and photoinduced *E*/*Z*-isomerization of azobenzene guests (**A39** and **A40**, Fig. 33b).[190] Host molecule **P92** formed amphiphilic pseudorotaxane structures with amphiphilic guest molecules **A39** or **A40** in water. Furthermore, pseudorotaxane **A39@P92** formed supramolecular micelles that gradually transformed into layered structures with liquid-crystalline properties, and pseudorotaxane **A40@P92** formed stable hollow vesicles. By adjusting the solution to pH 6.2, the Tyndall effect disappeared from the **A40@P92** solution owing to **P92** in its acid form precipitating out of the acidic aqueous solution. Furthermore, the vesicle could be reformed when the pH value was adjusted back to 7.4. More importantly, TEM images showed that, when the **A40@P92** vesicular solution was irradiated with UV light, most vesicles collapsed and only a few irregularly aggregates could be observed. In contrast, visible-light irradiation facilitated the reformation of vesicles. The **A40@P92** vesicle efficiently encapsulates anticancer drug mitoxantrone (MTZ) with good stability in a simulated normal physiological environment, and the encapsulated drug is promptly released in acidic environments similar to that of tumour cells or with external UV irradiation.

Hu, Wang, and coworkers fabricated a supramolecular assembly of a pseudorotaxane consisting of water-soluble pillar[6]arene **P92** and salicylaldehyde azine guest **A41** (Fig. 33c),[191] and used it to construct artificial light-harvesting systems. Light harvesting is based on efficient energy transfer from closely packed donors to acceptor fluorophores through a FRET process. Therefore, fluorescence quenching of the aggregated donor chromophores should be avoided to reduce energy loss. Upon addition of **P92** to the aqueous solution of **A41**, the trimethylammonium terminals of **A41** formed a stable pseudorotaxane with **P92** and further self-assembled into spherical nanoparticles with AIE behaviour, which is an ideal property for light harvesting. After simply mixing the pseudorotaxane assembly with hydrophobic fluorescent acceptors Nile red (NiR) and Eosin Y (ESY), two artificial light-harvesting systems were successfully constructed based on a highly efficient FRET process that occurs from the donor to the acceptor (NiR or ESY). More importantly, both artificial light-harvesting systems showed very high antenna effects with high donor/acceptor ratios (up to 150:1 for NiR system and 200:1 for ESY system), which were similar to those of natural light-harvesting systems.

Stang and coworkers synthesized pillar[5]arene-based hexagonal Pt(II) metallacycle **P95** from pillar[5]arene donor **P93** and acceptor **P94**, and discovered that its pseudorotaxane form with 1-butyl-4-[4-(diphenylamino)styryl]pyridinium (guest, **36**) showed significant AIE behaviour (Fig. 33d).[192] Guest compound **36** was designed to be a potential AIE-active fluorophore. In fluorescence spectra, no significant fluorescence emission was detected for **P93**, **P94**, **36@P96** (a pillararene complex of **36**), and **36@P95** (a metallacycle complex of **36**) in acetone solution, while **36@P95** showed strong emission in an acetone/water (5:95) mixture, which was >166 times higher than that in acetone, clearly indicating AIE behaviour. The drastic increase in fluorescence intensity observed only for **36@P95** in an acetone/water (5:95) mixture indicated that the metallacycle facilitated coaggregation between the guests and pillar[5]arenes through a synergistic effect. In contrast, after adding 1,6-dibromohexane as a competitive guest, the fluorescence in acetone/water (5:95) was almost completely quenched because **36** was no longer in the aggregated state. Therefore, the formation of a pseudorotaxane structure with the pillar[5]arene-based metallacycle played a critical role in realizing emission enhancement effects.

## Mechanically interlocked polymeric materials

### Rotaxane dendrimers based on pillar[5]arenes

Dendrimers are highly ordered, branched polymeric molecules.[193] This 3D branched morphology makes them a versatile platform for constructing practical macrocycles with multiple applications. Along the dendritic wedges of dendrimers, mechanically interlocked structures can be introduced to functionalize dendrimers with unexpected properties.[194,195]

Yang and coworkers established a practical approach to synthesize high-generation dendrimers with rotaxanes. Based on the host–guest interactions between pillar[5]arenes and neutral alkyl chains, rotaxanes containing monosubstituted platinum acetylide as one of the stoppers were constructed. The platinum metal core underwent a coupling reaction with other building blocks to build up the rotaxane dendrimers. Using this strategy, the shapes, sizes, and number of rotaxane rings, and the functional cores, can all be controlled or introduced into the assemblies.[196,197]

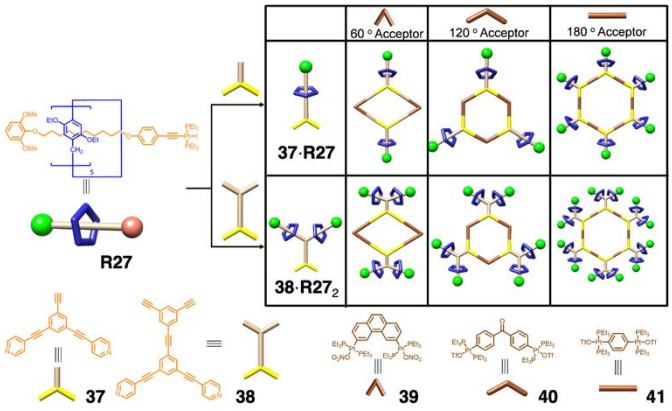


**Fig. 34** Structures of different rotaxane dendrimers based on rotaxane **R27**.

For example, coupling rotaxane **R27** as the starting material with **37** and **38** produced building blocks **37**·**R27** and **38**·$\mathbf{R27}_2$. The subsequent coupling with linkers **39–41**, which had binding

angles were 60°, 120°, and 180°, respectively, furnished rotaxane dendrimers with different shapes and sizes (Fig. 34) Furthermore, the synthesis of high-generation rotaxane dendrimers, which is a key challenge in this area, was achieved.[198,199] By introducing rotaxane branches into the dendrimers, the solubility and stability of the dendrimers were enhanced, enabling the synthesis of high-generation rotaxane dendrimers.[199]

Using this novel synthetic strategy, rotaxane dendrimers with stimuli-responsive or luminescent properties were prepared. Urea moieties, which interacted with pillar[5]arene more strongly compared with the alkyl chain, were incorporated into rotaxane **R28**. Therefore, pillar[5]arenes encircled the urea moieties on the dendrimers. After adding external stimuli, such as DMSO or acetate anions, which bind with urea tightly, the macrocycle wheels moved along the axles to the alkyl chain moieties. After removing the stimuli, the wheels moved back to the urea moieties (Fig. 35). This dual stimuli-responsive process made the dendrimers stretch or contract, leading to reversible size switching that enables the rotaxane dendrimers to serve as dynamic functional materials.[200,201]

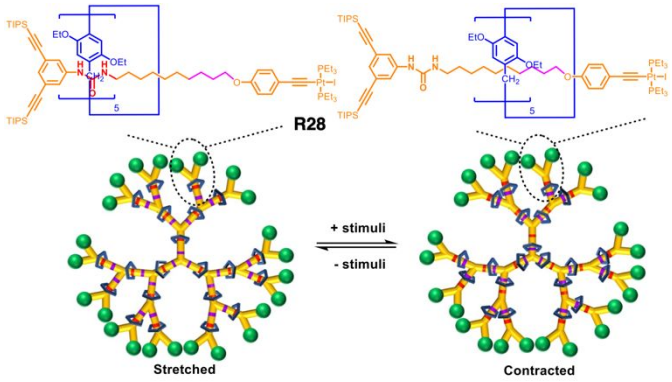


**Fig. 35** Structure of rotaxane dendrimer based on rotaxane **R28** and its dual stimuli-responsive behaviour.

Based on pillar[5]arene and urea-containing axles, daisy chain dendrimers decorated with daisy chain **P97** were also synthesized (Fig. 36). Similar to the aforementioned studies where external stimuli were applied, the dendrimers also showed dual stimuli-responsive properties. However, after interacting with DMSO or acetate, the dendrimers shrank rather than swelling. This might be attribute to self-folding of the branches, whose lengths increased after external stimuli. When the dendrimers were incorporated into poly(vinylidene difluoride) (PVDF), the molecular motion led to controllable shape transformation behaviour of the polymer film. Therefore, the motion at a molecular level was amplified to the macroscopic scale.[202]

As platinum acetylide subunits in the rotaxane dendrimers might have a heavy-atom effect on photosensitization, the Yang group introduced pillar[5]arene with two anthracene substituents as photosensitizer moieties to enhance the photosensitization efficiency. Rotaxane dendrimers based on rotaxane **R29** were then synthesized (Fig. 37). As expected, with increasing generations of rotaxane dendrimers, the efficiency was indeed enhanced. For example, the $^1O_2$ generation efficiency increased owing to boosted intersystem crossing (ISC), which benefited from enhanced spin-orbit coupling (SOC). These results were attributed to the regular arrangement of the anthracene and platinum moieties.[203]

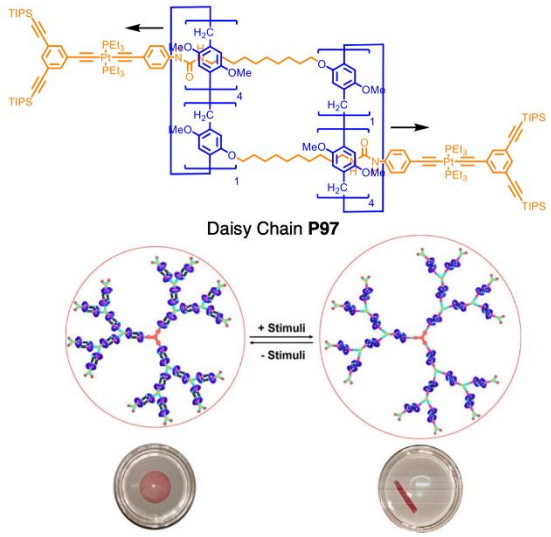


**Fig. 36** Structure of rotaxane dendrimer based on daisy chain **P97** and its dual stimuli-responsive behaviour. Reproduced with permission from ref. 202. Copyright 2020 American Chemical Society.

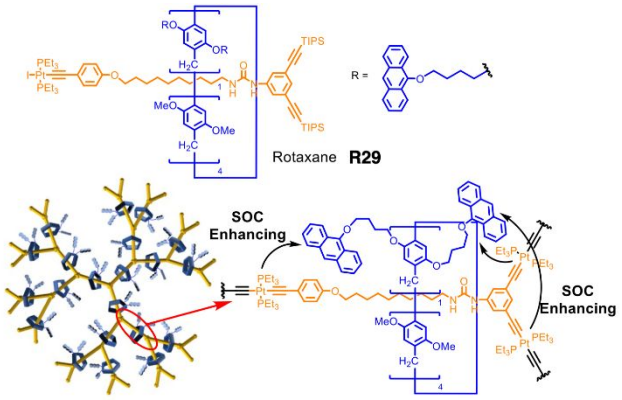


**Fig. 37** Structure of rotaxane dendrimer based on rotaxane **R29** and enhanced intersystem crossing between the naphthalene rings on the pillar[5]arenes and platinum on the axles.

The anthracene moieties also served as energy donors when zinc(II) porphyrin moieties located at the centre of rotaxane dendrimers **R30** as energy acceptors in light harvesting (Fig. 38). Owing to the unique structure of the dendrimers, the ratio of donors to acceptors was high. Meanwhile, donors were distributed around the acceptor in a monodispersed and well-defined manner. Therefore, the rotaxane dendrimers exhibited high energy transfer efficiency and antenna effects. Notably,

the rotaxane dendrimers contained urea moieties on the axles. Therefore, upon adding external stimuli, the wheels moved closer to the porphyrin cores through self-movement and skeleton-shrinking, which enhanced both the energy transfer efficiency and antenna effects. This process was reversed after removing the stimuli.[204]

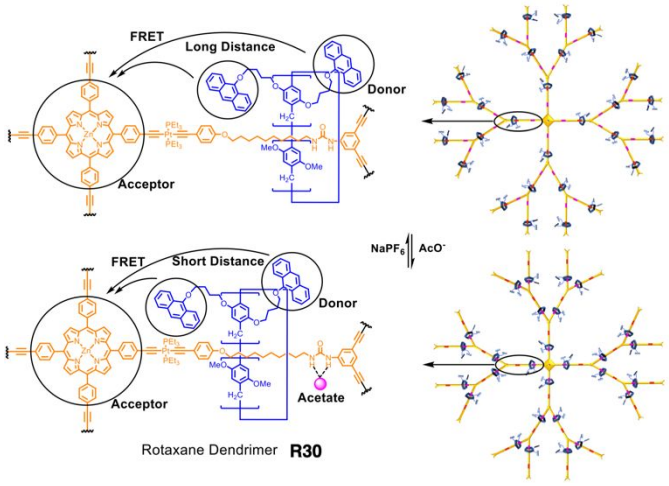


**Fig. 38** Structure of rotaxane dendrimer **R30** and its dynamic energy transfer.

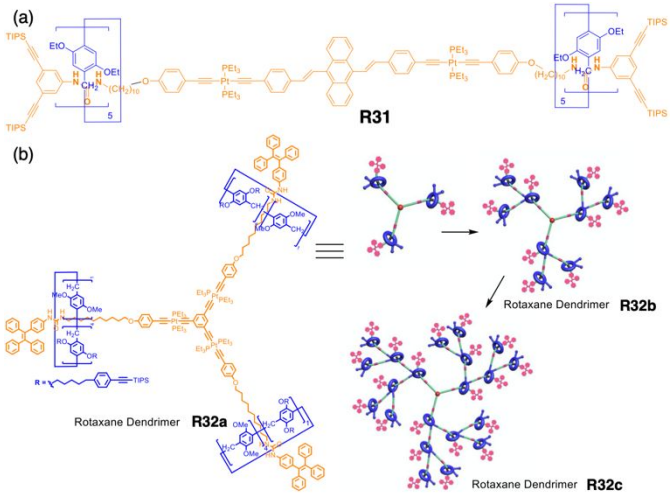


**Fig. 39** (a) Structure of rotaxane **R31**. (b) Structures of rotaxanes **R32a–c**. Reproduced with permission from ref. 206. Copyright 2021 Wiley-VCH Verlag GmbH & Co. KGaA.

To prevent the possible ACQ effect of anthracene-incorporated rotaxane dendrimers, a 9,10-distyrylanthracene moiety, which is extensively used in AIE materials, was introduced as the core (Fig. 39a). Based on rotaxane **R31**, all synthesized rotaxane dendrimers exhibited AIE effects and the efficiency was enhanced as the generations of dendrimers increased.[205]
The AIEgens can be located on the branches, affording AIEgen-branched rotaxane dendrimers **R32a–c** (Fig. 39b). The resulting assemblies also showed better light-harvesting properties with increasing generations. Meanwhile, the dendrimers served as efficient photocatalysts in both photo-oxidation and aerobic cross-dehydrogenative (CDC) reactions, where the catalytic efficiency was also generation-dependent.[206]

**Branched polymers based on pillar[5]arenes**

Branched polymers with mechanically interlocked structures are polymers in which the poly(pseudorotaxane)s are located on the side chains. Therefore, the peripheries of the polymer chains are modified by the supramolecular assembles, affording intriguing properties such as fluorescent sensing, drug delivery, and self-healing.

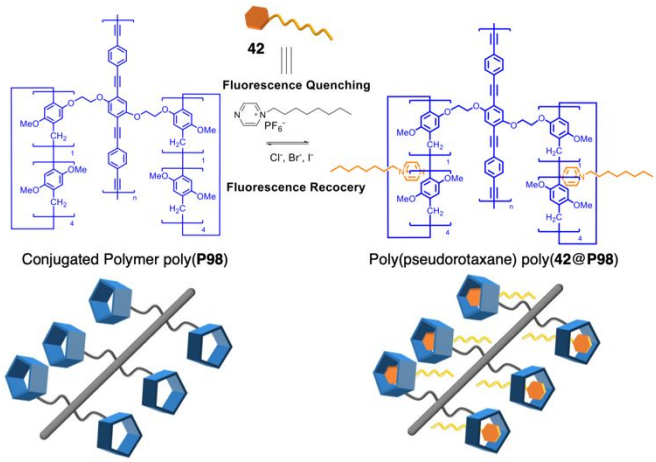


**Fig. 40** Structures of conjugated polymer poly(**P98**) and poly(pseudorotaxane) poly(**42@P98**), and their response to halogen anions.

With pillar[5]arene-modified poly(phenylene-ethynylene-butadiynylene)s poly(**P98**) and *n*-octylpyrazinium hexafluorophosphate (**42**), the first side-chain poly(pseudorotaxane), poly(**42@P98**), was synthesized by the Wang group. Owing to electron transfer from the electron-rich backbone to the *n*-octylpyrazinium cations, the fluorescence intensity of the poly(pseudorotaxane) was weaker than that of the pristine conjugated polymer. Upon interacting with halogen anions, fluorescence recovered owing to the strong binding between *n*-octylpyrazinium cations and halogen anions (Fig. 40). Therefore, the fluorescence was enhanced in the order of $I^- > Br^- > Cl^-$, which was consistent with their binding affinities for *n*-octylpyrazinium cations. Furthermore, under UV light, the differences in fluorescence intensity were easily distinguished by the naked eye, enabling the poly(pseudorotaxane)s to sense anions efficiently.[207,208]
Arunachalam and coworkers reported an anion-responsive poly(pseudorotaxane), poly(**43@P99**), based on polymer poly(**P99**) with pillar[5]arenes on the side chains and bispyridinium guests (Fig. 41a). The polymer was constructed by the ring-opening metathesis polymerization of pillar[5]arene **P99**, which was monofunctionalized with an oxanorbornene subunit. Pillar[5]arenes hosted bispyridinium **43** through supramolecular interactions, affording a crosslinked

poly(pseudorotaxane) assembly. Owing to the strong attraction between pyridinium cations and chloride anions, the assembly was destroyed when mixed with chloride anions.[209]

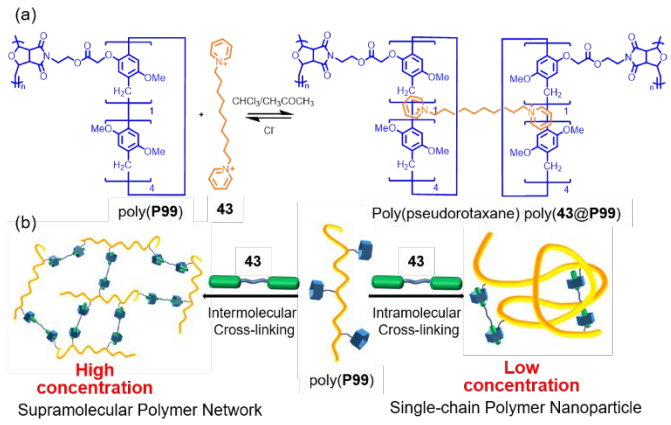


**Fig. 41** (a) Structure of poly(pseudorotaxane) poly(**43**@**P99**) and its response to chloride. (b) Formation of supramolecular network and single-chain polymer nanoparticles from polymer poly(**P99**).

When polymer poly(**P99**) interacted with the bisimidazolium guest at high concentration, a supramolecular network formed through intermolecular crosslinking. In contrast, highly dilute conditions promoted dominant intramolecular crosslinking, which resulted in single-chain polymer nanoparticle formation (Fig. 41b). These assemblies are based on the formation of poly(pseudorotaxane)s between pillar[5]arenes on the side chain and the bisimidazolium guest, which was attributed to their host–guest interaction.[210]

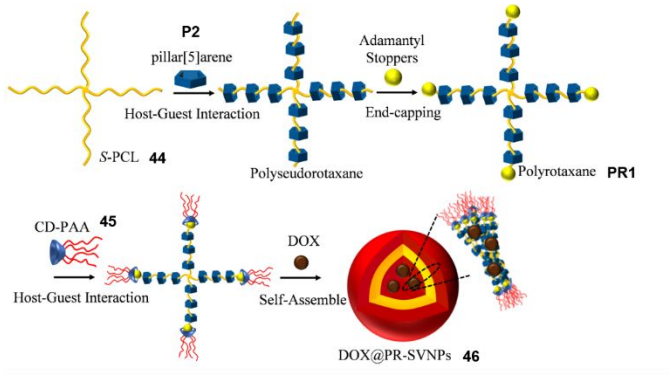


**Fig. 42** Synthesis of vesicle nanoparticles **46** from polyrotaxane **PR1** and its encapsulation of drug DOX.

Using star-poly(ε-caprolactone) (*S*-PCL) as the axles, perethylated pillar[5]arene **P2** as the wheels, and adamantane as the end-capping group, Li and coworkers synthesized polyrotaxane **PR1**, which was further assembled with β-cyclodextrin (CD) end-capped poly(acrylic acid) (CD-PAA) **45** through host–guest interactions between the macrocycles and the adamantane stoppers. In aqueous solution, this supramolecular polymer self-assembled to yield supramolecular vesicle nanoparticles **46** (PR-SVNPs), which showed a significantly improved drug loading capacity for DOX, probably due to the decreased crystallinity of *S*-PCL after polyrotaxane formation (Fig. 42). The loaded drugs were released selectively in an acidic microenvironment owing to the installed pH-stimulated CD-PAA. Furthermore, DOX@PR-SVNPs exhibited extremely low toxicity, highly efficient intra-tumoral accumulation, and substantial antitumor efficacy *in vivo*.[211]

Through strain-promoted azide–alkyne cycloaddition, conjugated polymers poly(**P100**) and poly(**47**), which contained pillar[5]arenes and cyanoalkane chains as side chains, respectively, were constructed (Fig. 43). Based on the host–guest interactions between pillar[5]arenes and cyanoalkanes when mixing the two polymers together, poly(pseudorotaxane) formed along the side chains, furnishing supramolecular organogels poly(**47**)@poly(**P100**). Upon exposing the gels to TFA vapor, imine bonds on the main chains were hydrolysed, causing degradation. The gels recovered after treatment with molecular sieves and triethylamine. Although the hydrolysis was reversible, gel reformation was not complete, resulting in a decreased Young's modulus for the reformed gels. Furthermore, as the gels originated from the crosslinked polymer chains via reversible supramolecular interactions, self-healing properties were observed after severing and reattaching.[212]

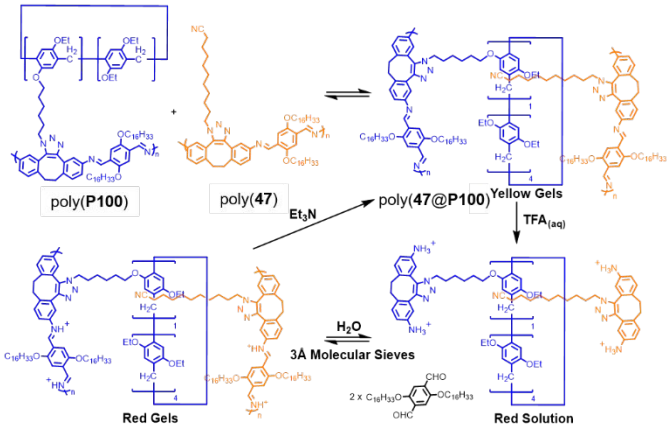


**Fig. 43** Reversible gel formation of the organo-gel based on poly(pseudorotaxane) poly(**47**)@poly(**P100**).

### Polyrotaxanes using linear polymers as axles

In 2010, our group reported new pseudopolyrotaxane **A42**@**P3**$_n$ and polyrotaxane **PR2** from a viologen polymer and perhydroxy-substituted pillar[5]arene (Fig. 44).[32,33] Based on supramolecular interaction between the cationic viologen and electron-rich pillar[5]arene cavity, complexation proceeded rapidly at room temperature. While heating the polyrotaxane solution, the colour changed from yellow to violet, which was a specific phenomenon not observed for the pseudopolyrotaxane counterpart. A mechanism was proposed, in which the viologen

radical cation partially forms at room temperature as the polymer chain is covered by pillar[5]arene electron donors, which shuttle slowly owing to intermolecular hydrogen bonds. Upon heating, the hydrogen bonds weaken, as deduced from the upfield shift of the OH proton signals in variable-temperature $^1$H NMR spectra, inducing faster movement along the polymer chain. Therefore, efficient electron transfer between pillar[5]arenes and viologen subunits occurred on the whole polymer and stabilized the radical cation species. This is the first electron transfer system based on a thermally sensitive polyrotaxane.

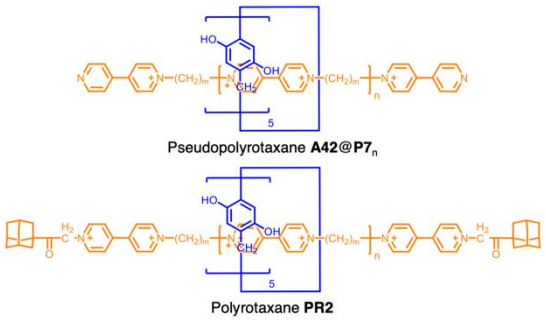


**Fig. 44** Structures of pseudopolyrotaxane **A42@P3**$_n$ and polyrotaxane **PR2**.

Electronic communication was also observed in pseudopolyrotaxane PANI@**P3**$_n$ from polyaniline (PANI) and perhydroxy-substituted pillar[5]arene (Fig. 45). After mixing the emeraldine base (EB) form of PANI and pillar[5]arene, the blue solution faded over time and become colourless after 180 min. The isosbestic point at 389 nm in UV–vis spectra and new emission at 416 nm in the emission spectra both confirmed formation of the leucoemeraldine base (LB) form of PANI. Meanwhile, a C=O stretching band appeared in the FT-IR spectra, which was attributed to the benzoquinone produced by oxidation of the hydroquinone subunits in pillar[5]arene. Therefore, PANI was reduced by the perhydroxy-substituted pillar[5]arene. Compared with hydroquinone, the macrocycle showed high efficiency in the reduction of PANI, because the formed pseudopolyrotaxane enabled close contact between reducing reagent pillar[5]arene and oxidizing substrate PANI. This is the first example of enhancing the reducing ability of a reductant by constructing supramolecular structures.[213]

In addition to forming pseudopolyrotaxanes with cationic or electron-deficient polymers, pillar[5]arenes also fit well with electron-neutral linear polymers, such as polyethylene (PE) and poly(ethylene oxide)s (PEOs).

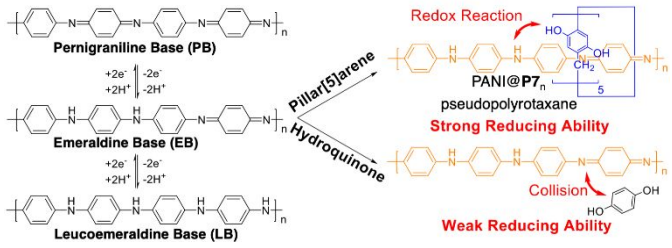


**Fig. 45** Structures of different PANIs and pseudopolyrotaxane PANI@**P3**$_n$; and the different reducing ability between pillar[5]arene and hydroquinone.

The lack of functional groups and low solubility in organic solvents of PE limits the preparation of PE-based pseudopolyrotaxanes (Fig. 46a).[214] However, multiple C–H/π interactions between PE and pillar[5]arene provide practical tools to overcome this challenge. At 140 °C, the melt mixing of per-*n*-pentylated pillar[5]arene **P101**, which melts at 83 °C, and high-density PE (HDPE), which melts at 126 °C, furnished pseudopolyrotaxane HDPE@**P101**$_n$. Complexation was indicated by solidification occurring after mixing the melted liquids. This was corroborated by measurements showing a new endothermic peak at 152 °C. The sample containing 70 wt% pillar[5]arene was optimal for forming pseudopolyrotaxane, because weak and no endothermic peaks were observed for HDPE and pillar[5]arene melting. Furthermore, the dual melting endothermic peaks at 126 and 152 °C indicated the increased melting point of PE chains, which was attributed to extension of the polymer chain through pseudopolyrotaxane formation. This provides a new chemical method for extending PE chains. By adding 1,4-dibromobutane (**48**) to the solid mixture of HDPE and pillar[5]arene at 140 °C, destruction of the pseudopolyrotaxane by the newly formed host–guest complex between **48** and pillar[5]arenes induced a solid-to-molten state transition.[215]

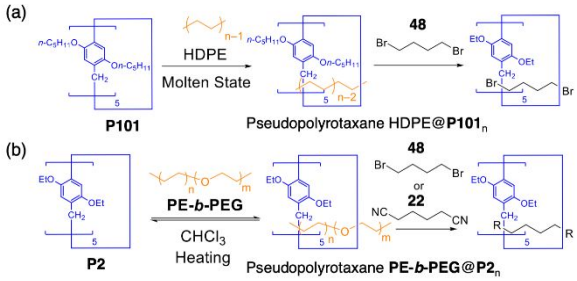


**Fig. 46** (a) Synthesis of pseudopolyrotaxane HDPE@**P101**$_n$ and its response to 1,4-dibromobutane. (b) Synthesis of pseudopolyrotaxane **PE-*b*-PEG@P2**$_n$ and its dual response to heat and competing guests.

Similar pseudopolyrotaxanes have also been constructed using monohydroxy-terminated **PE-*b*-PEG1400** or **PE-*b*-PEG2250** and perethylated pillar[5]arene **P2** in chloroform (Fig. 46b). The formation of pseudopolyrotaxane **PE-*b*-PEG@P2**$_n$ was evidenced by the upfield shift and splitting of the $^1$H NMR signal for the methylene proton on the PE chain, which was attributed to the shielding effect of the surrounding pillar[5]arenes, and NOE correlation signals between the methylene protons on the PE chain and the methyl and methylene protons on the pillar[5]arene. The solution of **PE-*b*-PEG1400** in chloroform was turbid at room temperature, and turned transparent after adding pillar[5]arene, indicating the higher solubility of the pseudopolyrotaxane compared with the polymer chain. Furthermore, adding a competing guest, such as 1,4-dibromobutane (**48**) or dicyanobutane (**22**), made the solution

turbid again. In the $^1$H NMR spectra of pseudopolyrotaxanes, the shielded methylene protons on PE chains became unshielded upon heating or adding competitive guests, which both suggested disassembly of the pseudopolyrotaxanes. Similar NMR changes were observed when heating the solution of **PE-*b*-PEG@P2**$_n$. Therefore, pseudopolyrotaxane **PE-*b*-PEG@P2**$_n$ is dual responsive to heating and competitive guests.[216]

Pseudopolyrotaxane PEO@**P7**$_n$ was prepared from poly(ethylene oxide)s (PEOs) and perhydroxy-substituted pillar[5]arene **P7** in a mixed methanol/water solvent (Fig. 47). The multiple hydrogen bonds and hydrophobic effect were the driving forces of threading. When using 1-adamantanamine (**49**) as the stopper, polyrotaxane **PR3** was constructed and showed higher thermal stability than its counterpart obtained from α-CD and PEOs. This was caused by the more rigid backbone in the pillar[5]arene, which was constructed by aromatic benzenes, than that in α-CD, which is constructed from sugar subunits. Furthermore, owing to the multiple hydrogen bonds inside, **PR3** exhibited thermoplastic behaviour and shape memory properties without further functionalization or crosslinking.[217]

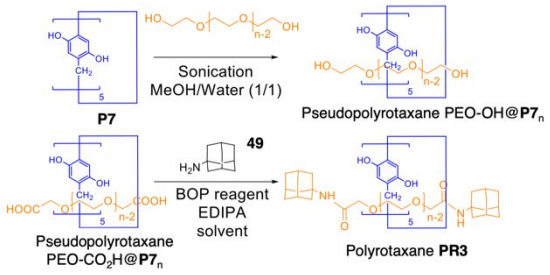


**Fig. 47** Synthesis of pseudopolyrotaxane PEO@**P7**$_n$ and polyrotaxane **PR3**.

Pseudopolyrotaxanes between PEOs and perethylated pillar[5]arene were prepared through crystalline-state complexation (Fig. 48). The macrocycle was first activated by removing solvents in the crystal through heating, and then immersed with excess melted PEOs at 80 °C. After filtration and washing with water, the pseudopolyrotaxanes were obtained. Dissolving the complex in $CDCl_3$ caused dethreading of the polymer chain, indicating the efficiency of crystalline-state complexation. According to PXRD measurements, as observed in the assembled structure of the pristine crystal, pillar[5]arene in the pseudopolyrotaxanes remained in a 1D channel, in which the PEO chains fitted. The motion of PEOs in the channel was considerably limited owing to the snug fit. When pillar[5]arene was immersed with an equal-weight mixture of PEOs with different molecular weights, selectively uptake of the PEOs with a high mass fraction occurred, which can be attributed to the multiple C–H/π interactions between the polymer chain and macrocycles preferring to guarantee effective coverage. The threading process was also affected by the end groups of the PEOs. OH- and $NH_2$-terminated PEOs showed slower speeds than PEO with OMe terminals owing to hydrogen bonding. For $CO_2H$ and tosyl derivatives, the threading process was much slower owing to electronic repulsion and steric hindrance, respectively.[218]

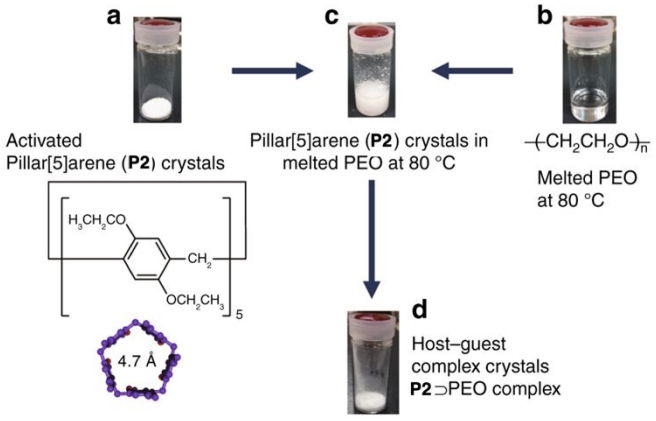


**Fig. 48** Encapsulation of PEOs with perethylated pillar[5]arene through crystalline-state complexation. Reproduced with permission from ref. 218. Copyright 2019 Springer Nature.

A topological gel based on the polyrotaxane of pillar[5]arene and poly(tetrahydrofuran) (PTHF) was prepared (Fig. 49a). Modifying pillar[5]arenes with tri(ethylene oxide) chains reduced the crystallinity of the macrocycles, making them liquid at room temperature. The cyclic host liquids (CHLs) can act as both hosts and solvents during complexation, yielding polyrotaxanes **PR4** and **PR5**, consisting of pillar[5]arene and PTHF, in moderate yield. Meanwhile, the yields in solvent were relatively low. By changing the feed ratio between CHLs and PTHF, the number of wheels changed. Terminal olefins on host molecule **PR5** were crosslinked by olefin metathesis to furnish a topological gel. The obtained gel swelled in solvents with intermediate dielectric constants ($4<\varepsilon<10$), such as dichloromethane, chloroform, and tetrahydrofuran.[219]

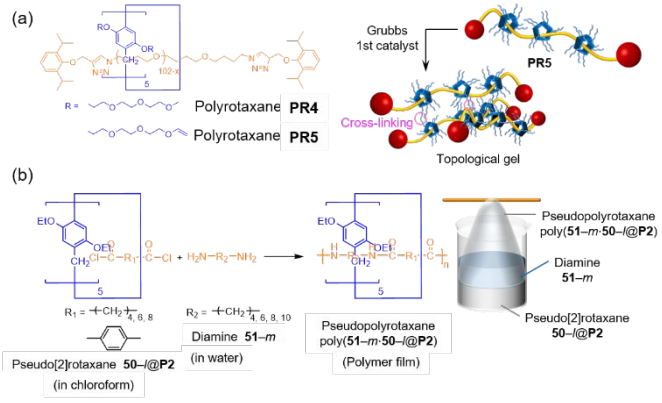


**Fig. 49** (a) Structures of polyrotaxanes **PR4** and **PR5**. (b) Synthesis of pseudopolyrotaxane poly(**51**–*m*·**50**–*l*@**P2**) from pseudo[2]rotaxane **50**–*l*@**P2** and diamine **51**–*m* through interfacial polymerization.

Our group recently reported the first example of a pseudopolyrotaxane based on pillar[n]arenes and polyamides

(Fig. 49b). As the low solubility of polyamides limited the construction of polyamide-based pseudopolyrotaxanes, interfacial polymerization was applied. To a chloroform solution of host–guest complex **50**–*l*@**P2** between perethylated pillar[5]arene and dicarbonyl chloride, an aqueous solution of diamine **51**–*m* was added slowly. Afterwards, at the interface between chloroform and water, a polymer film was generated, which was purified by washing with hot water, methanol, and chloroform. As the sample was not soluble in typical solvents, solid-state NMR and FT-IR measurements were conducted to confirm the formation of pseudopolyrotaxane poly(**51**–*m*·**50**–*l*@**P2**). To produce a high coverage ratio of pillar[5]arenes, the lengths of dicarbonyl chloride and the association constants between the dicarbonyl chloride and pillar[5]arenes should be balanced, with longer lengths increasing the polymerization efficiency, but decreasing the host–guest interaction efficiency. Compound **50**–8 was found to be optimal for obtaining the highest coverage ratio.[220]

## Conclusions and Perspectives

The first examples of MIMs, such as catenanes and rotaxanes, were reported in the 1960s.[221,222] Since then, MIMs using various host molecules, such as crown ethers, cyclodextrins, calix[*n*]arenes, cucurbit[*n*]urils, and blue boxes have been synthesized. In 2008, we first reported pillar[*n*]arenes, which initiated research on the synthesis of pillar[*n*]arene-based MIMs. In the last 14 years, numerous pillar[*n*]arene-based MIMs have been reported,[223–225] because pillar[*n*]arenes have various advantages for MIM design, synthesis, and applications. The highly symmetrical pillar-shaped and regular polygonal structures of pillar[*n*]arenes are advantageous for the characterization of MIMs with complex structures and analysis of their ring motion. Good solubility, which depends on the substituents, and superior host–guest properties in organic media are important for preparing MIMs in high yields, because host–guest complexes before interlocked structures are stable in organic media, and various synthetic reactions that mainly proceed in organic solvents can be used for MIMs synthesis. The versatile functionality of pillar[*n*]arenes has led to the synthesis of MIMs with functions and controlled molecular motion by introducing functional groups into pillar[*n*]arenes. However, the further expansion of pillar[*n*]arene-based MIMs is still needed, and the challenges faced based on unique pillar[*n*]arene properties are as follows:

(i) Control of planar chirality: Asymmetric synthesis of planar chiral MIMs, chiral transfer, and amplification of the planar chirality of pillar[*n*]arenes through MIMs formation are interesting topics based on the planar chirality of pillar[*n*]arenes.

(ii) Complex dynamics: Units in higher pillar[*n*]arene ($n > 6$) rings can rotate, even though formation of the [2]rotaxane,[83,88] because there are still spaces in the cavity, even in the presence of the axle. Therefore, the motion of the constituent units, in addition to the rotational and shuttling motion of the pillar[*n*]arene rings, are unique properties in pillar[*n*]arene-based MIMs.

(iii) Solid-state complexation: As pillar[*n*]arenes can even form host–guest complexes in the solid state,[226] the solid-state synthesis of MIMs and motion of the pillar[*n*]arene rings of MIMs in the solid state are new research directions for pillar[*n*]arene-based MIMs.

Therefore, despite various examples of pillar[*n*]arene-bead MIMs having been reported, many exciting long-term possibilities have yet to be investigated.

## Conflicts of interest

There are no conflicts to declare.

## Acknowledgements

This work was supported by JSPS KAKENHI Grant Numbers JP20K22528 (Research Activity Start-up, K.K.), JP21K14611 (Early-Career Scientists, K.K.), JP21K14612 (Early-Career Scientists, S.F.), JP21K20533 (Research Activity Start-up, S.O.), JP15H00990, JP17H05148, JP18H04510, and JP20H04670 (Scientific Research on Innovative Areas, T.O.), and JP19H00909 (Scientific Research (A), T.O.), JST CREST Grant Number JPMJCR18R3 (T.O.), and the MEXT World Premier International Research Center Initiative (WPI), Japan. We thank Simon Partridge, PhD, from Edanz (https://jp.edanz.com/ac) for editing a draft of this manuscript.

## Notes and references

1. B. Champin, P. Mobian and J.-P. Sauvage, *Chem. Soc. Rev.*, 2007, **36**, 358.
2. A. Coskun, M. Banaszak, R. D. Astumian, J. F. Stoddart and B. A. Grzybowski, *Chem. Soc. Rev.*, 2012, **41**, 19.
3. J. D. Crowley, S. M. Goldup, A.-L. Lee, D. A. Leigh and R. T. McBurney, *Chem. Soc. Rev.*, 2009, **38**, 1530.
4. K. D. Hanni and D. A. Leigh, *Chem. Soc. Rev.*, 2010, **39**, 1240.
5. C. Pezzato, C. Cheng, J. F. Stoddart and R. D. Astumian, *Chem. Soc. Rev.*, 2017, **46**, 5491.
6. J. F. Stoddart, *Chem. Soc. Rev.*, 2009, **38**, 1802.
7. M. Baroncini, S. Silvi and A. Credi, *Chem. Rev.*, 2020, **120**, 200.
8. R. S. Forgan, J.-P. Sauvage and J. F. Stoddart, *Chem. Rev.*, 2011, **111**, 5434.
9. M. Xue, Y. Yang, X. Chi, X. Yan and F. Huang, *Chem. Rev.*, 2015, **115**, 7398.
10. F. M. Raymo and J. F. Stoddart, *Chem. Rev.*, 1999, **99**, 1643.
11. Y. Okumura and K. Ito, *Adv. Mater.*, 2001, **13**, 485.
12. T. Sakai, H. Murayama, S. Nagano, Y. Takeoka, M. Kidowaki, K. Ito and T. Seki, *Adv. Mater.*, 2007, **19**, 2023.
13. H. Gotoh, C. Liu, A. B. Imran, M. Hara, T. Seki, K. Mayumi, K. Ito and Y. Takeoka, *Sci. Adv.*, 2018, **4**, eaat7629.
14. G. Crini, *Chem. Rev.*, 2014, **114**, 10940.
15. G. Wenz, B.-H. Han and A. Müller, *Chem. Rev.*, 2006, **106**, 782.
16. A. Harada, A. Hashidzume, H. Yamaguchi and Y. Takashima, *Chem. Rev.*, 2009, **109**, 5974.
17. J. W. Lee, S. Samal, N. Selvapalam, H.-J. Kim and K. Kim, *Acc. Chem. Res.*, 2003, **36**, 621.

18. J. Lagona, P. Mukhopadhyay, S. Chakrabarti and L. Isaacs, *Angew. Chem. Int. Ed.*, 2005, **44**, 4844.
19. C. J. Pedersen, *J. Am. Chem. Soc.*, 1967, **89**, 7017.
20. A. Ikeda and S. Shinkai, *Chem. Rev.*, 1997, **97**, 1713.
21. N. Morohashi, F. Narumi, N. Iki, T. Hattori and S. Miyano, *Chem. Rev.*, 2006, **106**, 5291.
22. D.-S. Guo and Y. Liu, *Acc. Chem. Res.*, 2014, **47**, 1925.
23. E. J. Dale, N. A. Vermeulen, M. Juríček, J. C. Barnes, R. M. Young, M. R. Wasielewski and J. F. Stoddart, *Acc. Chem. Res.*, 2016, **49**, 262.
24. I. Neira, A. Blanco-Gómez, J. M. Quintela, M. D. García and C. Peinador, *Acc. Chem. Res.*, 2020, **53**, 2336.
25. W. Liu and J. F. Stoddart, *Chem*, 2021, **7**, 919.
26. T. Ogoshi, S. Kanai, S. Fujinami, T. Yamagishi and Y. Nakamoto, *J. Am. Chem. Soc.*, 2008, **130**, 5022.
27. M. Xue, Y. Yang, X. D. Chi, Z. B. Zhang and F. H. Huang, *Acc. Chem. Res.*, 2012, **45**, 1294.
28. T. Ogoshi, T. Yamagishi and Y. Nakamoto, *Chem. Rev.*, 2016, **116**, 7937.
29. N. Song, T. Kakuta, T. Yamagishi, Y. W. Yang and T. Ogoshi, *Chem*, 2018, **4**, 2029.
30. W. Si, P. Xin, Z. T. Li and J. L. Hou, *Acc. Chem. Res.*, 2015, **48**, 1612.
31. N. L. Strutt, H. C. Zhang, S. T. Schneebeli and J. F. Stoddart, *Acc. Chem. Res.*, 2014, **47**, 2631.
32. T. Ogoshi, Y. Nishida, T. Yamagishi and Y. Nakamoto, *Macromolecules*, 2010, **43**, 3145.
33. T. Ogoshi, Y. Nishida, T. Yamagishi and Y. Nakamoto, *Macromolecules*, 2010, **43**, 7068.
34. N. L. Strutt, R. S. Forgan, J. M. Spruell, Y. Y. Botros and J. F. Stoddart, *J. Am. Chem. Soc.*, 2011, **133**, 5668.
35. T. Kakuta, T. Yamagishi and T. Ogoshi, *Acc. Chem. Res.*, 2018, **51**, 1656.
36. L.-J. Chen and H.-B. Yang, *Acc. Chem. Res.*, 2018, **51**, 2699.
37. T. Ogoshi, K. Demachi, K. Kitajima and T. Yamagishi, *Chem. Commun.*, 2011, **47**, 10290.
38. Z. Zhang, Y. Luo, J. Chen, S. Dong, Y. Yu, Z. Ma and F. Huang, *Angew. Chem. Int. Ed.*, 2011, **50**, 1397.
39. T. Ogoshi, R. Sueto, K. Yoshikoshi, Y. Sakata, S. Akine and T. Yamagishi, *Angew. Chem. Int. Ed.*, 2015, **54**, 9849.
40. T. Kakuta, T. Yamagishi and T. Ogoshi, *Chem. Commun.*, 2017, **53**, 5250.
41. K. Han, Y. Zhang, J. Li, Y. Yu, X. Jia and C. Li, *Eur. J. Org. Chem.*, 2013, 2057.
42. T. Ogoshi, S. Takashima and T. Yamagishi, *J. Am. Chem. Soc.*, 2015, **137**, 10962.
43. T. Ogoshi, D. Kotera, S. Nishida, T. Kakuta, T. Yamagishi and A. M. Brouwer, *Chem. Eur. J.*, 2018, **24**, 6325.
44. G. Yu, C. Han, Z. Zhang, J. Chen, X. Yan, B. Zheng, S. Liu and F. Huang, *J. Am. Chem. Soc.*, 2012, **134**, 8711.
45. W. Xia, X. Y. Hu, Y. Chen, C. Lin and L. Y. Wang, *Chem. Commun.*, 2013, **49**, 5085.
46. T. Ogoshi, K. Demachi, K. Kitajima and T. Yamagishi, *Chem. Commun.*, 2011, **47**, 7164.
47. T. Ogoshi, H. Kayama, D. Yamafuji, T. Aoki, K. Kitajima and T. Yamagishi, *Chem. Sci.*, 2012, **3**, 3221.
48. T. Ogoshi, D. Yamafuji, D. Kotera, T. Aoki, S. Fujinami and T. Yamagishi, *J. Org. Chem.*, 2012, **77**, 11146.
49. C. Han, Z. Zhang, G. Yu and F. Huang, *Chem. Commun.*, 2012, **48**, 9876.
50. T. Ogoshi, M. Hashizume, T. Yamagishi and Y. Nakamoto, *Chem. Commun.*, 2010, **46**, 3708.
51. T. Ogoshi, K. Kida and T. Yamagishi, *J. Am. Chem. Soc.*, 2012, **134**, 20146.
52. J. Ding, J. Chen, W. Mao, J. Huang and D. Ma, *Org. Biomol. Chem.*, 2017, **15**, 7894.
53. W. Yang, K. Samanta, X. Wan, T. U. Thikekar, Y. Chao, S. Li, K. Du, J. Xu, Y. Gao, H. Zuilhof and A. C.-H. Sue, *Angew. Chem. Int. Ed.*, 2020, **59**, 3994.
54. M. Guo, X. Wang, C. Zhan, P. Demay-Drouhard, W. Li, K. Du, M. A. Olson, H. Zuilhof and A. C.-H. Sue, *J. Am. Chem. Soc.*, 2018, **140**, 74.
55. Y. Chao and A. C.-H. Sue, *Supramol. Chem.*, 2022, DOI:10.1080/10610278.2022.2039653.
56. T. Ogoshi, K. Umeda, T. Yamagishi and Y. Nakamoto, *Chem. Commun.*, 2009, 4874.
57. N. L. Strutt, D. Fairen-Jimenez, J. Iehl, M. B. Lalonde, R. Q. Snurr, O. K. Farha, J. T. Hupp and J. F. Stoddart, *J. Am. Chem. Soc.*, 2012, **134**, 17436.
58. T. Ogoshi, D. Yamafuji, T. Akutsu and T. Yamagishi, *Chem. Commun.*, 2013, **49**, 8782.
59. H. Zhang, J. Han and C. Li, *Polym. Chem.*, 2021, **12**, 2808.
60. S. Fa, T. Kakuta, T. Yamagishi and T. Ogoshi, *Chem. Lett.*, 2019, **48**, 1278.
61. T. Ogoshi, D. Yamafuji, T. Aoki, K. Kitajima, T. Yamagishi, Y. Hayashi and S. Kawauchi, *Chem. Eur. J.*, 2012, **18**, 7493.
62. X.-B. Hu, L. Chen, W. Si, Y. Yu and J.-L. Hou, *Chem. Commun.*, 2011, **47**, 4694.
63. G. Liang, G. Wu, H. Wang, J. Su, H. Li, Q. Lin, Y. Zhang and T. Wei, *J. Incl. Phenom. Macrocycl. Chem.*, 2016, **86**, 173.
64. T. Ogoshi, D. Yamafuji, T. Aoki and T. Yamagishi, *Isr. J. Chem.*, 2018, **58**, 1246.
65. C. Li, L. Zhao, J. Li, X. Ding, S. Chen, Q. Zhang, Y. Yu and X. Jia, *Chem. Commun.*, 2010, **46**, 9016.
66. H. Chen, X. Jia and C. Li, Chin. J. Chem., 2015, 33, 343.
67. Y. Zhou, K. Jie, C. Thompson, N. Li and Y. Yao, *Tetrahedron Lett.*, 2015, **56**, 2091.
68. J. Kiruthika, S. Srividhya and M. Arunachalam, *Org. Lett.*, 2020, **22**, 7831.
69. T. Ogoshi, T. Akutsu, Y. Shimada and T. Yamagishi, *Chem. Commun.*, 2016, **52**, 6479.
70. T. Ogoshi, D. Yamafuji, T. Aoki and T. Yamagishi, *J. Org. Chem.*, 2011, **76**, 9497.
71. S. Xiong, X. Zhang, L.-B. Meng, J. Jiang, C. Lin and L. Wang, *Chem. Commun.*, 2015, **51**, 6504.
72. X. Yan, P. Wei, Z. Li, B. Zheng, S. Dong, F. Huang and Q. Zhou, *Chem. Commun.*, 2013, **49**, 2512.
73. S. Dong, C. Han, B. Zheng, M. Zhang and F. Huang, *Tetrahedron Lett.*, 2012, **53**, 3668.
74. R. Milev, A. Lopez-Pacheco, I. Nierengarten, T. M. N. Trinh, M. Holler, R. Deschenaux and J.-F. Nierengarten, *Eur. J. Org. Chem.*, 2015, 479.
75. I. Nierengarten, E. Meichsner, M. Holler, P. Pieper, R. Deschenaux, B. Delavaux-Nicot and J.-F. Nierengarten, *Chem. Eur. J.*, 2018, **24**, 169.
76. M. Holler, T. Stoerkler, A. Louis, F. Fischer and J.-F. Nierengarten, *Eur. J. Org. Chem.*, 2019, 3401.
77. T. Ogoshi, T. Aoki, R. Shiga, R. Iizuka, S. Ueda, K. Demachi, D. Yamafuji, H. Kayama and T. Yamagishi, *J. Am. Chem. Soc.*, 2012, **134**, 20322.
78. T. Ogoshi, Y. Tamura, D. Yamafuji, T. Aoki and T. Yamagishi, *Chem. Commun.*, 2016, **52**, 10297.
79. T. Ogoshi, R. Iizuka, D. Kotera and T. Yamagishi, *Org. Lett.*, 2015, **17**, 350.
80. P. Wei, X. Yan, J. Li, Y. Ma, Y. Yao and F. Huang, *Tetrahedron*, 2012, **68**, 9179.
81. J. Ye, R. Zhang, W. Yang, Y. Han, H. Guo, J. Xie, C. Yan and Y. Yao, *Chin. Chem. Lett.*, 2020, **31**, 1550.

82. C. Ke, N. L. Strutt, H. Li, X. Hou, K. J. Harlieb, P. R. McGonigal, Z. Ma, J. Iehl, C. L. Stern, C. Cheng, Z. Zhu, N. A. Vermeulen, T. J. Meade, Y. Y. Botros and J. F. Stoddart, *J. Am. Chem. Soc.*, 2013, **135**, 17019.
83. X. Hou, C. Ke, C. Cheng, N. Song, A. K. Blackburn, A. A. Sarjeant, Y. Y. Botros, Y.-W. Yang and J. F. Stoddart, *Chem. Commun.*, 2014, **50**, 6196.
84. N. Pearce, K. E. A. Reynolds, S. Kayal, X. Z. Sun, E. S. Davies, F. Malagreca, C. J. Schürmann, S. Ito, A. Yamano, S. P. Argent, M. W. George and N. R. Champness, *Nat. Commun.*, 2022, **13**, 415.
85. L. Yang, P. Langer, E. S. Davies, M. Baldoni, K. Wickham, N. A. Besley, E. Besley and N. R. Champness, *Chem. Sci.*, 2019, **10**, 3723.
86. K. Kitajima, T. Ogoshi and T. Yamagishi, *Chem. Commun.*, 2014, **50**, 2925.
87. W.-B. Hu, W.-J. Hu, X.-L. Zhao, Y. A. Liu, J.-S. Li, B. Jiang and K. Wen, *Chem. Commun.*, 2015, **51**, 13882.
88. T. Ogoshi, D. Yamafuji, T. Aoki, T. Yamagishi, *Chem. Commun.* 2012, **48**, 6842.
89. N. Sun, X. Xiao, W. Li and J. Jiang, *Adv. Sci.*, 2015, **2**, 1500082.
90. S. Dong, J. Yuan and F. Huang, *Chem. Sci.*, 2014, **5**, 247.
91. Z. Zhang, C. Han, G. Yu, F. Huang, *Chem. Sci.*, 2012, **3**, 3026.
92. W. J. Li, Q. Gu, X. Q. Wang, D. Y. Zhang, Y. T. Wang, X. He, W. Wang and H. B. Yang, *Angew. Chem. Int. Ed.*, 2021, **60**, 9507.
93. Y. Liu, C. Chipot, X. Shao and W. Cai, *J. Phys. Chem. C*, 2016, **120**, 6287.
94. S. Wang, X. Shao and W. Cai, *J. Phys. Chem. C*, 2017, **121**, 25547.
95. P. Langer, L. Yang, C. R. Pfeiffer, W. Lewis and N. R. Champness, *Dalton Trans.*, 2019, **48**, 58.
96. T. Ogoshi, D. Kotera, S. Fa, S. Nishida, T. Kakuta, T. Yamagishi and A. M. Brouwer, *Chem. Commun.*, 2020, **56**, 10871.
97. T. Ogoshi, D. Yamafuji, T. Yamagishi and A. M. Brouwer, *Chem. Commun.*, 2013, **49**, 5468.
98. L. Ma, S. Wang, C. Li, D. Cao, T. Li and X. Ma, *Chem. Commun.*, 2018, **54**, 2405.
99. E. Meichsner, I. Nierengarten, M. Holler, M. Chessé, J.-F. Nierengarten, *Helv. Chim. Acta*, 2018, **101**, e1800059.
100. M. Rémy, I. Nierengarten, B. Park, M. Holler, U. Hahn, J. F. Nierengarten, *Chem. Eur. J.*, 2021, **27**, 8492.
101. N. Sun, X. Xiao, W. Li and J. Jiang, *Adv. Sci.*, 2015, **2**, 1500082.
102. T. M. N. Trinh, I. Nierengarten, M. Holler, J.-L. Gallani, J.-F. Nierengarten, *Chem. Eur. J.*, 2015, **21**, 8019.
103. M. Steffenhagen, A. Latus, T. M. N. Trinh, I. Nierengarten, I. T. Lucas, S. Joiret, J. Landoulsi, B. Delavaux-Nicot, J. F. Nierengarten, E. Maisonhaute, *Chem. Eur. J.*, 2018, **24**, 1701.
104. S. P. Vincent, K. Buffet, I. Nierengarten, A. Imberty, J. F. Nierengarten, *Chem. Eur. J.* 2016, **22**, 88.
105. G. Yu, D. Wu, Y. Li, Z. Zhang, L. Shao, J. Zhou, Q. Hu, G. Tang and F. Huang, *Chem. Sci.*, 2016, **7**, 3017.
106. N. Song, D.-X. Chen, Y.-C. Qiu, X.-Y. Yang, B. Xu, W. Tian and Y.-W. Yang, *Chem. Commun.*, 2014, **50**, 8231.
107. W. J. Li, Q. Gu, X. Q. Wang, D. Y. Zhang, Y. T. Wang, X. He, W. Wang, H. B. Yang, *Angew. Chem. Int. Ed.*, 2021, **60**, 9507.
108. Q. Li, Y. Wu, Y. Liu, L. Shangguan, B. Shi and H. Zhu, *Org. Lett.*, 2020, **22**, 6662.
109. H. Chong, Y. Xu, Y. Han, C. Yan, D. Su, and C. Wang, *ChemistrySelect*, 2021, **6**, 9363.
110. L. Liu, D. Cao, Y. Ji, H. Tao, Y. Kou and H. Meier, *Org. Biomol. Chem.*, 2011, **9**, 7007.
111. Y. Chen, D. Cao, L. Wang, M. He, L. Zhou, D. Schollmeyer and H. Meier, *Chem. Eur. J.*, 2013, **19**, 7064.
112. W.-X. Zhang, L.-Z. Liu, W.-G. Duan, Q.-Q. Zhou, C.-G. Ma and Y. Huang, *Molecules*, 2019, **24**, 2693.
113. B. Xia and M. Xue, *Chem. Commun.*, 2014, **50**, 1021.
114. Y. Han, G.-F. Huo, J. Sun, J. Xie, C.-G. Yan, Y. Zhao, X. Wu, C. Lin and L. Wang, *Sci. Rep.*, 2016, **6**, 28748.
115. S. Jiang, Y. Han, J. Sun, C.-G. Yan, *Tetrahedron*, 2017, **73**, 5107.
116. L.-L. Zhao, Y. Han and C.-G. Yan, *Chin. Chem. Lett.*, 2020, **31**, 81.
117. R. Zhang, C. Wang, R. Long, T. Chen, C. Yan and Y. Yao, *Front. Chem.*, 2019, **7**, 508.
118. X.-S. Du, C.-Y. Wang, Q. Jia, R. Deng, H.-S. Tian, H.-Y. Zhang, K. Meguellati and Y.-W. Yang, *Chem. Commun.*, 2017, **53**, 5326.
119. Y. Han, G.-F. Huo, J. Sun, C.-G. Yan, Y. Lu and C. Lin, *Supramol. Chem.*, 2017, **29**, 547.
120. H. Tian, C. Wang, P.-H. Lin and K. Meguellati, *Tetrahedron Lett.*, 2018, **59**, 3416.
121. C.-L. Sun, J.-F. Xu, Y.-Z. Chen, L.-Y. Niu, L.-Z. Wu, C.-H. Tung and Q.-Z. Yang, *Chin. Chem. Lett.*, 2015, **26**, 843.
122. M. Ni, X.-Y. Hu, J. Jiang and L. Wang, *Chem. Commun.*, 2014, **50**, 1317.
123. Y. Guan, P. Liu, C. Deng, M. Ni, S. Xiong, C. Lin, X.-Y. Hu, J. Ma and L. Wang, *Org. Biomol. Chem.*, 2014, **12**, 1079.
124. X. Wu, M. Ni, W. Xia, X.-Y. Hu and L. Wang, *Org. Chem. Front.*, 2015, **2**, 1013.
125. X. Wu, L. Gao, J. Sun, X.-Y. Hu and L. Wang, *Chin. Chem. Lett.*, 2016, **27**, 1655.
126. Z. Zhao, Y. Chen, B. Sun, C. Qian, M. Cheng, J. Jiang, C. Lin and L. Wang, *Eur. J. Org. Chem.*, 2019, 3396.
127. H. Tian, R. Li, P.-H. Lin and K. Meguellati, *New. J. Chem.*, 2020, **44**, 10628.
128. T. Ogoshi, T. Furuta, Y. Hamada, T. Kakuta and T. Yamagishi, *Mater. Chem. Front.*, 2018, **2**, 597.
129. Y. Wang, Y. Tian, Y.-Z. Chen, L.-Y. Niu, L.-Z. Wu, C.-H. Tung, Q.-Z. Yang and R. Boulatov, *Chem. Commun.*, 2018, **54**, 7991.
130. Y.-H. Cui, R. Deng, Z. Li, X.-S. Du, Q. Jia, X.-H. Wang, K. Meguellati and Y.-W. Yang, *Mater. Chem. Front.*, 2019, **3**, 1427.
131. Z. Zhang, B. Xia, C. Han, Y. Yu and F. Huang, *Org. Lett.*, 2010, **12**, 3285.
132. T. Ogoshi, T. Akutsu, D. Yamafuji, T. Aoki and T. Yamagishi, *Angew. Chem. Int. Ed.*, 2013, **52**, 8111.
133. S.-H. Li, H.-Y. Zhang, X. Xu and Y. Liu, *Nat. Commun.*, 2015, **6**, 7590.
134. M. Cheng, Q. Wang, Y. Cao, Y. Pan, Z. Yang, J. Jiang and L. Wang, *Tetrahedron Lett.*, 2016, **57**, 4133.
135. Y.-F. Yang, W.-B. Hu, L. Shi, S.-G. Li, X.-L. Zhao, Y. A. Liu, J.-S. Li, B. Jiang and W. Ken, *Org. Biomol. Chem.*, 2018, **16**, 2028.
136. T. Ogoshi, T. Akutsu, T. Yamagishi, *Beilstein J. Org. Chem.*, 2018, **14**, 1937.
137. E. Lee, H. Ju, I.-H. Park, J. H. Jung, M. Ikeda, S. Kuwahara, Y. Habata and S. S. Lee, *J. Am. Chem. Soc.*, 2018, **140**, 9669.
138. H. Liang, B. Hua, F. Xu, L.-S. Gan, L. Shao and F. Huang, *J. Am. Chem. Soc.*, 2020, **142**, 19772.
139. J. Yao, W. Wu, W. Liang, Y. Feng, D. Zhou, J. J. Chruma, G. Fukuhara, T. Mori, Y. Inoue and C. Yang, *Angew. Chem. Int. Ed.*, 2017, **56**, 6869.
140. C. Fan, J. Yao, G. Li, C. Guo, W. Wu, D. Su, Z. Zhong, D. Zhou, Y. Wang, J. J. Chruma and C. Yang, *Chem. Eur. J.*, 2019, **25**, 12526.
141. J. Yao, H. Mizuno, C. Xiao, W. Wu, Y. Inoue, C. Yang and G. Fukuhara, *Chem. Sci.*, 2021, **12**, 4361.
142. C. Xiao, W. Wu, W. Liang, D. Zhou, K. Kanagaraj, G. Cheng, D. Su, Z. Zhong, J. J. Chruma and C. Yang, *Angew. Chem. Int. Ed.*, 2020, **59**, 8094.
143. J. Yao, W. Wu, C. Xiao, D. Su, Z. Zhong, T. Mori and C. Yang, *Nat. Commun.*, 2021, **12**, 2600.
144. W.-B. Hu, H.-M. Yang, W.-J. Hu, M.-L. Ma, X.-L. Zhao, X.-Q. Mi, Y. A. Liu, J.-S. Li, B. Jiang and K. Wen, *Chem. Commun.*, 2014, **50**, 10460.
145. W.-B. Hu, W.-J. Hu, Y. A. Liu, J.-S. Li, B. Jiang and K. Wen, *Org. Lett.*, 2015, **17**, 2940.

146. Q. Wang, M. Cheng, Y. Zhao, L. Wu, J. Jiang, L. Wang and Y. Pan, *Chem. Commun.*, 2015, **51**, 3623.
147. X.-L. Wu, Y. Chen, W.-J. Hu, Y. A. Liu, X.-S. Jia, J.-S. Li, B. Jiang and K. Wen, *Org. Biomol. Chem.*, 2017, **15**, 4897.
148. M. Cheng, J. Sun, C.-G. Yan, J. Jiang and L. Wang, *New J. Chem.*, 2018, **42**, 7603.
149. D. Li, Y. Han, J. Sun, W.-L. Liu and C.-G. Yan, *J. Incl. Phenom. Macrocycl. Chem.*, 2021, https://doi.org/10.1007/s10847-021-01115-0
150. Y. Han, C.-Y. Nie, S. Jiang, J. Sun and C.-G. Yan, *Chin. Chem. Lett.*, 2020, **31**, 725.
151. S. Jiang, Y. Han, L.-L. Zhao, J. Sun and C.-G. Yan, *Supramol. Chem.*, 2018, **30**, 642.
152. Y. Han, C.-Y. Nie, S. Jiang, J. Sun and C.-G. Yan, *J. Incl. Phenom. Macrocycl. Chem.*, 2022, **102**, 89.
153. M. Wang, X. Du, H. Tian, Q. Jia, R. Deng, Y. Cui, C. Wang and K. Meguellati, *Chin. Chem. Lett.*, 2019, **30**, 345.
154. Y. Han, L.-M. Xu, C.-Y. Nie, S. Jiang, J. Sun and C.-G. Yan, *Beilstein J. Org. Chem.*, 2018, **14**, 1660.
155. Z. Zhang, G. Yu, C. Han, J. Liu, X. Ding, Y. Yu and F. Huang, *Org. Lett.*, 2011, **13**, 4818.
156. L. Liu, L. Wang, C. Liu, Z. Fu, H. Meier and D. Cao, *J. Org. Chem.*, 2012, **77**, 9413.
157. T. F. Al-Azemi and M. Vinodh, *RSC Adv.*, 2021, **11**, 2995.
158. K. Wang, C.-Y. Wang, Y. Zhang, S. X.-A. Zhang, B. Yang and Y.-W. Yang, *Chem. Commun.*, 2014, **50**, 9458.
159. Z. Zhang, C. Han, G. Yu and F. Huang, *Chem. Sci.*, 2012, **3**, 3026.
160. W.-B. Hu, C.-D. Xie, W.-J. Hu, X.-L. Zhao, Y. A, Liu, J.-C. Huo, J.-S. Li, B. Jiang and K. Wen, *J. Org. Chem.*, 2015, **80**, 7994.
161. K. Wan, S.-C. Gap, X. Fang, M.-Y. Xu, Y. Yang and M. Xue, *Chem. Commun.*, 2020, **56**, 10155.
162. N. L. Strutt, H. Zhang, M. A. Giesener, J. Lei and J. F. Stoddart, *Chem. Commun.*, 2012, **48**, 1647.
163. T. Ogoshi, H. Kayama, D. Yamafuji, T. Aoki and T. Yamagishi, *Chem. Sci.*, 2012, **3**, 3221. (47)
164. Y. Guan, M. Ni, X. Hu, T. Xiao, S. Xiong, C. Lin and L. Wang, *Chem. Commun.*, 2012, **48**, 8529.
165. C. Li, K. Han, J. Li, Y. Zhang, W. Chen, Y. Yu and X. Jia, *Chem. Eur. J.*, 2013, **19**, 11892.
166. X. Wang, K. Han, J. Li, X. Jia and C. Li, *Poym. Chem.*, 2013, **4**, 3998.
167. S. Wang, Y. Wang, Z. Chen, Y. Lin, L. Weng, K. Han, J. Li, X. Jia and C. Li, *Chem. Commun.*, 2015, **51**, 3434.
168. Q. Wang, P. Zhang, Y. Li, L. Tian, M. Cheng, F. Lu, X. Liu, Q. Fan and W. Huang, *RSC Adv.*, 2017, **7**, 29364.
169. T. Ogoshi, K. Yoshikoshi, T. Aoki and T. Yamagishi, *Chem. Commun.*, 2013, **49**, 8785.
170. Y. Wang, J.-F. Xu, Y.-Z. Chen, L.-Y. Niu, L.-Z. Wu, C.-H. Tung and Q.-Z. Yang, *Chem. Commun.*, 2014, **50**, 7001.
171. N. Song, D.-X. Chen, M.-C. Xia, X.-L. Qiu, K. Ma, B. Xu, W. Tian and Y.-W. Yang, *Chem. Commun.*, 2015, **51**, 5526.
172. L.-B. Meng, D. Li, S. Xiong, X.-Y. Hu, L. Wang and G. Li, *Chem. Commun.*, 2015, **51**, 4643.
173. M. Fathalla, N. L. Strutt, S. Sampath, K. Katsiev, K. J. Hartlieb, O. M. Bakr and J. F. Stoddart, *Chem. Commun.*, 2015, **51**, 10455.
174. X.-W. Sun, Z.-H. Wang, Y.-J. Li, Y.-F. Zhang, Y.-M. Zhang, H. Yao, T.-B. Wei and Q. Lin, *Macromolecules*, 2021, **54**, 373.
175. X. Y. Hu, X. Wu, Q. Duan, T. Xiao, C. Lin and L. Wang, *Org. Lett.*, 2012, **14**, 4826.
176. X. Y. Hu, P. Zhang, X. Wu, W. Xia, T. Xiao, J. Jiang, C. Lin and L. Wang, *Polym. Chem.*, 2012, **3**, 3060.
177. K. Eichstaedt, B. Wicher, M. Gdaniec and T. Połoński, *CrystEngComm*, 2016, **18**, 5807.
178. P. Liu, Z. Li, B. Shi, J. Liu, H. Zhu, F. Huang, *Chem. Eur. J.*, 2018, **24**, 4264.
179. D. Xia, X. Lv, K. Chen and P. Wang, *Dalton Trans.*, 2019, **48**, 9954.
180. H. Xing and B. Shi, *Polym. Chem.*, 2016, **7**, 6159.
181. L. Gao, Z. Zhang, B. Zheng and F. Huang, *Polym. Chem.*, 2014, **5**, 5734.
182. X. Wu, Y. Yu, L. Gao, X. Y. Hu and L. Wang, *Org. Chem. Front.*, 2016, **3**, 966.
183. J. D. Ding, J. F. Chen, Q. Lin, H. Yao, Y. M. Zhang and T. B. Wei, *Polym. Chem.*, 2018, **9**, 5370.
184. Q. Lin, Z. H. Wang, T. T. Huang, T. B. Wei, H. Yao and Y. M. Zhang, *J. Mater. Chem. C*, 2021, **9**, 3863.
185. X. Zeng, H. Deng, X. Jia, L. Cui, J. Li, C. Li and J. Fang, *Chem. Commun.*, 2018, **54**, 11634.
186. E. Lee, I. Park, H. Ju, S. Kim, J. H. Jung, Y. Habata and S. S. Lee, *Angew. Chem. Int. Ed.*, 2019, **58**, 11296.
187. Z. Y. Li, Y. Zhang, C. W. Zhang, L. J. Chen, C. Wang, H. Tan, Y. Yu, X. Li and H. B. Yang, *J. Am. Chem. Soc.*, 2014, **136**, 8577.
188. H. Guo, J. Ye, Z. Zhang, Y. Wang, X. Yuan, C. Ou, Y. Ding, C. Yan, J. Wang and Y. Yao, *Inorg. Chem.*, 2020, **59**, 11915.
189. H. Zhang, K. T. Nguyen, X. Ma, H. Yan, J. Guo, L. Zhu and Y. Zhao, *Org. Biomol. Chem.*, 2013, **11**, 2070.
190. X. Y. Hu, K. Jia, Y. Cao, Y. Li, S. Qin, F. Zhou, C. Lin, D. Zhang and L. Wang, *Chem. Eur. J.*, 2015, **21**, 1208.
191. S. Guo, Y. Song, Y. He, X.-Y. Hu and L. Wang, *Angew. Chem. Int. Ed.*, 2018, **130**, 3217.
192. W. Tuo, Y. Sun, S. Lu, X. Li, Y. Sun and P. J. Stang, *J. Am. Chem. Soc.*, 2020, **142**, 16930.
193. F. Vögtle, G. Richardtand and N. Werner, Dendrimer Chemistry, WILEY-VCH, Weinheim, 2009.
194. J. W. Lee and K. Kim. Rotaxane Dendrimers. In: C. A. Schalley, F. Vögtle (eds) Dendrimers V. Topics in Current Chemistry, vol 228. Springer, Berlin, Heidelberg, 2003.
195. X. Q. Wang, W. J. Li, W. Wang and H. B. Yang, *Acc. Chem. Res.*, 2021, **54**, 4091.
196. W. Wang, B. Sun, X. Q. Wang, Y. Y. Ren, L. J. Chen, J. Ma, Y. Zhang, X. Li, Y. Yu, H. Tan and H. B. Yang, *Chem. Eur. J.,* 2015, **21**, 6286.
197. M. He, L. Chen, B. Jiang, H. Tan, C. Wang and H. Yang, *Chin. Chem. Lett.*, 2019, **30**, 131.
198. Y. X. Wang, Q. F. Zhou, L. J. Chen, L. Xu, C. H. Wang, X. Li and H. B. Yang, *Chem. Commun.,* 2018, **54**, 2224.
199. W. Wang, L. J. Chen, X. Q. Wang, B. Sun, X. Li, Y. Zhang, J. Shi, Y. Yu, L. Zhang, M. Liu and H. B. Yang, *Proc. Natl. Acad. Sci. U. S. A.*, 2015, **112**, 5597.
200. X. Q. Wang, W. Wang, W. J. Li, L. J. Chen, R. Yao, G. Q. Yin, Y. X. Wang, Y. Zhang, J. Huang, H. Tan, Y. Yu, X. Li, L. Xu and H. B. Yang, *Nat. Commun.*, 2018, **9**, 3190.
201. X. Q. Wang, W. J. Li, W. Wang, J. Wen, Y. Zhang, H. Tan and H. B. Yang, *J. Am. Chem. Soc.*, 2019, **141**, 13923.
202. W. J. Li, W. Wang, X. Q. Wang, M. Li, Y. Ke, R. Yao, J. Wen, G. Q. Yin, B. Jiang, X. Li, P. Yin and H. B. Yang, *J. Am. Chem. Soc.*, 2020, **142**, 8473.
203. W. J. Li, Z. Hu, L. Xu, X. Q. Wang, W. Wang, G. Q. Yin, D. Y. Zhang, Z. Sun, X. Li, H. Sun and H. B. Yang, *J. Am. Chem. Soc.*, 2020, **142**, 16748.
204. W.-J. Li, X.-Q. Wang, W. Wang, Z. Hu, Y. Ke, H. Jiang, C. He, X. Wang, Y.-X. Hu, P.-P. Jia, P. Yin, J. Chen, H. Sun, Z. Sun, L. Xu and H.-B. Yang, *Giant*, 2020, **2**, 100020.
205. X.-Q. Wang, W. Wang, W.-J. Li, Y. Qin, G.-Q. Yin, W.-L. Jiang, X. Li, S. Wu and H.-B. Yang, *Org. Chem. Front.*, 2019, **6**, 1686.
206. W. J. Li, X. Q. Wang, D. Y. Zhang, Y. X. Hu, W. T. Xu, L. Xu, W. Wang and H. B. Yang, *Angew. Chem. Int. Ed.*, 2021, **60**, 18761.
207. S. Sun, X.-Y. Hu, D. Chen, J. Shi, Y. Dong, C. Lin, Y. Pan and L. Wang, *Polym. Chem.,* 2013, **4**, 2224.
208. S. Sun, J.-B. Shi, Y.-P. Dong, C. Lin, X.-Y. Hu and L.-Y. Wang, *Chin. Chem. Lett.*, 2013, **24**, 987.

209. M. Boominathan, J. Kiruthika and M. Arunachalam, *J. Polym. Sci. Part A: Polym. Chem.*, 2019, **57**, 1508.
210. M. Boominathan and M. Arunachalam, *ACS Appl. Polym. Mater.*, 2020, **2**, 4368.
211. J. He, J. Chen, S. Lin, D. Niu, J. Hao, X. Jia, N. Li, J. Gu, Y. Li and J. Shi, *Biomacromolecules*, 2018, **19**, 2923.
212. V. Kardelis, K. Li, I. Nierengarten, M. Holler, J.-F. Nierengarten and A. Adronov, *Macromolecules*, 2017, **50**, 9144.
213. T. Ogoshi, Y. Hasegawa, T. Aoki, Y. Ishimori, S. Inagi and T. Yamagishi, *Macromolecules*, 2011, **44**, 7639.
214. J. Li, A. Harada and M. Kamachi, *Bull. Chem. Soc. Jpn.*, 1994, **67**, 2808.
215. T. Ogoshi, H. Kayama, T. Aoki, T. Yamagishi, R. Ohashi and M. Mizuno, *Polym. J.*, 2013, **46**, 77.
216. J. Chen, N. Li, Y. Gao, F. Sun, J. He and Y. Li, *Soft Matter*, 2015, **11**, 7835.
217. K. Kato, K. Onishi, K. Maeda, M. Yagyu, S. Fa, T. Ichikawa, M. Mizuno, T. Kakuta, T. Yamagishi and T. Ogoshi, *Chem. Eur. J.* 2021, **27**,6435.
218. T. Ogoshi, R. Sueto, M. Yagyu, R. Kojima, T. Kakuta, T. Yamagishi, K. Doitomi, A. K. Tummanapelli, H. Hirao, Y. Sakata, S. Akine and M. Mizuno, *Nat. Commun.*, 2019, **10**, 479.
219. T. Ogoshi, T. Aoki, S. Ueda, Y. Tamura and T. Yamagishi, *Chem. Commun.*, 2014, **50**, 6607.
220. T. Ogoshi, M. Yoshiki, T. Kakuta, T. Yamagishi and M. Mizuno, *Chem. Commun.,* 2021, **57**, 12468.
221. I. T. Harrison, S. Harrison, *J. Am. Chem. Soc.*, 1967, **89**, 5723.
222. E. Wasserman, *J. Am. Chem. Soc.* 1960, **82**, 4433.
223. K. Yang, S. Chao, F. Zhang, Y. Pei and Z. Pei, *Chem. Commun.*, 2019, **55**, 13198.
224. X.-Y. Lou and Y.-W. Yang, *Adv. Mater.*, 2020, **32**, 2003263.
225. T. Ogoshi, T. Kakuta and T. Yamagishi, *Angew. Chem. Int. Ed.*, 2019, **58**, 2197.
226. K. Jie, Y. Zhou, E. Li and F. Huang, *Acc. Chem. Res.*, 2018, **51**, 2064.